

UNIVERSITA' VITA-SALUTE SAN RAFFAELE

CORSO DI DOTTORATO DI RICERCA

INTERNAZIONALE IN MEDICINA MOLECOLARE

Curriculum in Basic and Applied Immunology and Oncology

Interferon $\alpha\beta$ -receptor subunit 1 (IFNAR1)

stabilization in the liver metastatic

microenvironment

DoS: Dr. Giovanni Sitia

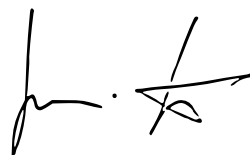
Second Supervisor: Prof. Stefano Indraccolo

Tesi di DOTTORATO di RICERCA di Andrea Monestiroli

matr. 015570

Ciclo di dottorato XXXV

SSD MED/04



Anno Accademico 2021/2022

Consultazione tesi di Dottorato di Ricerca

Il/la sottoscritto/I Andrea Monestiroli
Matricola / *registration number* 015570
nato a/ *born at* Milano
il/on 28/04/1984

autore della tesi di Dottorato di ricerca dal titolo / *author of the PhD Thesis titled*

Interferon $\alpha\beta$ -receptor subunit 1 (IFNAR1) stabilization in the liver metastatic microenvironment

AUTORIZZA la Consultazione della tesi / *AUTHORIZES the public release of the thesis*
 NON AUTORIZZA la Consultazione della tesi per tempo indeterminato / *DOES NOT AUTHORIZE the public release of the thesis for indeterminate time*

a partire dalla data di conseguimento del titolo e precisamente / *from the PhD thesis date, specifically*

Dal / *from* 17/01/2023

Poiché / *because*:

l'intera ricerca o parti di essa sono potenzialmente soggette a brevettabilità/ *The whole project or part of it might be subject to patentability*;

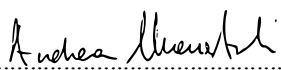
ci sono parti di tesi che sono già state sottoposte a un editore o sono in attesa di pubblicazione/ *Parts of the thesis have been or are being submitted to a publisher or are in press*;

la tesi è finanziata da enti esterni che vantano dei diritti su di esse e sulla loro pubblicazione/ *the thesis project is financed by external bodies that have rights over it and on its publication*.

E' fatto divieto di riprodurre, in tutto o in parte, quanto in essa contenuto / *Copyright the contents of the thesis in whole or in part is forbidden*

Data /Date 14/11/2022

Firma /Signature



Declaration

This thesis has been:

- composed by myself and has not been used in any previous application for a degree. Throughout the text, I use both 'I' and 'We' interchangeably.
- has been written according to the editing guidelines approved by the University.

Permission to use images and other material covered by copyright has been sought and obtained. For the following images (Fig. 1.6, 1.13, 1.20-21), it was not possible to obtain permission and are therefore included in the thesis under the "fair use" exception (Italian legislative Decree no. 68/2003).

The data and descriptions presented in the introduction on pages 42-47 are taken from a recently published paper by my group, in which I am a co-author (Tran NL, Ferreira LM, Alvarez-Moya B, Buttiglione V, Ferrini B, Zordan P, Monestiroli A, Fagioli C, Bezzecchi E, Scotti GM, *et al* (2022) Continuous sensing of IFN α by hepatic endothelial cells shapes a vascular antimetastatic barrier. *Elife* 11). Some of the figures presented in the Introduction section were created using BioRender software (BioRender) under an active institutional license.

All the results presented here were obtained by myself, except for:

- 1. The surgical procedures to obtain in vivo metastatic models reported in this thesis, because of their complexity, required the collaboration of a team of micro-surgeons and collaborators to be successfully performed. I participated in all of these experiments, in all roles except intra-mesenteric injection of cells, which was performed by Dr. Ngoc Lan Tran, Dr. Maria Ferreira and Dr. Giovanni Sitia.*
- 2. The digital PCR experiments shown in Figure 3.3.1 C-D were performed by Dr. Ilaria Marzinotto, Diabetes Research Institute, San Raffaele Scientific Institute, Milan, Italy.*
- 3. Confocal immunofluorescence staining and imaging in Figure 3.6.1. and quantification of IHC staining in Figure 3.6.2. B and 3.10.7 F were performed in collaboration with Dr. Maria Ferreira from my group.*

4. *The data in Figures 3.10.1, 3.10.3, and 3.10.6 A-C were designed and obtained by Dr. Paola Zordan, a former member of my group. All other experiments using the OT-ISA model were performed in collaboration with Dr. Zordan.*

5. *The data from Figure 3.11. D-E were produced by Chiara Stambazzi, Valentina Buttiglione, former members of my group in collaboration with Dr. Federica Pedica in the Pathology dept. of OSR and Prof. Luca Aldrighetti and Prof. Riccardo Rosati from Hepatobiliary Surgery Unit and Gastroenterology Surgery Unit of OSR.*

All sources of information are acknowledged by means of reference.

Acknowledgments

I thank C. Fagioli, C. B. Ekalle-Soppo, F. Caruso, B. Mendicino, and E. Daoud from the Experimental Hepatology Unit; A. Fiocchi, M. Raso, and M. Ravà from the HSR Animal Histopathology Facility; T. Canu and C. Gnasso from the HSR Preclinical Imaging Facility; G. Torri, C. Lorenzi, and D. Lazarevic from the HSR Center for Omics Sciences for technical support. I thank all the members of the Experimental Hepatology Unit and the San Raffaele AIRC 5X1000 team for helpful discussions; V Russo for his tutoring support.

Confocal immunofluorescence histology was performed at the Alembic facility at HSR. Flow cytometry was performed at the FRACTAL facility at HSR.

I'm very grateful to the Francesco Fronzaroli Memorial Fellowship, which supported me and allowed me to perform this Ph.D. work.

Abstract

Liver metastases from colorectal cancer (CRC) are the second leading cause of cancer-related deaths worldwide. Therefore, new therapeutic approaches are highly needed. Type I IFNs contribute to anti-tumor immunity by stimulating specific CD8⁺ DCs to cross-present antigens to cytotoxic CD8⁺ T cells (CTLs) and by providing a "third signal" to stimulate clonal expansion of tumor-specific CTLs. However, tumors in mice and humans activate immune escape mechanisms that target the type I IFNs signaling pathway. Indeed, down-regulation of IFNAR1 by components of the CRC tumor microenvironment reduces the viability and accumulation of CTLs within CRC tumors, establishing an immune-privileged niche. Mechanistically, degradation of IFNAR1 on the cell surface follows ubiquitination by a specific E3 ligase that binds to phosphorylated Ser⁵²⁶ IFNAR1 in mice, or Ser⁵³⁵ in humans. Importantly, a genetic variant of IFNAR1 with a single Ala substitution of Ser⁵²⁶ or Ser⁵³⁵ (IFNAR1^{SA}), renders cell surface IFNAR1 undegradable and restores tumor-specific CTL viability, accumulation within CRC tumors and efficacy of adoptive T cell therapies. It is currently unknown whether this pathway is also deregulated in liver CRC metastases and what are the cellular and molecular drivers of this deregulation.

Using murine models of CRC liver metastases as well as human liver CRC metastasis samples, we tested the hypothesis that cells of the hepatic CRC metastatic microenvironment deregulate IFNAR1, and that overcoming this phenotype may restore tumor-specific CTL viability, accumulation within CRC tumors, and efficacy of adoptive T cell therapies.

To define the liver microenvironmental clues associated with IFNAR1 downregulation in the liver we monitored a panel of different genes associated with immune-privileged niches in murine CRC tumor models with increasing volume. We found that several type I IFN subtypes are upregulated in metastatic liver lesions and this is associated with increased numbers of interferon-regulated genes (IRGs), checkpoint inhibitors, inflammatory cytokines, and genes associated with the IFNAR1 degradation machinery, which is typical of an immunosuppressive microenvironment. To elucidate the cellular source of type I interferons, we examined various MSI and MSS CRC mouse cell lines and tumor organoids (MTO) and found that CRCs express the same type I IFN subtypes

in vitro, whereas pancreatic ductal adenocarcinoma (PDAC) cells did not. Next, we developed a continuous delivery strategy to administer recombinant type I IFN molecules with different affinities for IFNAR1 (IFN α 1 and IFN α 11) to mice with established intrahepatic CRC and PDAC tumors. However, the use of these molecules did not significantly reduce intrahepatic tumor growth in CRC tumors. Differently, we obtained data showing that pharmacological stabilization of IFNAR1 by p38/PDK inhibitors reduced tumor burden and improved survival in mice with CRC liver metastases. Moreover, independent experiments using anti-tumor T cells showed that CD8⁺ T cells with a non-degradable IFNAR1 significantly reduced tumor burden. Mechanistically, IFNAR1 stabilization reversed the immune deregulation associated with intrahepatic tumor growth by promoting infiltration, persistence, and anti-tumor effector functions of CD8⁺ T cells. Finally, we found a correlation between IFN signature expression and survival in patients with CRC tumors, we confirmed that IFNAR1 is downregulated in primary human CRC lesions and corresponding synchronous liver lesions in a cohort of patients undergoing combined surgery for CRC and liver metastases. In conclusion, stabilization of IFNAR1 in liver CRC metastases represents a promising new therapeutic approach to improve immunotherapies.

Table of contents

Table of contents	1
Acronyms and Abbreviations	4
List of Figures and Tables	6
1. Introduction.....	9
1.1 Colorectal cancer.....	9
1.1.1 Incidence and risk factors.....	9
1.1.2 Carcinogenesis.....	11
1.1.3 Signs and symptoms, investigations and diagnosis	16
1.1.4 Colorectal cancer staging and histopathology.....	18
1.1.5 Guidelines for colorectal cancer treatment	26
1.1.6 Post-operative recurrence in colorectal cancer.....	29
1.1.7 Colorectal cancer with synchronous liver metastases.....	31
1.1.8 Synchronous liver metastases surgery and chemotherapy treatment	31
1.2 Liver metastatization process.....	35
1.3 Adoptive cell therapy (ACT) in cancer treatment.....	37
1.4 Interferons	39
1.4.1 Type I interferons signaling and activity	40
1.5 Continuous sensing of IFN α by hepatic endothelial cells shapes a vascular antimetastatic barrier	44
1.5.1 Continuous perioperative IFN α administration reduces liver CRC metastatic burden and improves survival.....	45
1.5.2 HECs mediate the anti-metastatic activity of IFN α	47
1.5.3 Continuous IFN α sensing improves immunostimulatory properties of HECs to provide lasting tumor protection	49
1.5.4 Type I Interferon subtypes display different <i>in vitro</i> and <i>in vivo</i> potencies...50	

1.6 Inactivation of Interferon receptor promotes the establishment of immune privileged tumor microenvironment.....	52
1.6.1 Inhibitors of stress-activated kinases for IFNAR1 stabilization.....	55
2. Aim of the work	58
3. Results	59
3.1 Adjuvant IFN α therapy does not significantly reduce intrahepatic CRC growth .	59
3.2 Endogenous Type I Interferons and several IRGs are expressed in the liver of MC38 bearing mice.....	62
3.3 CRC cell lines and tumor organoids express type I Interferon subtypes <i>in vitro</i> .	66
3.4 CRC cell lines express functional type I Interferon proteins.....	69
3.5 CRC liver tumors of different origin express type I Interferon genes <i>in vivo</i>	71
3.6 CRC liver metastatic lesions show a reduced IFNAR1 expression and IFN activation capacity.....	73
3.7 CRC and PDAC liver metastases show different sensibility to IFN based therapeutic approaches	76
3.8 CRC and PDAC cell lines display different cell autonomous susceptibility to IFN stimulation	79
3.9 Pharmacological IFNAR1 degradation inhibitors reduce CRC metastases growth and improve survival.....	82
3.10 OT-ISA effector T cells ACT have an improved therapeutic index, survival/killing advantage and increases tumor CD3 ⁺ cell recruitment in combinatorial IFN α therapy.....	86
3.11 IRF7 increased expression correlates with worse prognosis in patients with primary CRC tumors, and IFNAR1 is downregulated in CRC tumors and synchronous liver metastases.....	97
4. Discussion.....	100
5. Materials and Methods	105
5.1 Animal studies.....	105

5.2 Tumor cell lines and organoids.	105
5.3 Mouse models of liver metastases.	106
5.4 Recombinant Mouse IFN α therapy.	107
5.5 Magnetic resonance imaging (MRI).....	107
5.6 Peripheral blood analyses.	108
5.7 B16-Blue TM IFN- α/β assay on cell protein extracts.	108
5.8 RNA extraction and quantitative real-time PCR gene expression analyses.	109
5.9 Digital PCR gene expression analyses.	110
5.10 Isolation of splenocytes and Generation of Effector CD8+ T Cells.....	110
5.11 Cell proliferation assays.....	111
5.12 Immunofluorescence and confocal microscopy.	112
5.13 Isolation of intra hepatic leukocytes (IHLs).....	112
5.14 Flow cytometry.....	114
5.15 Kinase inhibitors preparation	115
5.16 Patients.....	115
5.17 Immunohistochemistry.	116
5.18 Statistical analysis.....	116
6. References.....	117
7. Appendix.....	130

Acronyms and Abbreviations

5-FU	5-fluorouracil
ACT	Adoptive Cell Therapy
AJCC	American Joint Committee on Cancer
CA 19-9	Cancer Antigen 19-9
CEA	Carcinoembryonic Antigen
CTL	Cytotoxic T Lymphocytes
CRC	Colorectal Carcinoma
CTC	Circulating Tumor Cell
CRLM	Colorectal Liver Metastases
dPCR	Digital PCR
EGFR	Epithelial Growth Factor Receptor
EMT	Epithelial-Mesenchymal Transition
FOLFIRI	5-FU/irinotecan
FOLFOX	5-FU/oxaliplatin
HEC	Hepatic Endothelial Cell
IC	Intestinal Crypts
IFN	Interferon
IFNAR1	Interferon Alpha And Beta Receptor Subunit 1
IHL	Intra Hepatic Leukocytes
ISG/IRG	Interferon Stimulated/Regulated Gene
LCC	Left-sided Colon Cancer
LOH	Loss of Heterozygosity
MDSC	Myeloid-Derived Suppressor Cell
MHC	major histocompatibility complex
MOP	Mini-Osmotic Pumps
MRI	Magnetic Resonance Imaging
MSI	Microsatellite Instability
MSS	Microsatellite Stable
MTO	Murine Tumor Organoid
NCCN	National Comprehensive Cancer Network

OVA	Ovalbumin
PDAC	Pancreatic Ductal Adenocarcinoma
PBMC	Peripheral Blood Mononuclear Cell
PD-1	Programmed Death 1
PD-L1	Programmed Death-Ligand 1
PRR	Pattern Recognition Receptors
RCC	Right-sided Colon Cancer
SCLM	Synchronous Colorectal Liver Metastases
TCGA	The Cancer Genome Atlas
TCR	T Cell Receptor
TGF	Transforming Growth Factor
TIL	Tumor-Infiltrating Lymphocytes
TME	Tumor Microenvironment
TNF	Tumor Necrosis Factor
UPR	Unfolded Protein Response
VEGF	Vascular Endothelial Growth Factor
WBC	White Blood Cells

List of Figures and Tables

1. Introduction

<i>Figure 1.1. Incidence of CRC in 2020.</i>	7
<i>Figure 1.2. The adenoma-carcinoma pathway.</i>	9
<i>Figure 1.3. The EGFR pathway.</i>	13
<i>Figure 1.4. The TNM System.</i>	19
<i>Figure 1.5. Colorectal cancer metastatic spreading.</i>	20
<i>Table 1.1. CRC Staging System.</i>	19
<i>Figure 1.6. Prognostic differences between right and left colon cancer.</i>	25
<i>Figure 1.7. Vascular and lymphatic supply of the colon.</i>	26
<i>Figure 1.8. Guidelines for treatment of colorectal cancer by stage.</i>	27
<i>Figure 1.9. Circulating tumor cells in colorectal cancer. CTCs as prognostic factor for CRC recurrence.</i>	30
<i>Figure 1.10. NCCN Guidelines for metastatic colorectal cancer.</i>	33
<i>Figure 1.11 The portal vein system.</i>	36
<i>Figure 1.12. The type I Interferons signaling pathway.</i>	41
<i>Figure 1.13. The dual role of type I IFN in immunity.</i>	40
<i>Figure 1.14. IFNα dosing regimen determination.</i>	44
<i>Figure 1.15. Continuous perioperative IFNα treatment effectively reduces liver CRC tumor burden and improves survival.</i>	46
<i>Figure 1.16. Continuous IFNα treatment inhibits spontaneous liver colonization of orthotopically injected CT26 cells.</i>	46
<i>Figure 1.17. IFNα perioperative antimetastatic action is mediated by HECs.</i>	48
<i>Figure 1.18. HECs continuous IFNα sensing confers lasting tumor protection.</i>	49
<i>Figure 1.19. Type I IFN subtypes show different potencies.</i>	50
<i>Figure 1.20. IFN signaling and IFNAR1 downregulation in CRC patients.</i>	53
<i>Figure 1.21. IFNAR1 positive cells are excluded from human CRC.</i>	54

3. Results

<i>Figure 3.1. Adjuvant IFNα therapy does not significantly reduce intrahepatic CRC growth.</i>	60
<i>Figure 3.2. Endogenous Type I Interferons and several IRGs are expressed in the liver of MC38 bearing mice.</i>	61
<i>Figure 3.3.1. CRC cell lines and tumor organoids express type I Interferon subtypes in vitro.</i>	67
<i>Figure 3.3.2. Intestinal crypts (IC) characterization.</i>	68
<i>Figure 3.4. CRC cell lines express functional type I Interferon proteins.</i>	69
<i>Figure 3.5. CRC liver tumors of different origin express type I Interferon genes in vivo.</i>	71
<i>Figure 3.6.1. CRC liver metastatic lesions show a reduced IFNAR1 expression.</i>	71
<i>Figure 3.6.2. CRC liver metastatic lesions show reduced pSTAT1 activation upon IFNα stimulation.</i>	72
<i>Figure 3.7.1. High potency IFNα11 treatment does not cause overt toxicity.</i>	76
<i>Figure 3.7.2. CRC and PDAC liver metastases show different sensibility to IFN based therapeutic approaches.</i>	77
<i>Figure 3.8. CRC and PDAC cell lines display different cell autonomous susceptibility to IFN stimulation.</i>	80
<i>Figure 3.9.1. Pharmacological IFNAR1 degradation inhibitors reduce CRC metastases growth and improve survival.</i>	81
<i>Figure 3.9.2. IFNAR1 degradation inhibitors treatment does not cause weight loss or overt toxicity.</i>	84
<i>Figure 3.10.1. MC38_NGFR-OVA are selectively recognized by OT1^{Eff} cells in vitro.</i>	86
<i>Figure 3.10.2. IFNAR1^{SA} mice show increased IFN signaling.</i>	87
<i>Figure 3.10.3. OT-I^{SA} and OT-I effector T cells show comparable proliferation rate and effector function in vitro.</i>	88
<i>Figure 3.10.4. OT-I^{SA} and OT-I effector T cells show comparable therapeutic index when administered 7 days after CRC challenge.</i>	90
<i>Figure 3.10.5. OT-I^{SA} effector T cells ACT have an improved therapeutic index when administered 14 days after CRC challenge.</i>	91

<i>Figure 3.10.6. OT-I^{SA} effector T cells have an improved survival/killing advantage.</i>	90
<i>Figure 3.10.7. IFNα therapy in combination with OT-I^{SA} ACT increases CD3⁺ cell recruitment in the tumor reducing tumor growth.</i>	95
<i>Figure 3.11. IRF7 increased expression correlates with worse prognosis in patients with primary CRC tumors, and IFNAR1 is downregulated in CRC tumors and synchronous liver metastases.</i>	98

7. Appendix

<i>Table 7.1. Custom Taqman Array Cards genes list.</i>	128
--	-----

1. Introduction

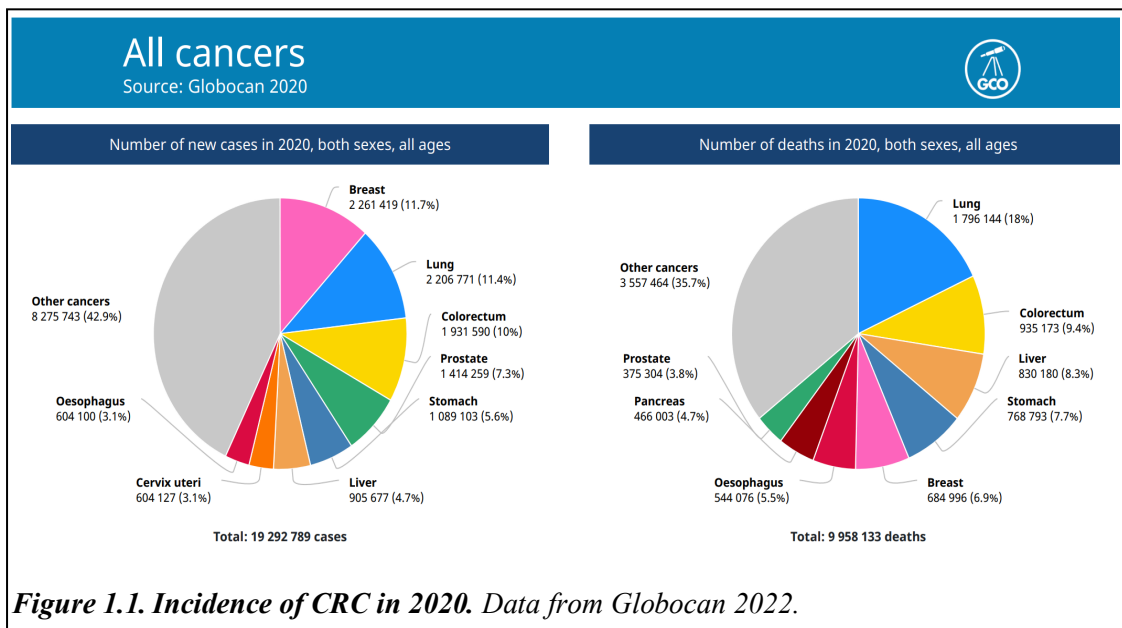
1.1 Colorectal cancer

1.1.1 Incidence and risk factors

Adenocarcinoma of Colon and Rectum (CRC) is a major clinical hurdle, with a high impact on both cancer morbidity and mortality. Accordingly, CRC is the third most common cancer (after breast and lung) and the second leading cause of cancer-related death (after lung) worldwide (Sung *et al*, 2021).

Incidence rate of CRC increases as function of age, reaching in the US approximatively the 80% of new cases in patients older than 55 years (with a median age at diagnosis of 66 years) (Reports from the National Cancer Institute, 2022).

Nevertheless, from 2002 the death rate for women and men decreased of the 4.3% annually. Accordingly, there has been a significant increase in 5-year survival rates over the last 30 years: nowadays 5-year survival for CRC is 65.1%, percentage that rise to 90.9% in patients with localized tumor (confined to primary site) at time of diagnosis (Reports from the National Cancer Institute, 2022). CRC is more common in men than women (23.4 versus 16,2 cases per 100,000 persons), with a higher mortality rate in the firsts (death rate of 16 per 100,000 men and 11.3 per 100,000 woman) (Reports from the



National Cancer Institute, 2022). Differently from other cancer types, as lung cancer, no single risk factor is responsible for most CRC cases (Brenner *et al*, 2014).

In this regard, excluding age and sex, others risk factors have been linked to CRC insurgence as family history of this malignancy, inflammatory bowel disease, smoking and alcohol consumption, high intake of red and processed meat, obesity and diabetes (Brenner *et al*, 2014). Particularly, the more common factor risks in the population are those related to habits (as smoking and alcohol consumption or high intake of red and processed meat) that are also the group of which correlation with CRC incidence is editable, modifying behavior. Differently, genetic CRC predisposition and inflammatory bowel disease are less frequent in general population but are responsible for a strong increase in CRC occurrence (Brenner *et al*, 2014). Among the preventive factors, physical activity, colonoscopy and a partially healthy diet are the most recognized (with a weak protective effect of a diet rich in fruits, vegetables, cereal fibers and whole grains) (Brenner *et al*, 2014).

There have been several hereditary factors associated with the development of CRC, although most cases occur sporadic and develop over the course of a long time, through the adenoma-carcinoma sequence (Brenner *et al*, 2014). Thirty five percent of the risk for CRC is due to hereditary components. Excluding hereditary forms such as familial adenomatous polyposis (FAP) and hereditary nonpolyposis colon cancer (Lynch syndrome), which are caused by recognized genetic aberrations but account for less than 5% of all colorectal cancers, the genetic factors that determine disease risk are still incompletely known (Taylor *et al*, 2010). A collective number of single nucleotide polymorphisms (SNPs) have been identified in the last years in genome-wide association studies, showing a statistical significance but generally very small associations with colorectal cancer risk (Theodoratou *et al*, 2012; Mimori *et al*, 2012).

CRC rate of incidence is four times higher in transitioned countries compared with transitioning countries, with an approximately equal mortality rates in the two, due to the poor health assistance in the latter. The highest incidences are among people who live in European regions, Australia/ New Zealand, and Northern America (Sung *et al*, 2021). When considered alone rectal cancer shows a similar regional distribution, although rates in Eastern Asia rank among the highest. From incidence data emerged as CRC can be considered a marker of socio-economic development, with incidence rates that tend to

rise in countries undergoing major transition and increasing their development index (Fidler *et al*, 2016). The surge of incidence in previously low-risk countries is probably associated to changes in diet and lifestyle factors, such as a shift toward increased consumption of animal foods and a sedentary lifestyle, leading to lower physical activity and higher prevalence of obesity, which are independently associated with colorectal cancer risk (Siegel *et al*, 2020). Furthermore, heavy alcohol consumption, cigarette smoking, and consumption of red or processed meat represent additional risks of developing CRC, though calcium supplements and adequate consumption of whole grains, fiber, and dairy products seem to be CRC protective factors (Clinton *et al*, 2019). All in all, primary prevention remains the most important strategy to reduce the growing global burden of colorectal cancer.

1.1.2 Carcinogenesis

Carcinogenesis is based on the accumulation of selected genetic mutations that lead to clonal proliferation of cells, bypassing the balance between cell death and proliferation. Usually, these mutations occur in genes known as oncogenes and tumor suppressor genes (Hanahan & Weinberg, 2000, 2011; Subramaniam *et al*, 2016). The majority of sporadic colon carcinomas arise from an adenomatous polyp (adenoma), which is associated with nearly 80% of colorectal carcinomas. As the adenoma progresses, it follows the adenoma-carcinoma pathway, characterized by the loss or inactivation of a large proportion of

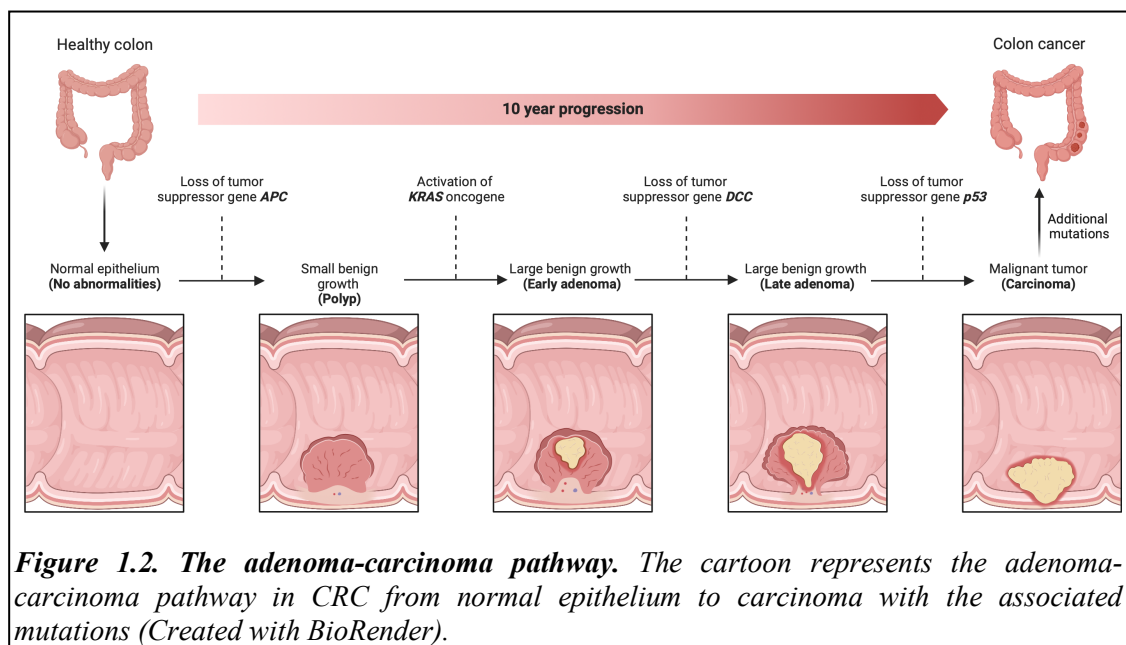


Figure 1.2. The adenoma-carcinoma pathway. The cartoon represents the adenoma-carcinoma pathway in CRC from normal epithelium to carcinoma with the associated mutations (Created with BioRender).

genes (Fig 1.2) (Weitz *et al*, 2005). The development of CRC from adenoma takes between 10 and 15 years. Over time, an adenomatous polyp becomes increasingly dysplastic, indicating an early neoplastic process that eventually leads to the formation of the underlying cancer (Weitz *et al*, 2005). Three different pathways of genomic instability have been identified in the context of the adenoma-carcinoma pathway: the chromosomal instability, the microsatellite instability, and the CpG island methylator phenotype pathways (Sieber *et al*, 2003; Armaghany *et al*, 2011; Li *et al*, 2021).

Chromosomal instability

Chromosomal instability (CIN) pathway consists of a known sequence of genetic alterations corresponding to very specific histological changes (Sieber *et al*, 2003; Weitz *et al*, 2005; Armaghany *et al*, 2011; Li *et al*, 2021). Genomic alterations include activation of proto-oncogenes (KRAS) and inactivation of at least three tumor suppression genes, in particular loss of Adenomatous Polyposis Coli (APC), loss of TP53, and loss of heterozygosity (LOH) for the long arm of chromosome 18 (18q) (Sieber *et al*, 2003; Armaghany *et al*, 2011; Li *et al*, 2021). APC gene, the most common initial mutation in familial/inherited and sporadic colon cancer, is a tumor suppressor gene, which acts as a negative regulator of the Wnt signaling pathway (Sieber *et al*, 2003; Michor *et al*, 2005; Li *et al*, 2021). The Wnt signaling pathway is involved in the maintenance of stem cells compartment in the colonic crypts (Shih *et al*, 2001; Michor *et al*, 2005; Bian *et al*, 2020).

Mechanistically, wild-type APC inhibits stem cell proliferation by degrading β -catenin, a key regulator of the Wnt signaling pathway; in contrast, in APC mutated CRC, high levels of intracellular β -catenin lead to prolonged activation of Wnt and thus enhanced proliferation of cancer stem cells (Shih *et al*, 2001; Michor *et al*, 2005; Bian *et al*, 2020). Otherwise debated, in sporadic CRC with wild-type APC gene, persistent activation of the Wnt pathway may occur as a result of hypermethylation of the APC gene promoter or point mutations in the β -catenin structure (Kinzler & Vogelstein, 1996; Morin *et al*, 1997; Esteller *et al*, 2000). In any case, the increase of undifferentiated cells in the colonic crypts may ultimately lead to the development of a polyp, which, as indicated in the adenoma-carcinoma pathway, with the accumulation of successive additional mutations affecting genes such as KRAS and TP53, eventually becomes a CRC

(Kinzler & Vogelstein, 1996; Morin *et al*, 1997; Esteller *et al*, 2000; Li *et al*, 2021). TP53 gene encoding p53 protein, a well-known tumor suppressor gene (Hanahan & Weinberg, 2000). This protein is involved in cell cycle control and apoptosis and is frequently mutated in CRC (Li *et al*, 2021). p53 triggers G1 cell cycle arrest in the presence of DNA damage to allow DNA repair before the cell proceeds to DNA replication and otherwise promotes cell apoptosis. p53 mutation occurs during the transition from adenoma to cancer leading to a significant increase of cells with a high mutation load (Hafner *et al*, 2019; Li *et al*, 2021).

In advanced CRC steps of the adenoma-carcinoma pathway, LOH of the chromosome 18q genetic aberration is described. LOH is the loss of one of the two alleles of a gene, often accompanied by the mutation of the second allele (Sieber *et al*, 2003; Ogino *et al*, 2009; Armaghany *et al*, 2011). Deleted in Colorectal Carcinoma (DCC) gene, encoding for the homonymous transmembrane protein, maps in chromosome 18q (Forcet *et al*, 2001). DCC is a "conditional tumor suppressor gene" that can inhibit cell growth in the absence of its ligand netrin-1, which is released by colorectal cells during their differentiation.

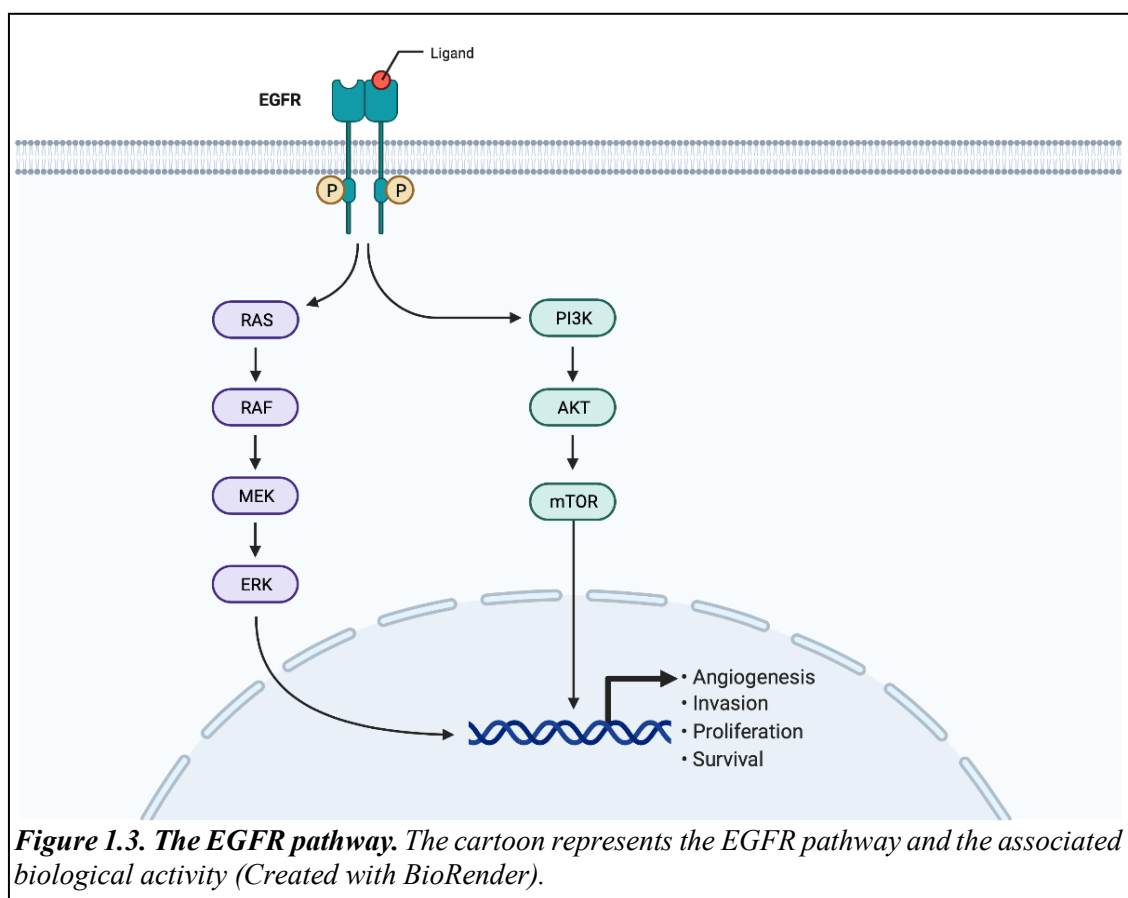


Figure 1.3. The EGFR pathway. The cartoon represents the EGFR pathway and the associated biological activity (Created with BioRender).

Consequently, LOH of the DCC gene results in abnormal cell survival (Forcet *et al*, 2001; Ogino *et al*, 2009). Moreover, also the SMAD4 gene, which inhibits TGF- β signaling, maps in chromosome 18q, and its loss can promote tumor progression (Zhao *et al*, 2018).

Another key pathway that can be affected during CRC carcinogenesis is the endothelial growth factor receptor (EGFR) pathway (Figure 1.3). EGFR, a transmembrane tyrosine kinase receptor, upon binding to its ligand endothelial growth factor (EGF), transduces signals through two intracellular pathways that activate cell proliferation and survival. Ligand binding to the extracellular domain of the receptor promotes receptor dimerization and the consequent auto phosphorylation of intracellular domains (Weitz *et al*, 2005; Hanahan & Weinberg, 2011; Li *et al*, 2021). Downstream signaling cascade involves multiple proteins belonging to RAS/RAF/MAPK and PI3K/AKT pathways. Cellular effects activated by this signaling cascade includes cell proliferation, angiogenesis, cell motility, and metastatization process (Krasinskas, 2011). Because of the possible constitutive activation of this pathway, monoclonal blocking antibodies against the extracellular domain of EGFR have been developed: Cetuximab and Panitumumab, which are used in combination with conventional chemotherapy or as single agents in the treatment of metastatic CRC (Armaghany *et al*, 2011). Not all patients with EGFR overexpression are able to respond to these drugs, as mutations in oncogenes coding for the downstream proteins are in part involved in this resistance. In CRC patients in whom all downstream EGFR effectors are not mutated (KRAS, BRAF PI3K, and PTEN wildtype, quadruple negative), anti-EGFR monoclonal antibodies show the highest response rate (Armaghany *et al*, 2011). Among the RAS oncogenes, which include HRAS, NRAS, and KRAS isoforms, KRAS is the most frequently mutated family member in CRC. Nearly 40% of patients affected by CRC have this mutation, which is associated with poor prognosis (Armaghany *et al*, 2011). KRAS, a member of the MAP kinase (MAPK) pathway downstream of EGFR signaling, promotes cell proliferation and invasion (Watanabe *et al*, 2001). KRAS is also considered a valid molecular biomarker candidate for anti-EGFR therapy, as it is the most commonly mutated factor downstream of the EGFR pathway, and there are several lines of evidence for a better outcome in patients who have a nonmutated wild-type RAS protein (Watanabe *et al*, 2001).

Microsatellite instability (MSI)

Mutations in DNA sequences can be caused by both environmental and spontaneous errors. The latter occur during cell replication and are caused by errors of DNA polymerase in synthesising an identical copy of the template DNA strand, resulting in mutations during DNA replication (Vilar & Gruber, 2010; Armaghany *et al*, 2011). The mismatch repair (MMR) system control and corrects errors missed by DNA polymerase. MMR system is often defective in CRC leading to an increased mutation in these tumors. Because microsatellites contain repetitive sequences, they are the genomic region most likely to mutate as a result of an abnormal MMR system. Microsatellites are indeed small, repetitive DNA sequences scattered throughout the genome, composed of mono-, di-, tri-, and tetranucleotide repeats, hundreds of nucleotide-long. When this phenomenon occurs, it is referred to as microsatellite instability (MSI). (Vilar & Gruber, 2010; Armaghany *et al*, 2011). MSI is the hallmark of Lynch syndrome Hereditary Non-Polyposis Colorectal Cancer (HNPCC) and occurs in more than 95% of these patients. Differently, in most sporadic colorectal cancers, the mechanisms underlying MSI remain elusive and account for only 15-20% of cases (Vilar & Gruber, 2010; Armaghany *et al*, 2011). MSI can be diagnosed by molecular testing if any of the four mismatched repair genes or promoters (MLH1, MSH2, MSH6, and PMS2) have mutations or aberrant methylation. “Microsatellite High” (MSI-H) status is defined by the presence of more than 30% instability in the MMR gene, whereas “Microsatellite Low” (MSI-L) is defined by the presence of between 10% and 29% instability in the MMR gene; “Microsatellite Stable” (MSS) is defined as wild type MMR gene. The higher the instability, the better the prognosis for CRC (Boland *et al*, 1998; Li *et al*, 2021).

CpG Island Methylator Phenotype

Several epigenetic regulatory mechanisms influence DNA expression without changing the nucleotide sequence (Armaghany *et al*, 2011). Aberrant epigenetic regulation by defective methylation of gene promoter regions is common in CRC and has the same significance as DNA mutations in inactivating tumor suppressor genes. In aberrant hypermethylation, a methyl group is covalently attached to the 5' position of

cytosine (C) near guanosine (G) in repetitive CG dinucleotides or CpG islands within the promoter region (Armaghany *et al*, 2011; Li *et al*, 2021). CpG islands are normally unmethylated, allowing the expression of target gene, whereas upon promoter methylation gene transcription is blocked. In this context, silencing of a tumor suppressor gene can be achieved by promoter hypermethylation in both alleles or by a combination of loss of one allele by deletion or mutation and suppression of the other by promoter hypermethylation (Armaghany *et al*, 2011; Li *et al*, 2021).

1.1.3 Signs and symptoms, investigations and diagnosis

CRC exhibit a diverse spectrum of signs and symptoms that are not specific and depend to some extent on the location of the tumor in the colon. Early stages, when cure rates are high, are often asymptomatic, and clinical presentation often does not predict disease. The most common symptoms are abdominal pain, altered stools, anorexia, constipation, diarrhea, fatigue, nausea or vomiting, obstructive symptoms, any visible rectal bleeding, rectal pain, and tenesmus. A change in bowel habits, i.e., one of three symptoms, including diarrhea, constipation, or altered stool, is considered another important variable, as is blood in the stool, which can change the feces color (bright red in 70% of patients, dark in 22%, and darker burgundy or maroon blood in 8%) and can be detected with a fecal occult blood test (Majumdar *et al*, 1999; John *et al*, 2011). Other relevant signs include hemoglobin measurements (anemia is defined when hemoglobin is ≤ 13.4 g/dL in men and ≤ 12.3 g/dL in women), weight loss, fecal occult blood test results, and a palpable mass on physical examination (rectal or abdominal). The median duration of symptoms from onset to diagnosis is 14 weeks, with no association between duration of symptoms and cancer stage (Majumdar *et al*, 1999; John *et al*, 2011). Patients may also present with signs and symptoms of metastatic disease. Approximately 20% of patients with CRC have distant metastases at the time of diagnosis. CRC can spread by lymphatic and hematogenous dissemination, as well as through adjacent and transperitoneal routes. Regional lymph nodes, liver, lungs, and peritoneum are the most common sites of metastasis. Patients may present with signs or symptoms related to any of these organs. The presence of right upper quadrant pain, abdominal distention, early satiety, supraclavicular adenopathy, or periumbilical nodes usually indicates advanced, often

metastatic, disease (Majumdar *et al*, 1999; John *et al*, 2011). CRC diagnostic process includes evaluation of the patient's medical history, physical examination, laboratory and imaging tests, and endoscopy. The first investigation is the physical examination and rectal exploration: 70% of rectal cancers and 30% of CRCs are detected during this examination. The gold standard for diagnosis of CRC is endoscopy (including sigmoidoscopy and colonoscopy) with a sensitivity of 92-97% (Świderska *et al*, 2014). Endoscopy also allows biopsies of lesions and removal of adenomas. Diagnostic imaging tests make an important contribution to the CRC examination: the opaque enema, virtual computed tomography (CT), or colon CT, used for non-stabbing lesions when endoscopy is not recommended. Magnetic resonance imaging (MRI) is considered the gold standard for rectal tumors, because it can provide a fairly accurate assessment of the extent of invasion of the bowel wall (Świderska *et al*, 2014). Ecoendoscopy (EUS) is a valid alternative to MRI that is less expensive and offers the ability to perform targeted biopsies, but it is operator-dependent and not available in every hospital. Ecoendoscopy has a diagnostic accuracy for tumor size of 80-95%, while for lymph node assessment it has a sensitivity and specificity of 55% and 78%, respectively (Świderska *et al*, 2014). Among laboratory tests, the aforementioned fecal occult blood test and tumor markers play an important role. Fecal occult blood test indicates hemoglobin in stool due to bleeding in the gastrointestinal tract. Tumor markers are molecules produced by tumor cells or healthy cells in response to a tumor (Brenner *et al*, 2014; Świderska *et al*, 2014). The markers can be detected in blood, urine, and other body fluids. The carcinoembryonic antigen (CEA), cancer antigen (CA) 19-9, tumor antigen of colorectal carcinoma (tumor-associated glycoprotein, TAG -72), and tissue polypeptide specific antigen (TPS) are used for diagnosis and monitoring of CRC (Brenner *et al*, 2014; Świderska *et al*, 2014). However, these markers have low sensitivity and specificity for CRC diagnosis. CEA is the most commonly screened marker for gastrointestinal tract tumors. It is a glycoprotein produced by cells of the large intestine (Brenner *et al*, 2014; Świderska *et al*, 2014). An elevated serum CEA level may be associated with carcinogenesis (above 5 µg/l is considered "high"). In 50% of patients, it is a marker of tumor recurrence after surgery. Unfortunately, an increase in CEA concentration rarely occurs in early disease stages, but is mostly observed in advanced tumors (Brenner *et al*, 2014; Świderska *et al*, 2014), and an elevated CEA level before surgery may correlate with an unfavorable prognosis

(Brenner *et al*, 2014; Świderska *et al*, 2014). Finally, it is recommended to assess the presence of metastases at the time of diagnosis using CT scan ultrasound examinations of the abdomen and chest, as the most common sites of metastasis are the lungs and liver.

1.1.4 Colorectal cancer staging and histopathology

Histologic variants

World Health Organization (WHO) classifies different variants of CRC, which can be mucinous, signet ring cell, medullary, micropapillary, serrated, cribriform comedo-type, adenosquamous, spindle cell, and undifferentiated (Compton, 2003).

TNM System

The TNM system, as defined by the Union for International Cancer Control (UICC) and American Joint Committee on Cancer (AJCC), is used to determine the stage of a tumor, and accordingly, a TNM for CRC is constantly updated. In this system, the designation "T" indicates the local extent of the untreated primary tumor at the time of diagnosis and initial examination. The designation "N" indicates the status of regional lymph nodes, and "M" indicates distant metastasis at the time of diagnosis (Chen *et al*, 2021) (Figure 1.4). The preceding symbol "p" refers to the pathologic determination of TNM as opposed to the clinical determination (denoted by the preceding "c") (Compton & Greene, 2004) Pathologic classification is based on gross and microscopic examination of the obtained specimen, both primary tumor and biopsy, nodes, and distant lesions. Clinical classification (cTNM) is determined by findings obtained by a variety of techniques, including physical examination, radiologic imaging, endoscopy, biopsy, and surgical exploration (Compton & Greene, 2004).

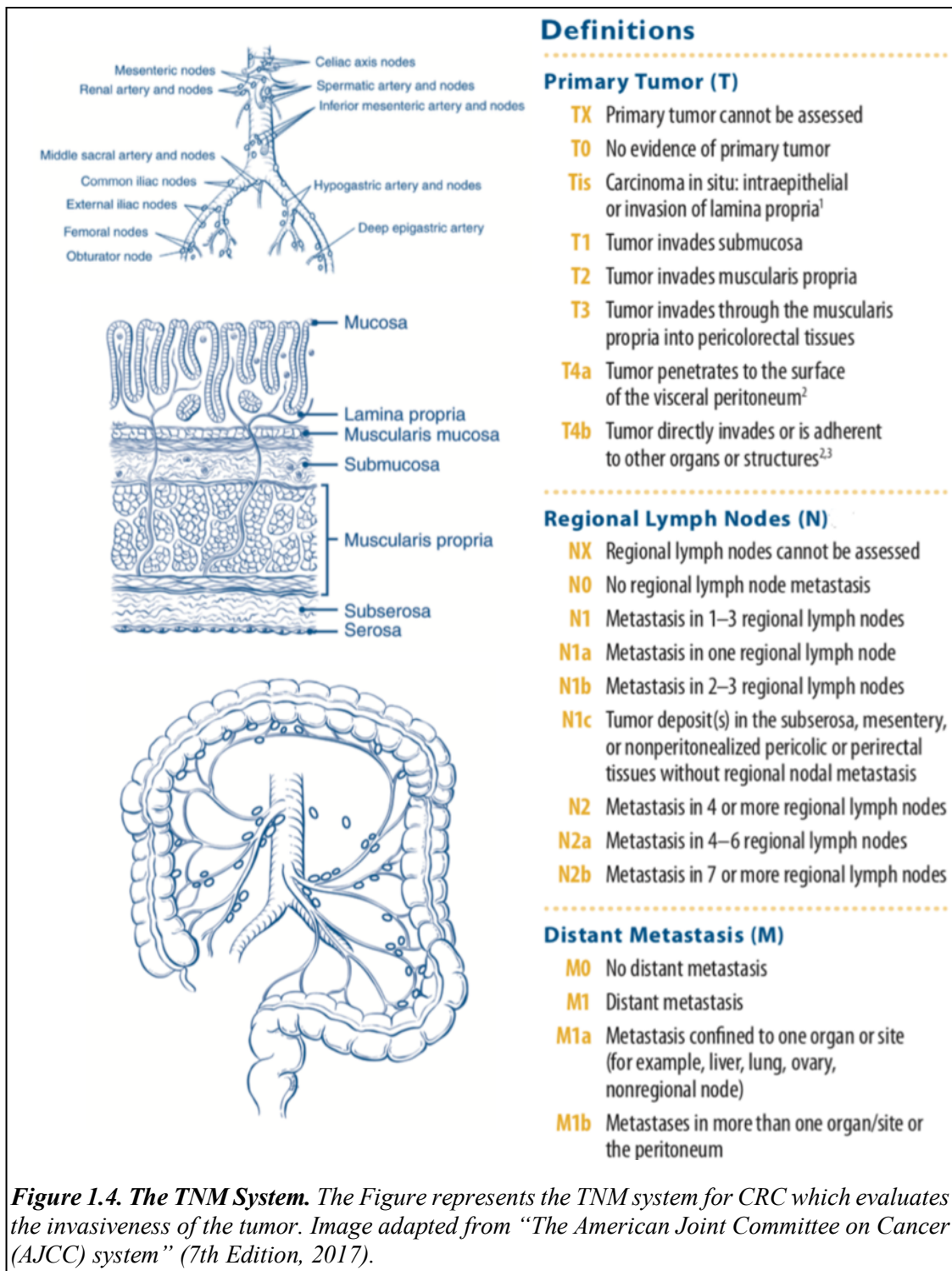


Figure 1.4. The TNM System. The Figure represents the TNM system for CRC which evaluates the invasiveness of the tumor. Image adapted from “The American Joint Committee on Cancer (AJCC) system” (7th Edition, 2017).

CRC metastatization process

The "anatomical-mechanical" hypothesis is usually used to explain metastatic spread. From the colon and proximal parts of the rectum, blood is directed to the liver via the portal vein system, so that the first organ reached by metastases is the liver (Fig. 1.5) (Riihimäki *et al*, 2016). From the liver, the blood reaches the lungs via the heart as the next organ. The distal parts of the rectum can surpass the liver, and the first organ they reach is the lung. Rectal cancers metastasize to thoracic organs more frequently than colon cancers, which metastasize mainly to the liver. In addition, metastases can spread

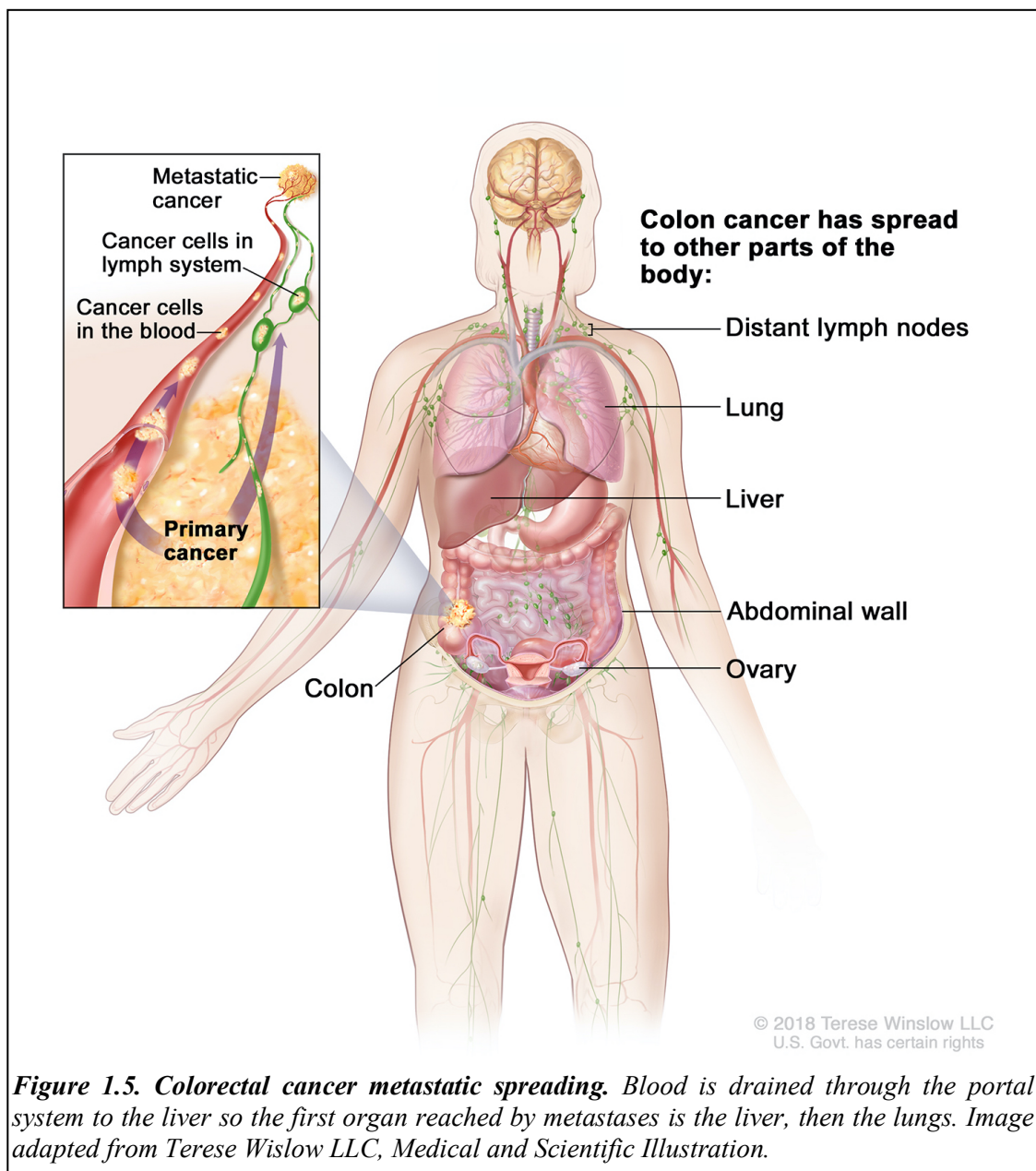


Figure 1.5. Colorectal cancer metastatic spreading. Blood is drained through the portal system to the liver so the first organ reached by metastases is the liver, then the lungs. Image adapted from Terese Wislow LLC, Medical and Scientific Illustration.

to the abdominal cavity through the peritoneal fluid (Riihimäki *et al*, 2016). Lung metastases are more common in patients who also have metastases to the bones or nervous system, while lung metastases together with metastases to the peritoneum and other gastrointestinal sites are rare (Riihimäki *et al*, 2016). Some distinct patterns can be identified: Apparently, CRC spreads to the liver via the portal circulation and from there to the lungs. It may also enter the lungs directly, possibly via lymphatic vessels or directly from the distal rectum (Riihimäki *et al*, 2016). However, there is evidence in several studies that the lung appears to be an important hub for further spread: metastases to the nervous system happened more frequently together with metastases to the respiratory tract than with liver metastases (Riihimäki *et al*, 2016). It is speculated that tumors that metastasize via the "normal" portal vein way are less mobile than more motile cells that may seek out the lungs or central nervous system (Riihimäki *et al*, 2016). CRC may also metastasize to the peritoneal cavity, resulting in non-hematogenous ovarian metastases that are often detected along with peritoneal metastases, particularly in colon cancer (Riihimäki *et al*, 2016). The peritoneum and ovaries are often considered a continuum, and ovarian metastases are much more common in women with colon cancer than rectal cancer, possibly due to anatomic factors (Riihimäki *et al*, 2016).

Staging

The staging system most commonly used for CRC is the American Joint Committee on Cancer (AJCC) system (7th edition, 2017). After determining a patient's TNM scores, this information is combined in a process known as "stage grouping" to assign an overall stage to assess disease severity and the best treatment modality (Table 1.1). According to the stage defined by the AJCC system, the specific 5-year survival rate for colorectal cancer is 93% for stage I, 87% for stage IIa, 63% for stage IIb, 89% for stage IIIa, 69% for stage IIIb, 53% for stage IIIc, and 11% for stage IV [Reports from the American Cancer Society, 2017].

Stage 0:	Tis	N0	M0
Stage I:	T1 - T2	N0	M0
Stage IIa:	T3	N0	M0
Stage IIb:	T4a	N0	M0
Stage IIc:	T4b	N0	M0
Stage IIIa:	T1 - T2	N1 / N1c	M0
	T1	N2a	M0
Stage IIIb:	T3 - T4a	N1 / N1c	M0
	T2 - T3	N2a	M0
	T1 - T2	N2b	M0
Stage IIIc:	T4a	N2a	M0
	T3 - T4a	N2b	M0
	T4b	N1 - N2	M0
Stage IVa:	any T	any N	M1a
Stage IVb:	any T	any N	M1b
Stage IVc:	any T	any N	M1c

Table 1.1. CRC Staging System.

Grading

Another prognostic factor for CRC is the degree of gland formation, commonly referred to as "grading." The prognostic role of grading is well described in the literature. Several findings indicate that the aggressiveness of tumor is reflected histopathologically by the presence of many poorly differentiated cell clusters and the loss of gland formations (Ueno *et al*, 2012). In the histopathological classification of the tumor, grade G1 tumors are defined as well differentiated, G2 tumors as moderately differentiated, G3 tumors as poorly differentiated, and G4 tumors as undifferentiated. Differentiation status is defined by the number of cancer cell clusters in a tumor without gland-like structures. A G1 tumor shows <5 clusters, a G2 tumor 5 to 9, and a G3 tumor >10. According to this classification, the disease-free survival rate is 96%, 85%, and 59% for G1, G2, and G3, respectively (Ueno *et al*, 2012). Poorly differentiated clusters affect survival independently of T and N stages, demonstrating that grading can contribute to an effective stratification of CRC patients (Ueno *et al*, 2012).

Tumoral budding

Tumor budding is defined as the presence of single cells and small clusters of tumor cells at the invasive front of carcinomas (Compton, 2003; Chen *et al*, 2021). The most commonly cited scoring system for tumor budding was developed by Ueno and defines "high-grade budding" as more than 10 buds consisting of fewer than 5 cells in a 25-fold field (Ueno *et al*, 2002). The biology of tumor budding is not fully understood, but the main hypothesis is that at least some types of budding are an example of epithelial-mesenchymal transition, a phenotypic change in cancer cells caused by loss of cell adhesion molecules, cytoskeletal alterations, increased production of extracellular matrix components, resistance to apoptosis, and the ability to degrade the basement membrane, resulting in a greater migratory capacity and invasiveness required to initiate seeding in other organs (Grigore *et al*, 2016). Tumor spread correlates to a poorer prognosis, higher tumor grade, the presence of lymphatic and perineural invasion, and lymph node metastases. In several studies, budding has been associated with local tumor recurrence

and distant metastases, as well as significantly worse overall and disease-free survival (Ueno *et al*, 2002).

Chron like Lymphoid Reaction

The lymphocytic reaction observed in CRC is indicative of an active immune response to the tumor. A significant association exists between increased lymphocytic reaction and favorable prognostic outcome (Ueno *et al*, 2013). The histologic feature of nodular lymphoid aggregates (LAs) at the periphery of CRC reflects the activation of the lymphoid system against the tumor (Ueno *et al*, 2013). Graham and Appelman refer to peritumoral LAs as a Crohn's-like response (CLR) because they resemble part of the inflammatory component of Crohn's disease (Ueno *et al*, 2013).

Microsatellite instability

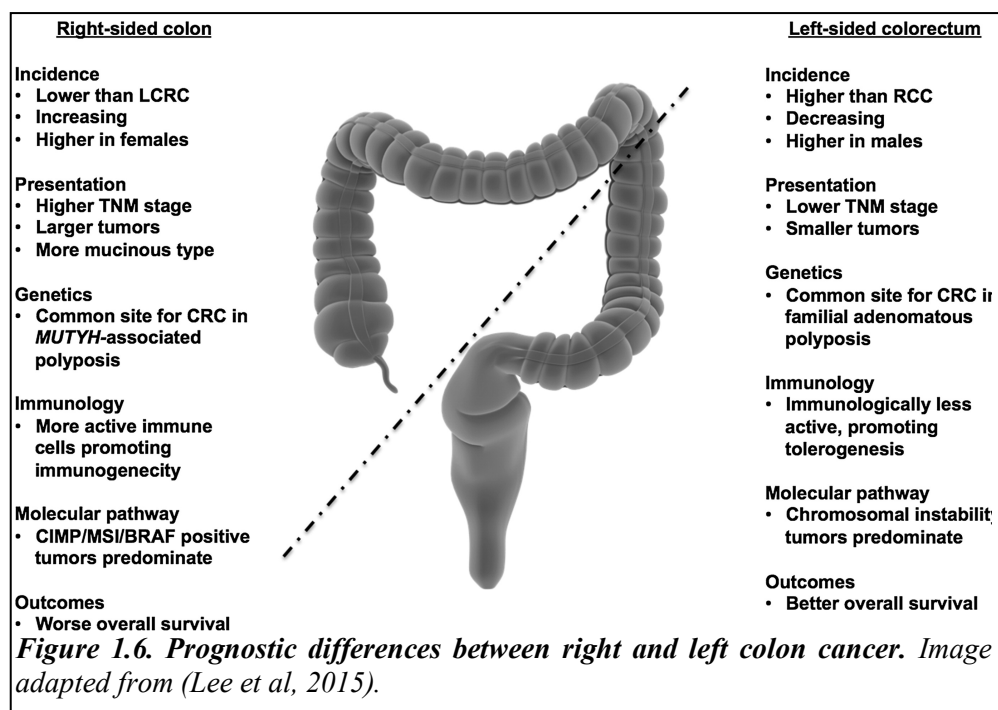
The pathogenesis of microsatellite instability (MSI) has been discussed previously. High-grade microsatellite instability (MSI-H) occurs in approximately 15% of all colorectal carcinomas (Li *et al*, 2021). Colorectal carcinomas of the MSI-H phenotype have several phenotypic features that distinguish them from their microsatellite-stable counterparts. MSI-H colorectal carcinomas are typically located in the proximal colon, where they can grow into large tumors. They exhibit several histopathologic features that have been grouped under the term "MSI-H histology," including a high density of tumor-infiltrating lymphocytes that are often accompanied by lymphoid follicles in the tumor environment (Crohn's-like reaction) (Geiersbach & Samowitz, 2011; Li *et al*, 2021). The growth pattern of MSI-H CRC is often an expansive type, without tumor budding and disseminated growth and histopathological appearance of MSI-H cancers indicates a marked local host immune response. They have a low incidence of distant metastases and a higher 5-year survival rate compared with patients at the same stage with microsatellite-stable cancer (Geiersbach & Samowitz, 2011; Li *et al*, 2021).

Molecular differences between right colon cancer and left colon cancer

Evidence exists that right-sided colon cancer (RCC) is distinct from left-sided colon cancer (LCC). RCC and LCC have different embryological origins as well as anatomical, histological, genetic, and immunological features (Lee *et al*, 2015) The right-sided colon (cecum, ascending colon, and proximal two-thirds of the transverse colon) arises from the midgut during embryonic development, though the left-sided colon (distal third of the transverse colon, descending colon, and sigmoid colon) arises from the hindgut (Lee *et al*, 2015). RCC involves usually bulky, exophytic, polypoid lesions that grow into the colon lumen. In contrast, LCC are infiltrating, constricting lesions that encircle the colonic lumen and cause obstruction (Saidi *et al*, 2008; Lim *et al*, 2017). Patients with RCC have been shown to be older and more often female, and the disease is associated with advanced tumor stages, increased tumor size, often poorly differentiated tumors, and specific molecular biology patterns described below (Lim *et al*, 2017).

As mentioned previously, CRC is characterized by genetic alterations that include mutations in oncogenes and/or tumor suppressor genes and distinct gene profiles define the proximal and distal colon even before cancer development (Missiaglia *et al*, 2014). In particular, higher transcriptional activity has been observed in the distal colon, which may explain some of the features of LCC (Missiaglia *et al*, 2014)(Lee *et al*, 2015). In the past, it has been described that almost all distal colon cancers have allelic losses in chromosomal regions 17p, 18q, and 5q, which are associated with genetic alterations in tumor suppressor genes. More recently, KRAS and TP53 mutations have been shown to be characteristic of LCC but not RCC, which are predominantly MSI-positive tumors. TP53 mutations in RCC and LCC have been pooled, with a higher proportion of TP53-positive tumors found in the distal colorectum compared with the proximal colon (Missiaglia *et al*, 2014; Lee *et al*, 2015). Mucosal immunology is also different between the compartments of the colorectum as intraepithelial T cells have been shown to be higher in the proximal colon than in the distal colorectum in healthy adults. If this difference reflects the mucosal immunology observed in CRC, proximal colon tumors would be subject to increased immunologic activity compared with LCC, suggesting immunologic differences that may account for the differential pathogenesis and outcome of RCC and LCC (Kirby *et al*, 2003). Moreover, the mutation frequencies of CpG island

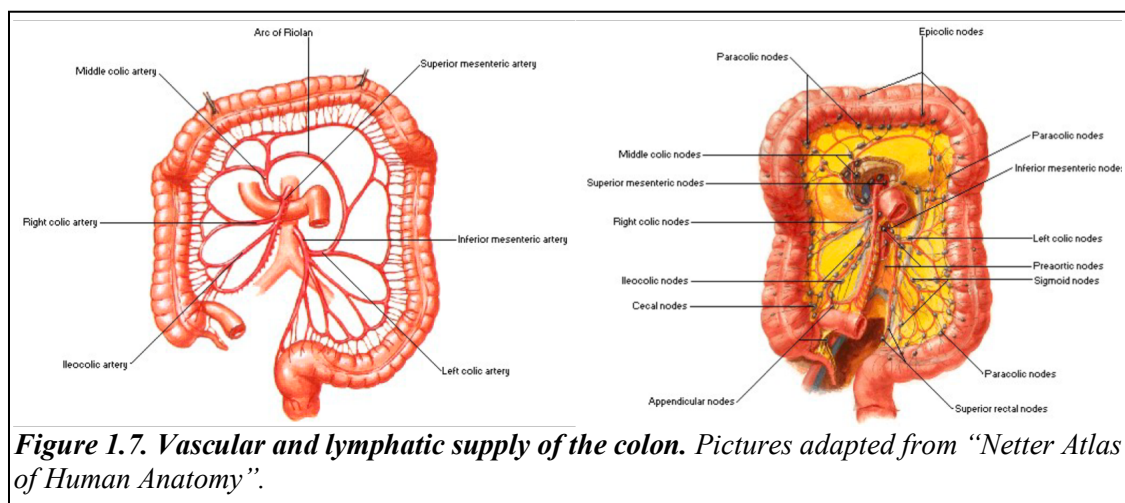
methylation phenotype (CIMP), MSI, and BRAF gradually increase from the rectum to the ascending colon without any immediate change at the splenic flexure (Lee *et al*, 2015; Missiaglia *et al*, 2014). Despite all these findings, several studies have shown that the overall picture is significantly worse in RCC compared with LCC (Lee *et al*, 2015), highlighting the need for a more precise characterization of the differences between RCC and LCC.



1.1.5 Guidelines for colorectal cancer treatment

The gold standard treatment for CRC is resective surgery. The goal of surgical treatment for colon adenocarcinoma is to remove the primary carcinoma with adequate margins, perform regional lymphadenectomy, and restore continuity of the gastrointestinal tract (GI) by anastomosis. The extent of resection depends on the location of the cancer, its blood supply (Figure 1.7), the draining lymphatic system (Figure 1.8), and the presence or absence of direct spread to adjacent organs. Wide resection of the lymphatics that parallel the arterial supply is also performed to attempt to render the abdomen free of lymphatic metastases. Right hemicolectomy is the procedure of choice for lesions involving the cecum, ascending colon, and hepatic flexure, whereas extended right hemicolectomy is performed for most lesions of the transverse colon. A left hemicolectomy (resection from the splenic flexure to the rectosigmoid junction) is the procedure of choice for tumors of the descending colon, and finally, a sigmoidectomy is appropriate for tumors of the sigmoid colon. Abdominal colectomy, or total colectomy, consists of removal of the entire colon from the ileum to the rectum, with continuity restored by ileorectal anastomosis. It is usually performed for multifocal tumors.

After surgery for the primary tumor, it is important to stratify patients according to their pathologic status to determine who might benefit from adjuvant chemotherapy. Guidelines for nonmetastatic CRC are published by the National Comprehensive Cancer Network (NCCN) (Figure 1.8). The three chemotherapeutic agents commonly used to treat patients with early-stage colon cancer are 5-fluorouracil (5-FU), capecitabine (Xeloda), and oxaliplatin (Eloxatin) (Benson *et al*, 2004; Wu, 2018). 5-FU is a nucleotide



analog that can inhibit thymidylate synthase (TS), an enzyme important for the synthesis of pyrimidine nucleotides. Leucovorin (folinic acid) is co-administered with 5-FU to enhance the clinical effect. Administration of capecitabine, a prodrug of 5-FU, has a similar effect. Both 5-FU and capecitabine showed the same efficacy in adjuvant and metastatic treatment (Benson *et al*, 2004; Wu, 2018). Oxaliplatin, differently, is a platinum-based drug that acts as an alkylating agent and directly inhibits DNA synthesis.

Adjuvant therapy is given over a 6-month period, either as single therapy with 5-FU or capecitabine or as a dual combination of 5-FU/oxaliplatin or capecitabine/oxaliplatin (Benson *et al*, 2004; Wu, 2018).

PATHOLOGIC STAGE	ADJUVANT TREATMENT
Tis; T1, N0, M0	Observation
T2, N0, M0	Observation
T3, N0, M0 (MSI-H or dMMR)	Observation
T3, N0, M0 (MSI-L or MSS and no high-risk features)	Clinical trial or Observation or Consider capecitabine or 5-FU/leucovorin
T3, N0, M0 at high risk for systemic recurrence or T4, N0, M0	Capecitabine or 5-FU/leucovorin or FOLFOX or CAPEOX or FLOX or Clinical trial or Observation
T any, N1-2, M0	FOLFOX or CAPEOX (both category 1 and preferred) Other options include: FLOX (category 1) or Capecitabine or 5-FU/leucovorin

Figure 1.8. Guidelines for treatment of colorectal cancer by stage.
NCCN, 2017.

The only group of patients not receiving any adjuvant treatment are stage I patients (Dunlop *et al*, 2013). For stage II patients, it is important to determine whether they should receive adjuvant chemotherapy based largely on cancer recurrence and on the extent of benefits patients receive from treatment (Benson *et al*, 2004; Wu, 2018) These patients generally have a good prognosis, with a 5-year overall survival rate of 80% and potential adjuvant chemotherapy may increase the 5-year overall survival rate by no more than 5%. Accordingly, several randomized trials compared observation versus 5-FU therapy and reported a small absolute improvement in survival of 3.6% for patients who received chemotherapy (André *et al*, 2009; Sargent *et al*, 2010). Stage II patients with MSI-high tumors have a better prognosis than patients with MSS tumors and, indeed do

not benefit from adjuvant 5-FU chemotherapy. In stage III CRC, the risk of recurrence after surgery is 50-60%, and adjuvant chemotherapy with 5-FU/oxaliplatin can reduce the risk of death by 20% (André *et al*, 2009; Sargent *et al*, 2010)

1.1.6 Post-operative recurrence in colorectal cancer

Clinically, recurrence after curative surgery remains a major clinical concern for patients with CRC. Recurrence is distinguished into early recurrence, within the first two years after curative surgery, and late recurrence, two years or more after curative surgery (Aghili *et al*, 2010).

In order to improve survival rates of patients with CRC following curative resection and to detect and treat metastatic disease early, it is crucial to identify prognostic factors for recurrence (Aghili *et al*, 2010). A number of factors have been identified as statistically significant markers of CRC recurrence, including tumor stage, depth of invasion, degree of vascular invasion and serum levels of CEA and CA 19-9. The use of these markers as predictors of recurrence interval may allow the identification of patients at high risk of recurrence (Aghili *et al*, 2010). In particular, high serum levels of CEA and CA 19-9 measured before surgery and at follow-up after curative resection are CRC prognostic factors. Elevated CEA is a reliable marker for liver metastases, while CA 19-9 appears to be associated with peritoneal recurrence; however, these antigens have not yet been studied in relation to recurrence interval (Aghili *et al*, 2010). Wall invasion depth by the primary tumor is another important prognostic factor, in addition to serum markers (Aghili *et al*, 2010). Several studies have reported that the involvement of adjacent organs and the depth of tumor invasion are significant prognostic factors for postoperative recurrence, but others dispute this hypothesis and suggest that venous invasion and lymph node metastasis are more important in predicting recurrence interval (Aghili *et al*, 2010). A recently introduced prognostic factor for CRC recurrence is circulating tumor cells (CTC), defined as circulating cells in the bloodstream derived from the primary tumor (Steinert *et al*, 2012). They can be collected from the central venous blood compartment, peripheral blood, tumor draining veins, portal vein system, or arterial blood system (Figure 1.9). It is estimated that about 10^6 cells per gram of primary tumor enter the systemic circulation every day (Steinert *et al*, 2012; Bork *et al*, 2014). Nevertheless, most of these cells are unable to survive in the circulation or form distant metastases because they ultimately undergo apoptosis or die due to shear forces in the circulation. Data from animal models show that less than 0.1% of CTCs in the bloodstream eventually form distant metastases (Steinert *et al*, 2012; Bork *et al*, 2014). On the contrary, an important

prerequisite for metastases formation is the spread of CTC from epithelial malignant cells during Epithelial-Mesenchymal Transition (EMT) (Thiery & Sleeman, 2006).

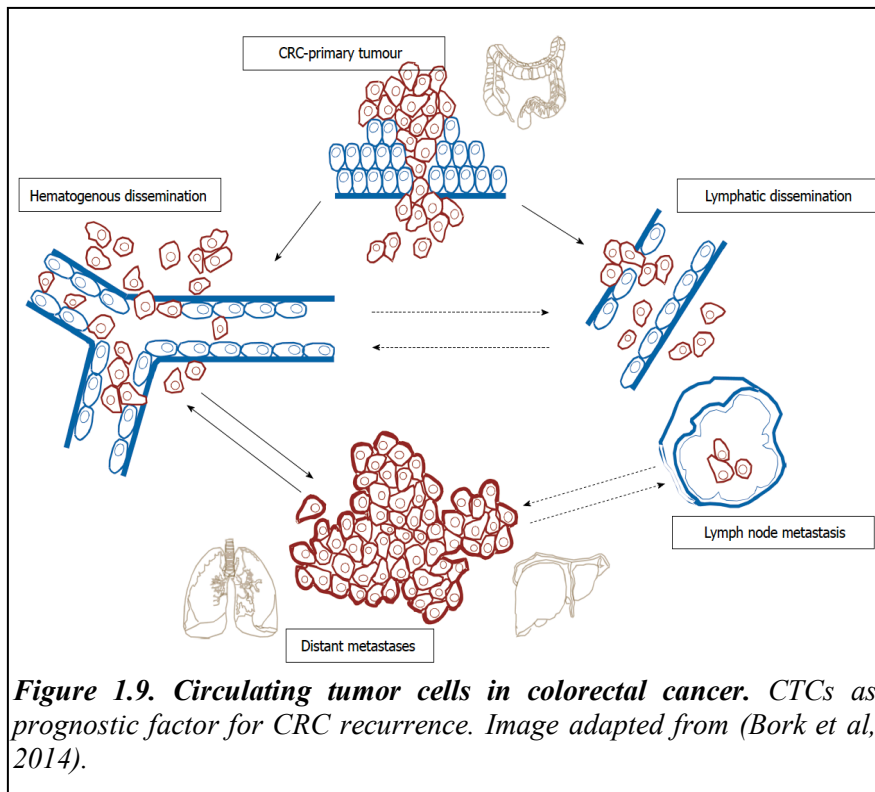


Figure 1.9. Circulating tumor cells in colorectal cancer. CTCs as prognostic factor for CRC recurrence. Image adapted from (Bork et al, 2014).

Adjuvant chemotherapy treatment is considered another prognostic factor for recurrence, although it is unclear whether adjuvant therapy and recurrence interval are related. Presumably, especially in high-risk patients (stage III), the absence of adjuvant chemotherapy could be a prognostic factor for early recurrence (Aghili *et al*, 2010). Evidence suggest also that spreading to recurrent organs can depend on the timing of recurrence. Based on a retrospective study of postoperative patients with CRC, the liver was the most common site of early recurrence and local recurrences were more common among rectal cancer patients than among colon cancer patients. In contrast, lung metastases were more common in late recurrences, and other sites of late recurrence include the bones and peritoneum (Aghili *et al*, 2010) In addition, 5-year overall survival and post-relapse survival are significantly lower in patients with early relapse than in patients with late relapse from CRC (Aghili *et al*, 2010).

1.1.7 Colorectal cancer with synchronous liver metastases

At CRC diagnosis, 20-25% of patients present with stage IV disease, with synchronous liver metastases (CRLM) present in 15-25% of cases. Synchronous metastases are defined as liver metastases discovered at the same time or before the diagnosis of the primary CRC tumor. They usually have a less favorable cancer biology and survival expectancy than metachronous metastases (liver metastases discovered in the subsequent 5 years after the diagnosis of the primary tumor CRC). In order to determine the best therapeutic strategy for synchronous liver metastases, operability and resectability are evaluated: resectable metastases and non-resectable metastases are distinguished (Adam *et al*, 2015). To assess the oncologic and clinical prognosis of CRLM patients, clinical risk scores (CRS) must be evaluated: Two CRSs are widely used, the Fong score and the Nordlinger score. The Fong and Nordlinger scores are calculated before liver resection (Schreckenbach *et al*, 2015). Both scores, however, are predictive for patients who have not received neoadjuvant chemotherapy while they are not predictive for patients who have received either neoadjuvant chemotherapy or biologic-targeted therapy (Schreckenbach *et al*, 2015).

1.1.8 Synchronous liver metastases surgery and chemotherapy treatment

Surgery is the most effective treatment for CRLM with a 5-year overall survival rate of 40% (Ratti *et al*, 2016). Approximately 15-25% of patients with CRC have synchronous liver metastases (SCLM), but only 10-20% of all patients with stage IV disease are eligible for potentially curative resection, which negatively impacts survival.

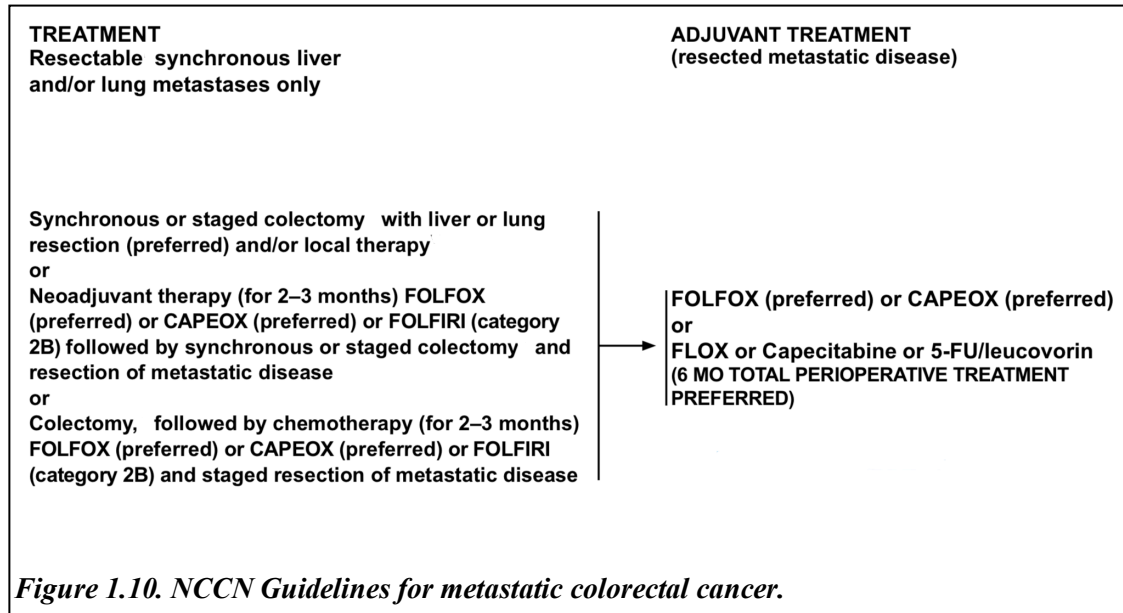
Radical resection of the primary tumor and liver metastases is the only potentially curative treatment for these patients, either as initial treatment or following neoadjuvant chemotherapy (Fiorentini *et al*, 2017; Adam *et al*, 2015). Even though the optimal management strategy for patients with SCLM is still debated, safety and efficacy of combined resection of CRC tumors and liver metastases have been demonstrated. (Fiorentini *et al*, 2017; Adam *et al*, 2015), also considering the widespread use of minimally invasive procedures, both for primary CRC and liver metastases deriving from

technological advances and the acquisition of appropriate surgical expertise (Fiorentini *et al*, 2017; Adam *et al*, 2015).

In addition to neoadjuvant therapy, new surgical strategies are increasingly used to improve resectability in patients with unresectable SCLM (Tournigand *et al*, 2003; Koopman *et al*, 2007; Cremolini *et al*, 2015). Portal vein embolization results in atrophy of the liver to be resected and hypertrophy of the remaining liver (i.e. increased FLR). Similarly, two-stage hepatectomies involve delayed re-hepatectomy after hypertrophy of the remaining liver, and can be used for large bilateral lesions in which a single-stage resection (resection of colon and liver metastases in the same procedure) of all affected segments would lead to liver failure (Fiorentini *et al*, 2017).

The multimodal approach to the treatment of SCLM also requires chemotherapy, which plays an extremely important role in the treatment of SCLM. It can be used to reduce tumor burden and allow secondary surgical resection, or neoadjuvantly in patients suitable for surgery (Tournigand *et al*, 2003; Koopman *et al*, 2007; Cremolini *et al*, 2015). Stage IV patients are generally treated with chemotherapeutic agents such as 5-FU, capecitabine (Xeloda), oxaliplatin (Eloxatin), and irinotecan, the last not combined with capecitabine because of overlapping toxicity, in the first- and second-line treatment of metastases (Tournigand *et al*, 2003; Koopman *et al*, 2007; Cremolini *et al*, 2015; Wu, 2018). Chemotherapy in metastatic patients usually consists of a combination of infusional 5-FU/irinotecan (FOLFIRI) or 5-FU/oxaliplatin (FOLFOX), that shown to be equally effective, with the addition of a biologic agent (Tournigand *et al*, 2003; Koopman *et al*, 2007; Cremolini *et al*, 2015; Wu, 2018). The choice of chemotherapy strategy is often based initially on the toxicities of therapy and the patient's existing comorbidities and preferences.

Among biological agents, bevacizumab, the monoclonal antibody against vascular endothelial growth factor (VEGF) that binds and neutralizes VEGF-A, has become a central player in the treatment of metastatic colorectal cancer (Zinser-Sierra *et al*, 2011).



Bevacizumab in addition to 5-FU/leucovorin, irinotecan plus 5-FU/leucovorin, or irinotecan plus infusional 5-FU/leucovorin significantly improves overall survival in patients with previously untreated CRC metastases (Zinser-Sierra *et al*, 2011). The addition of bevacizumab to oxaliplatin plus FOLFOX was also associated with increased overall survival in patients with metastatic colorectal cancer who had previously progressed on an unbevacizumab-containing regimen (Zinser-Sierra *et al*, 2011). Monoclonal antibodies such as cetuximab (Erbix) and panitumumab (Vectibix) bind and inhibit EGFR activity. Currently, both of these drugs are approved for the treatment of metastatic CRC. They are administered intravenously as either a combination with chemotherapy or as a single agent. The NCCN guidelines for CRC with resectable liver metastases are summarized in Fig. 1.10.

The role of percutaneous ablation in the treatment of CRC liver metastases oligometastatic disease (typically one to five clinically or radiographically detectable metastases) is well recognized in patients who are not candidates for surgery (Venkat *et al*, 2018). The NCCN guidelines recommend ablation alone or ablation in combination with resection when feasible to treat all disease foci (Venkat *et al*, 2018). The most common ablative technique for treating CRC liver metastases is radiofrequency ablation (RFA). However, the major limitation of this technique is the proximity to vessels larger

than 3 mm (Venkat *et al*, 2018). Median survival after RFA for colorectal liver metastases ranges from 24 to 45.3 months, with a 5-year overall survival rate of 18-33%. In contrast, the median survival after surgical resection is 41-80 months with a 5-year overall survival rate of 48-71% (Venkat *et al*, 2018).

1.2 Liver metastatization process

In order to metastasize, cancer cells must have the ability to migrate through body compartments and enter the bloodstream. Subsequently, the tumor cells must exit the vessels to invade the tissues. This process takes place mainly at the level of capillaries, where cancer cells begin to interact through various proteins with the organ they have entered thanks to the bloodstream. As previously sentenced, the organ where CRC cells most frequently metastasize is the liver. Metastasis occurs when tumor cells detach from the primary tumor and enter the portal circulation (Kow, 2019). In particular, the liver drains blood from the entire intestine through the portal system, and as the first blood-filtering organ, the cells that have found a way into the portal circulation can easily reach it (Fig.1.11). CTCs are thought to settle in small branches of the portal vein or at the beginning of the hepatic sinusoids, mainly because of size constraints. It is also believed that these microanatomical properties prevent the spread of tumor cells from the periportal to the centrilobular area, and to the general circulation (Vidal-Vanaclocha, 2008; Catarinella *et al*, 2016). This evidence is consistent with studies showing that most CRC-derived CTCs are found in the portal vein in CRC patients undergoing surgery (Denève *et al*, 2013). In addition, procedures such as surgical removal of colorectal cancer and liver surgery itself may influence various aspects of the process of liver metastasis. These include increased tumor cell motility and loss of CRC cells during surgery, as well as increased adhesion of CRC cells to activated liver endothelium. Similarly, transient immunosuppression with decreased leukocyte antitumor activity may awaken existing dormant intrahepatic micrometastases, that may spread secondarily in the liver parenchyma before a clinically detectable tumor emerges (Shakhar & Ben-Eliyahu, 2003; Park *et al*, 2018). Consequently, adjuvant immunotherapies that can target the early stages of CRC colonization of the liver represent a unique treatment window chance to limit the growth of occult liver metastases (i.e., when the size is less than the current radiological resolution capability) (Tran *et al*, 2022). Interferon based therapies are among those currently used for other cancer types (Snell *et al*, 2017; Borden, 2019).

During tumor growth, many of the cancer cells show altered mobility due to phenotypic and morphological changes, such as epithelial-mesenchymal transition (EMT), collective-amoeboid transition (CAT), and the mesenchymal-amoeboid transition

(MAT) (Zijl *et al*, 2011). In particular, epithelial-mesenchymal transition is a highly conserved process that occurs during embryogenesis, chronic inflammation, and fibrosis and is recognized as one of the most important events during cancer progression and metastasis. To form metastases, extravasated tumor cells must be able to survive in the unknown microenvironment they find in the parenchyma of tissues distant from the primary tumor. One of the theories of cancer cell survival is based on the presence of a "pre-metastatic niche", that can solve the problem of a microenvironment incompatible for cancer cell growth (Kelly *et al*, 2005; Hanahan & Weinberg, 2011; Strilic & Offermanns, 2017; Peinado

et al, 2017; Gui *et al*, 2020). According to this model, it is the primary tumor itself that releases the signals necessary for niche formation, thus favoring the establishment of an environment suitable for metastatic growth (Kaplan *et al*, 2005). Recently, there has been an increased focus on the microenvironment of hepatic metastases, as the liver is the main site of metastasis of gastrointestinal tract tumors (Milette *et al*, 2017). Tumor seeding into the liver microenvironment and subsequent growth involves cancer cells, immune cells, and liver resident hepatocytes and non-parenchymal cells. It has been proposed that when the primary tumor secretes factors that promote metastatic growth, non-parenchymal cells are recalled to the premetastatic niche, including Kupffer cells, hepatic stellate cells, suppressor cells of myeloid origin (MDSC), and neutrophils.

Consequently, strategies that harness the protumoral immune response to target both cells and molecules within liver metastases have emerged as valid approaches that deliver highly effective and long-lasting therapeutic outcomes (Milette *et al*, 2017). Finally, metastatic tumors that grow into the liver often secrete neoangiogenic factors that induce neovascularization from hepatic artery blood, and adjuvant cell-based strategies targeting immune cells involved in the tumor vascularization program showed important effects against CRC liver metastases (Catarinella *et al*, 2016).

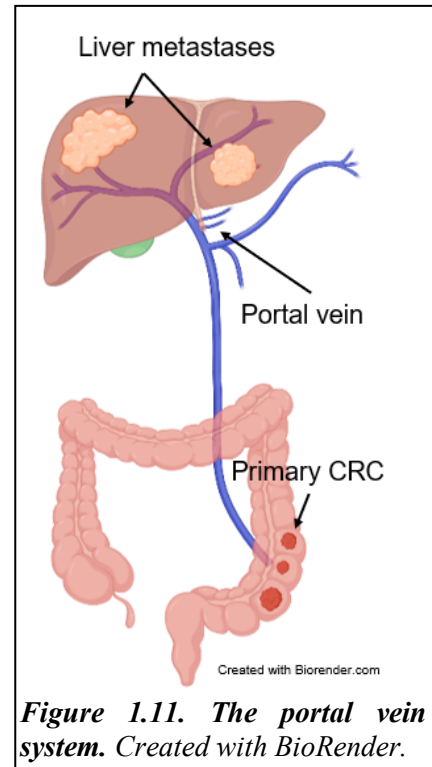


Figure 1.11. The portal vein system. Created with BioRender.

1.3 Adoptive cell therapy (ACT) in cancer treatment

Cancer immunotherapy is a new and leading-edge therapy for the treatment of oncological patients. In particular, adoptive cell therapy (ACT) consists of intravenous transfer into cancer patients of tumor-resident or circulating immune cells modified to mediate antitumor function (Perica *et al*, 2015; Rohaan *et al*, 2019; Kirtane *et al*, 2021).

CD8⁺ T cells are among the primary cells of the immune system responsible for tumor immune surveillance and are able to recognize antigens presented by tumor cells and growing tumors (Jiang *et al*, 2019). The presence of CD8⁺ T cells in tumor lesions is important to block tumor growth and completely eliminate the tumor, and for this reason, (Duong *et al*, 2015). In particular, CD8⁺ T lymphocytes are activated when the TCR recognizes their specific antigen, and subsequently they begin to proliferate and differentiate into cytotoxic T lymphocytes (CTLs) to eliminate tumor cells after CTL tumor recognition. These lymphocytes, called tumor-infiltrating lymphocytes (TILs), are often found with other leukocytes in the tumor microenvironment, and increased infiltration of TILs is usually associated with a better prognosis (Jiang *et al*, 2019). However, several resistance mechanisms occur in the complex interaction between tumor-specific CD8⁺ T lymphocytes and cancer cells, often leading to a T cells dysfunctional phenotype (Thommen & Schumacher, 2018; Xia *et al*, 2019; Zhang *et al*, 2020). In the clinic, specific CD8⁺ T lymphocytes are isolated from the patient's blood, lymph nodes, or tumor to perform ACT, and then expanded *in vitro* and re-injected into the patient (Jiang Xiaotao, et al., 2019).

The use of TILs has shown surprising results in the treatment of melanoma tumor, whereas it is difficult to use them in other tumor types, especially solid tumors, due to leukocyte isolation difficulties, target antigen heterogeneity and antigen escape, and, more importantly, the immunosuppressive mechanisms that are often present (Kirtane *et al*, 2021; Duong *et al*, 2015). Other T cell targeting strategies rely on modifying T cells isolated from patient peripheral blood mononuclear cells (PBMCs). Genetic engineering strategies are used to express modified TCRs in these cells that recognize a specific tumor antigen (TCR-T), or to express a chimeric antigen receptor (CAR-T) that combines binding to a specific antigen with T cell activation functions (Rohaan *et al*, 2019). The advantages of this strategy are based on the different antigen repertoire that can be used

and the broader alternatives in the choice of receptor-antigen pair. However, the TCR of interest must be specific for tumor antigens only, to avoid a possible graft-versus-host reaction, and be restricted to at least one HLA allele corresponding to that of the patient to be treated (Jiang *et al*, 2019). Furthermore, the hurdles in the treatment of solid tumors are essentially the same as in the use of TILs (Kirtane *et al*, 2021). Growing tumors develop various resistance mechanisms to evade specific immune responses. The discovery of upregulation of immune checkpoint molecules in tumors changed the way some cancers were clinically approached by introducing treatment with monoclonal antibodies against inhibitory molecules such as, programmed death 1 (PD-1)/programmed death-ligand 1 (PD-L1) or Cytotoxic T-Lymphocyte Antigen 4 (CTLA-4) (Kalbasi & Ribas, 2020), but these strategies show fluctuating results depending on the patient and tumor type, mainly caused by tumor resistance to immune checkpoint blockade. It has also been reported that CRC tumors upregulate TGF- β pathway molecules to block T cell infiltration (Tauriello *et al*, 2018), and that IFNAR1 downregulation on tumor-specific T cells in primary CRC leads to the formation of an immune-privileged niche within the tumor (Katlinski *et al*, 2017). Accordingly, recent evidence indicates that the immunosuppressive tumor microenvironment promotes IFNAR1 downregulation on tumor-specific T cells through adenosine and regulatory T cell activity (Zhang *et al*, 2022). It is thus clear that new effective therapeutic approaches are needed both as mono or combination therapy to curb patients' CRC metastases.

1.4 Interferons

Interferons (IFNs) are a family of secreted α -helical cytokines produced in response to specific intracellular and extracellular stimulation. IFNs act in a paracrine or autocrine manner and stimulate intra- and inter-cellular networks to regulate innate and acquired immunity, resistance to viral infections, and survival or death of cells (González-Navajas *et al*, 2012; Snell *et al*, 2017). Upon binding to high-affinity cell surface receptors, IFNs trigger a signaling cascade that leads to the transcription of interferon-stimulated genes (ISGs). IFNs are divided into three major subgroups based on their ability to bind to common receptor types. Type I IFNs all bind to a heterodimeric receptor complex composed of the IFN- α R1 and IFN- α R2 subunits, and in humans include IFN α , IFN β , IFN ω , and IFN τ . IFN γ is the only type II IFN and binds to its own type II cell receptor (IFNGR1) (González-Navajas *et al*, 2012; Snell *et al*, 2017), whereas III interferons (IFN- λ s) bind to a heterodimeric receptor consisting of two subunits: IFNLR1 and IL -10R2 (Kotenko *et al*, 2003; Lin *et al*, 2016). Almost all cell types produce type I IFNs. The cells that release IFN α and IFN β most frequently are leukocytes and fibroblasts, respectively, generally upon contact with viruses, double-stranded RNA, polypeptides, and cytokines (González-Navajas *et al*, 2012; Snell *et al*, 2017). Type II IFN γ is produced by T and natural killer (NK) cells after a series of immunological stimuli, including T-cell-specific antigens, staphylococcal enterotoxin A, and the combination of phytohemagglutinin and phorbol esters. Unlike IFN α and - β , it is not released directly after viral infection. Type III IFNs are produced by mucosal epithelial cells and bind to the IFN- λ receptor, mainly expressed by epithelial cells and plasmacytoid dendritic cells (Kotenko *et al*, 2003; Cheon *et al*, 2014; Lin *et al*, 2016). IFNs have a broad spectrum of activity and are involved in complex interactions (González-Navajas *et al*, 2012; Snell *et al*, 2017). In particular, they act in antiviral response, cellular metabolism and differentiation, and orchestrate antitumor activity. IFNs antitumor effect is mostly due to a combination of direct antiproliferative and indirect immune-mediated effects (González-Navajas *et al*, 2012; Snell *et al*, 2017).

1.4.1 Type I interferons signaling and activity

Type I IFNs signal through a dimeric receptor (IFNAR $\alpha\beta$) comprising of the IFNAR1 and IFNAR2 chains, primarily through Janus kinase 1 (Jak1) and tyrosine kinase 2 (Tyk2), leading to phosphorylation of signal transducers and activators of transcription Stat1 and Stat2 (Fig. 1.12) (Zitvogel *et al*, 2015). After phosphorylation, the Stat1 and Stat2 complex translocates to the nucleus. There, STAT1-STAT2 heterodimers bind interferon (IFN)-regulating factor 9 (IRF9), resulting in the heterotrimeric transcription complex known as IFN-stimulated gene factor 3 (ISGF3). After binding to specific DNA response elements, ISGF3 activates transcription of ISGs (IFN-stimulated genes) (Fig. 1.11). The proteins encoded by ISGs primarily serve to block pathogens by various mechanisms, including inhibition of viral transcription, translation, and replication, degradation of viral nucleic acids, and alteration of cellular lipid metabolism (Ivashkiv & Donlin, 2014). Moreover, the activity of type I IFNs supports CTLs through several mechanisms, including promoting cross-priming by stimulating dendritic cells (DCs), enhancing the immune effector functions of CTLs by increasing the expression of perforin 1 and granzyme B, and promoting the survival of memory CTLs. In addition, type I IFNs can prevent the elimination of antigen-activated CTLs by NK cells and stimulate the release of pro-inflammatory cytokines (such as interleukin-1 β (IL -1 β) and IL -18) by macrophages. Type I IFNs, in turn, can inactivate the suppressive function of regulatory T cells (Treg) (Trinchieri, 2010; Zitvogel *et al*, 2015). Importantly, Type I IFNs have been shown to be able to provide a "third signal" for CD8⁺ T cells to stimulate clonal expansion and differentiation (Curtsinger *et al*, 2005), and that inadequate availability of this signal limits the CTL response to solid tumors (Curtsinger *et al*, 2007).

In this context, Type I IFNs are known to have antineoplastic effects in various malignancies. Experimental data strongly suggest the existence of a process within the immune system that protects the host from oncogenesis and controls the immunological characteristics of developing tumors (Zitvogel *et al*, 2015; Snell *et al*, 2017). This process, termed cancer immunoediting, consists of three phases: first, the elimination of malignant cells by the immune system; second, the establishment of a balance between genetically unstable malignant cells and the immune system, reflecting the immunoediting that the immune system imposes on cancer cells; and third, the escape of neoplastic cell variants

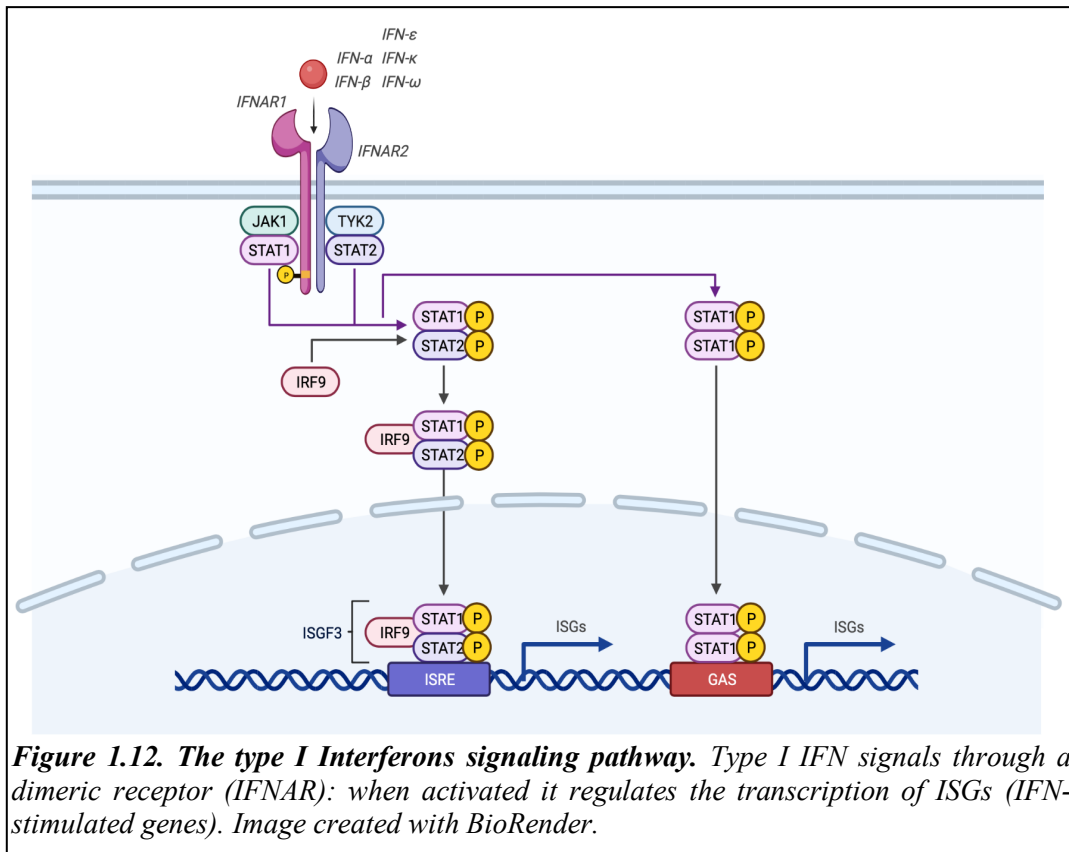


Figure 1.12. The type I Interferons signaling pathway. Type I IFN signals through a dimeric receptor (IFNAR): when activated it regulates the transcription of ISGs (IFN-stimulated genes). Image created with BioRender.

with reduced immunogenicity that eventually form clinically manifest neoplasms. Type I IFNs intervene in all of these phases (Zitvogel *et al*, 2015; Snell *et al*, 2017).

In cancer, the role of Type I IFNs is considered necessary to promote T-cell responses and prevent metastasis. Type I IFNs can directly inhibit proliferation of normal and tumor cells *in vitro* and *in vivo* and exert other direct effects on tumor cells, as downregulation of oncogene expression, induction of tumor suppressor genes, increase in major histocompatibility complex (MHC) class I expression and direct inhibition of cancer cell proliferation and angiogenesis (Bracci *et al*, 2007; Indraccolo, 2010; Zitvogel *et al*, 2015; Snell *et al*, 2017). In addition to direct effects on tumor cells, type I IFNs exert various effects on host immune cells, which may play a central role in the overall antitumor response (Bracci *et al*, 2007; Zitvogel *et al*, 2015; Snell *et al*, 2017). Several studies provided evidence for the importance of type I IFNs in the differentiation of the Th1 subset of T lymphocytes and in the proliferation, survival, and activity of CTLs, as previously described, in response to specific antigens (Trinchieri, 2010; Zitvogel *et al*, 2015; Snell *et al*, 2017). Type I IFNs exert also important effects on plasmacytoid dendritic cell (pDC) differentiation and function. Upon stimulation, these cells produce large amounts of type I interferon (mainly IFN α and IFN β) and serve as a bridge between

innate and adaptive immunity. The ability of pDC is to stimulate T cells and activate them by antigen presentation. Such effects may play an important role in the induction of IFN-induced antitumor immunity. Type I IFNs act as a key signal for differentiation and activation of DCs. In particular, IFN promotes the rapid differentiation of monocytes into highly active pDCs (Cella *et al*, 1999).

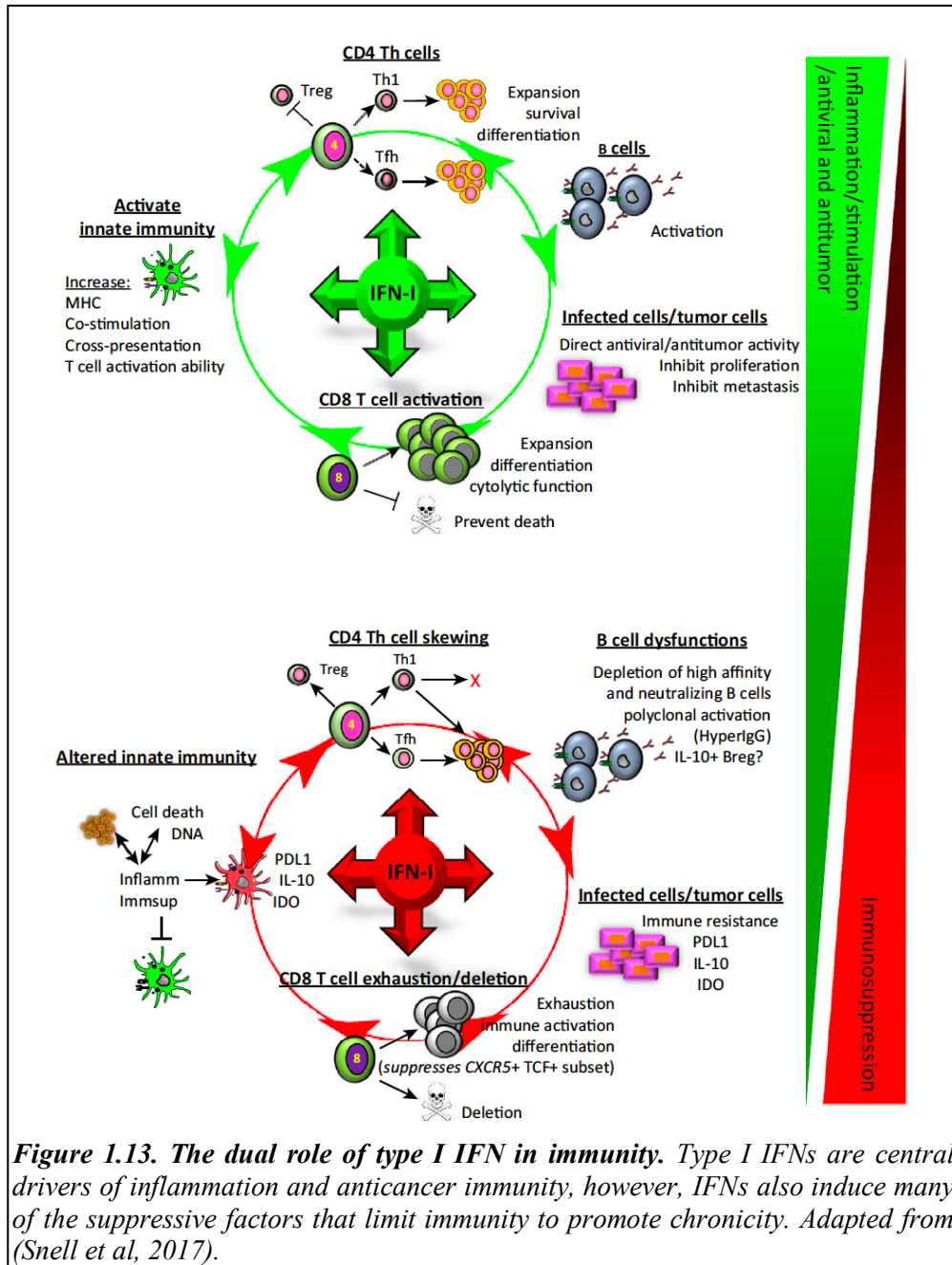


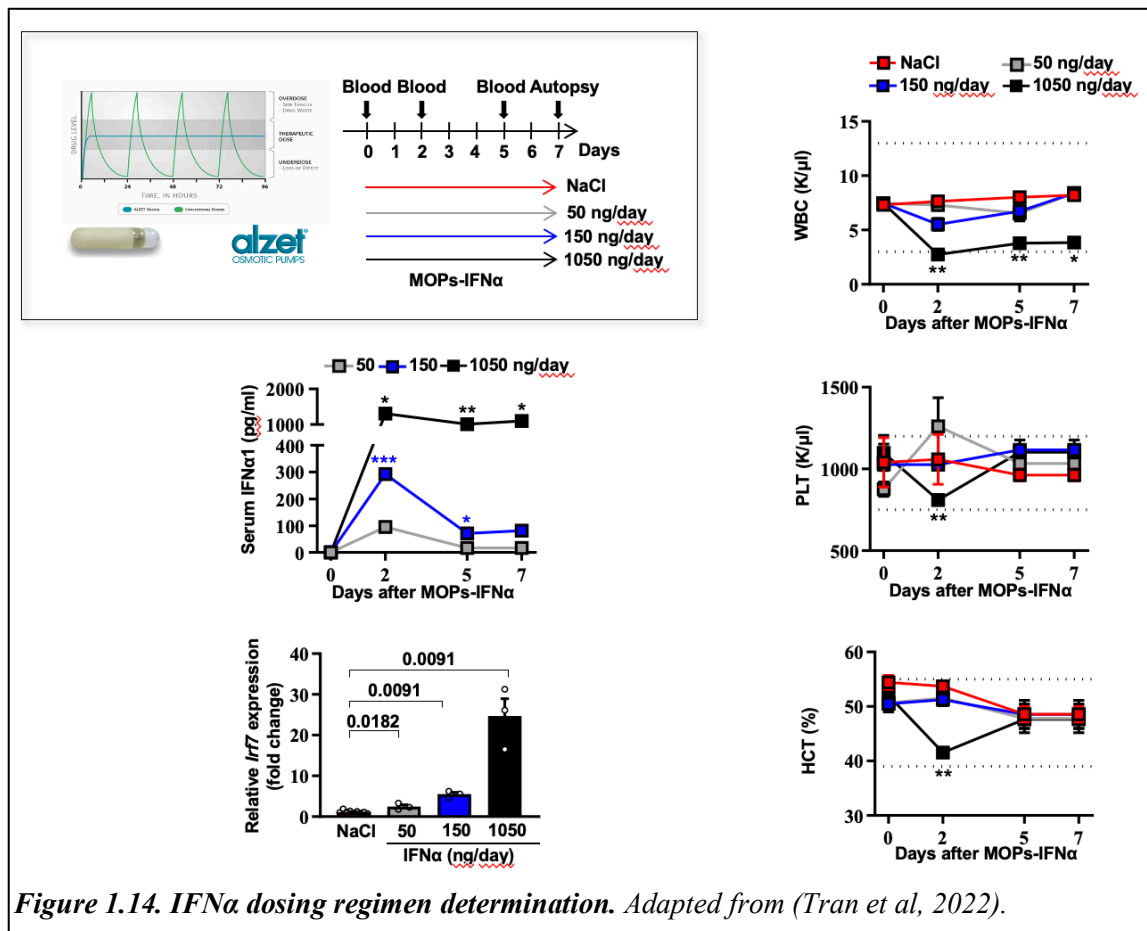
Figure 1.13. The dual role of type I IFN in immunity. Type I IFNs are central drivers of inflammation and anticancer immunity, however, IFNs also induce many of the suppressive factors that limit immunity to promote chronicity. Adapted from (Snell *et al*, 2017).

Despite the various evidence on the antitumoral effects of Type I IFNs recent studies have highlighted the fact that many cancers are characterized by concurrent immune suppression and inflammation (Snell *et al*, 2017). Type I IFNs have emerged as central

drivers of inflammation, but IFNs are also able to induce many of the suppressive factors that limit immunity and promote induction of chronic state (Fig.1.13). Accordingly, growing evidence show that type I IFNs may also play a negative role by promoting negative feedback and immunosuppression (Snell *et al*, 2017). It is widely recognized that, as mentioned, type I IFNs are critical in the early phase of cancer containment for activating DCs to cross-priming tumor-specific CTLs. Type I IFNs are usually induced by the recognition of nucleic acids in intracellular compartments, from sensors belonging to the family of pattern recognition receptors (PRRs) (Zitvogel *et al*, 2015). Several cytosolic DNA receptors have been identified, that trigger IFN production via a signaling cascade involving the master adaptor molecule stimulator of IFN genes (STING) (Demaria *et al*, 2015). Recently, spontaneous activation of STING was found to be required for induction of antitumor immunity (Demaria *et al*, 2015), on the other hand, there is evidence that in cancer, an accumulation of plasmacytoid DCs (pDCs) at the tumor margin and in sentinel lymph nodes, especially in melanoma and breast cancer, correlates with a lack of decrease in proinflammatory cytokine production and poorer prognosis (Sisirak *et al*, 2012; Snell *et al*, 2017). The question arises as to why an IFN-I-producing cell should be negatively associated with cancer progression. One explanation is that tumor-associated pDCs are specifically defective for IFN-I production and response, and expression of indoleamine 2,3-dioxygenase (IDO) by pDC has been mentioned as a possible immunomodulatory mechanism for its known capacity to restrict T-cell function and activate mechanisms of immune tolerance, suppress T-cell responses, and promote Treg expansion. IDO expression by plasmacytoid dendritic cells and macrophages is induced by IFN, leading to upregulation of checkpoint inhibitor expression that attenuates antitumor T cell responses (González-Navajas *et al*, 2012; Snell *et al*, 2017). Thus, similar to chronic viral infections, persistent Type I IFN signaling may be an important factor in immune system dysfunction in some cancers. Accordingly, low STING activity resulting from tumor cell turnover and phagocytosis by macrophages may lead to persistent, comparatively lower, IFN production that promotes IDO, PD-L1, and IL-10-dependent regulatory mechanisms, and production of these cytokines may lead to suppression of the immune response against tumors (Snell *et al*, 2017).

1.5 Continuous sensing of IFN α by hepatic endothelial cells shapes a vascular antimetastatic barrier

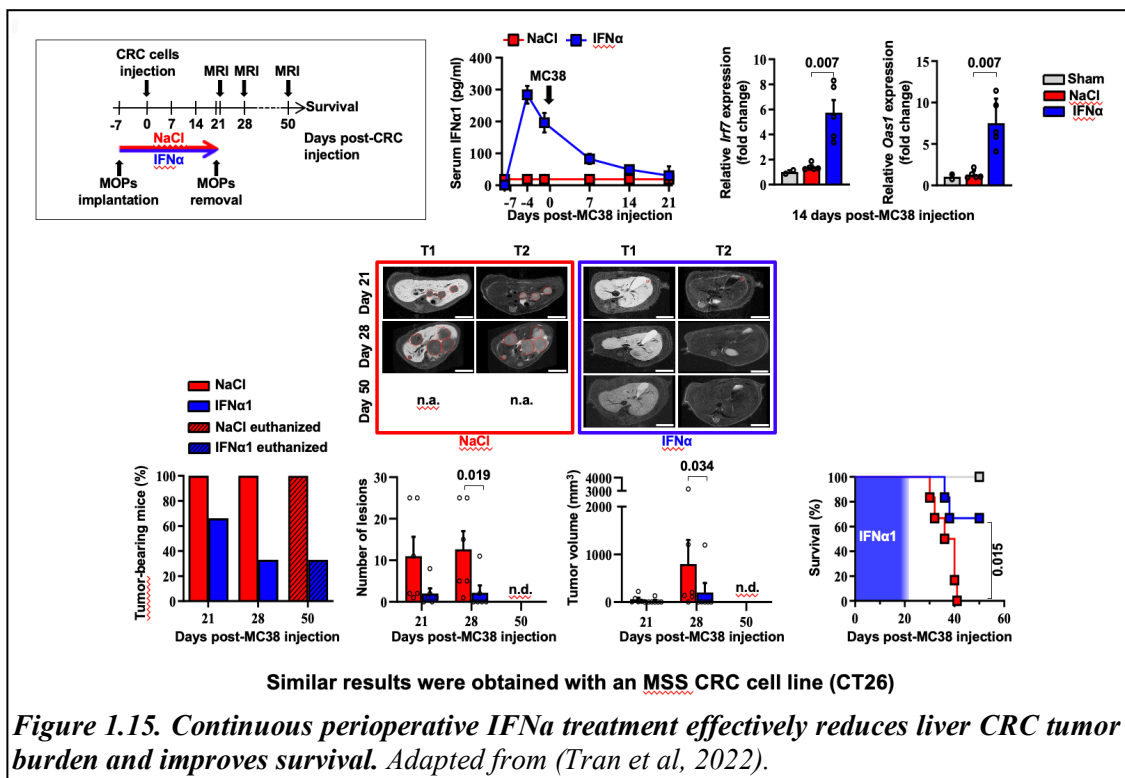
Recently published work from our laboratory (Tran *et al*, 2022) has shown that perioperative continuous IFN α therapy can curb the growth of liver CRC metastases through IFN α sensing by hepatic endothelial cells, which can form a vascular antimetastatic barrier. The starting point of this work was the limited clinical efficacy observed with systemic administration of IFN α , possibly due to its short plasma half-life (~1 hour) (Bocci, 1994) and the use of high and pulsed doses that often resulted in systemic side effects (Weber *et al*, 2015). To avoid the known toxicities, especially myelotoxicity, caused by high doses of IFN α (Weber *et al*, 2015) and to define a delivery strategy able to ensure long-lasting and nonfluctuating IFN α levels in blood and tissues, in the work were used mini-osmotic pumps (MOP) (Alzet), that were initially tested using different release rates of recombinant mouse IFN α 1 over time (i.e., 50 ng/day, 150 ng/day, or 1050 ng/day) (Fig.1.14). As shown, serum IFN α levels peaked on day 2 after



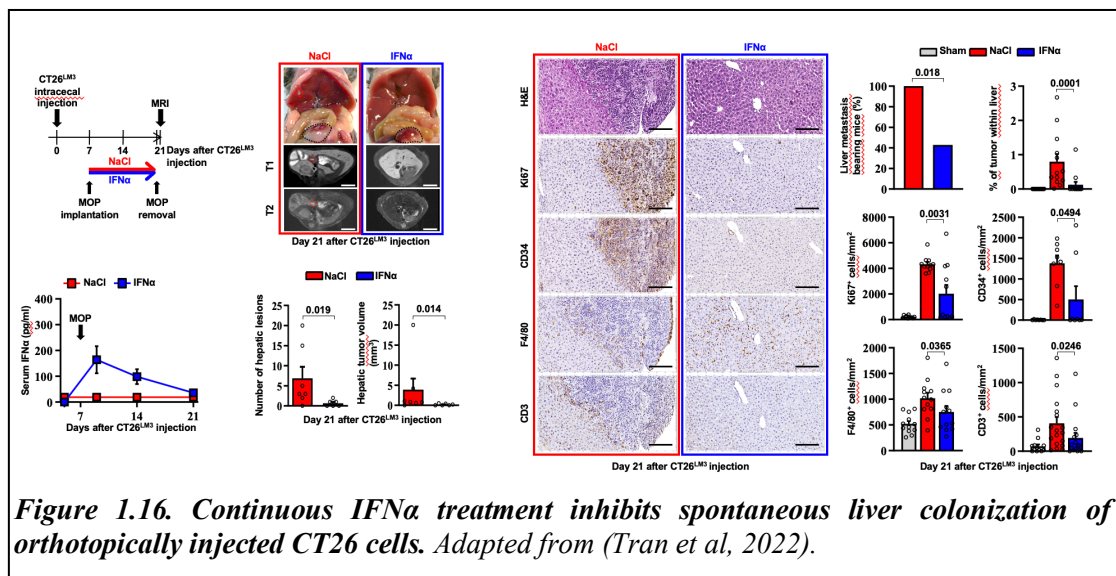
implantation of MOP, with relative IFN α reflecting different MOP loading doses. A significant decrease in white blood cell (WBC) count was observed only at the highest dose, with no change in platelet count (PLT) or hematocrit (HCT). Intrahepatic induction of the interferon-stimulated gene (ISG) *Irf7* (Cheon *et al*, 2014) at day 7 after treatment initiation showed a proportional dose effect with a sixfold increase in *Irf7* expression at a dosing regimen of 150 ng/day. In light of these results showing no bone marrow and liver toxicity while significantly induction of hepatic *Irf7* expression, dosing regimen of 150 ng/day was chosen to be tested in perioperative trials.

1.5.1 Continuous perioperative IFN α administration reduces liver CRC metastatic burden and improves survival

The ability of continuous IFN α administration (150 ng/day for 28 days) to reduce the growth of CRC metastases in the liver was next tested by challenging experimental animals with CRC cells seven days after MOP-IFN α treatment initiation, a time frame compatible with the perioperative period in humans (Horowitz *et al*, 2015). To test the efficacy of continuous IFN α administration, either the MSI MC38 CRC cell line (Corbett *et al*, 1975; Efremova *et al*, 2017) or the low immunogenicity MSS CT26 CRC cell line (Corbett *et al*, 1975; Castle *et al*, 2014) was used (Fig.1.14). Continuous IFN α administration resulted in well-tolerated serum IFN α levels of ~300 pg/ml at day 2 and ~100 pg/ml thereafter, which subsequently declined to undetectable levels, that is reflected by intrahepatic *Irf7* expression at day 21 after continuous IFN α therapy that was similar to that previously observed. Importantly, magnetic resonance imaging (MRI)-based longitudinal analyzes in MC38- or CT26-treated animals showed that 100% of NaCl-treated mice had liver lesions of increasing size that eventually led to human euthanasia, whereas 45% and 66% of IFN α -treated mice treated with MC38 and CT26 cells, respectively, had no liver metastases throughout the experimental period (Fig.1.15). All remaining IFN α treated mice, that were classified as disease-positive, had lesions that were reduced in number and size compared with those detected in NaCl-treated.



Remarkably, the metastatic lesions eventually regressed and achieved complete remission by day 50 in approximately 33% of IFN α -treated mice challenged with MC38 cells, which were classified as disease-positive by day 21 whereas none of the few CT26-challenged mice that were classified as disease-positive at Day 21 survived long-term. Finally, continuous administration of IFN α also improved survival, with similar rates for MC38- and CT26-stressed mice. This evidence suggests that continuous IFN α administration safely and efficiently limits metastatic colonization of the liver from CRC cell lines that have different immunogenic or genetic characteristics. Importantly the same results were

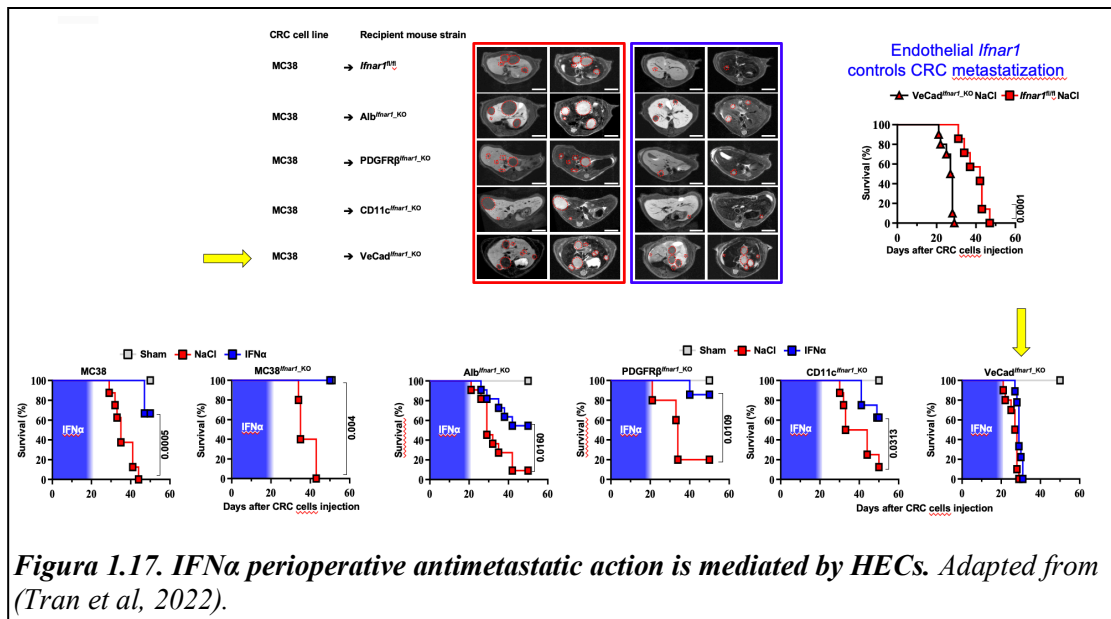


obtained for CRC liver metastases colonization curb in a orthotopic model of CRC (Fig.1.16).

1.5.2 HECs mediate the anti-metastatic activity of IFN α

Following experimental evidence that continuous IFN α administration effectively blocks the growth of CRC liver metastases, we performed a series of experiments in CRC and selected conditional IFNAR1-KO animal strains to decipher the possible contribution of different cells of the tumor microenvironment in sensing of continuous IFN α . Because the surface receptor subunit *Ifnar1* is necessary to mediate the pleiotropic anti-tumor properties of IFN α (Cheon *et al*, 2014), we removed this molecule from CRC cells and from liver parenchymal and non-parenchymal cells. Analyzes of IFN α action on MC38*Ifnar1*^{-KO} cell lines revealed that lesions generated by MC38 or MC38*Ifnar1*^{-KO} cells in IFN α -treated mice were similarly reduced in number and size compared with liver metastases in NaCl-treated controls, resulting in comparable mouse survival rates (Fig.1.17), supporting the hypothesis that continuous IFN α administration in this experimental setup has no direct antiproliferative activity against CRC cells, consistent with our previously reported data (Catarinella *et al*, 2016). To investigate the contribution of IFN α sensing in parenchymal and non-parenchymal cells of the liver, conditional specific IFNAR1- KO and *Ifnar1*fl/fl control mice were used. *Ifnar1*fl/fl control mice and mice lacking *Ifnar1* in hepatocytes (designated *AlbIfnar1*_ KO), hepatic stellate cells (designated *PdgfrbIfnar1*_ KO), *Itgax*⁺ (CD11c) DCs/KCs/LCMs (designated *ItgaxIfnar1*_ KO), or *Cdh5*⁺ endothelial cells (designated *VeCadIfnar1*_ KO) were injected with MC38 cells 7 days after initiation of NaCl or IFN α therapy. MRI analysis at day 21 after tumor challenge showed that loss of *Ifnar1* on hepatocytes, hepatic stellate cells, or DCs/KCs/LCMs did not significantly alter the anti-metastatic activity of IFN α treatment (Fig. 1.17).

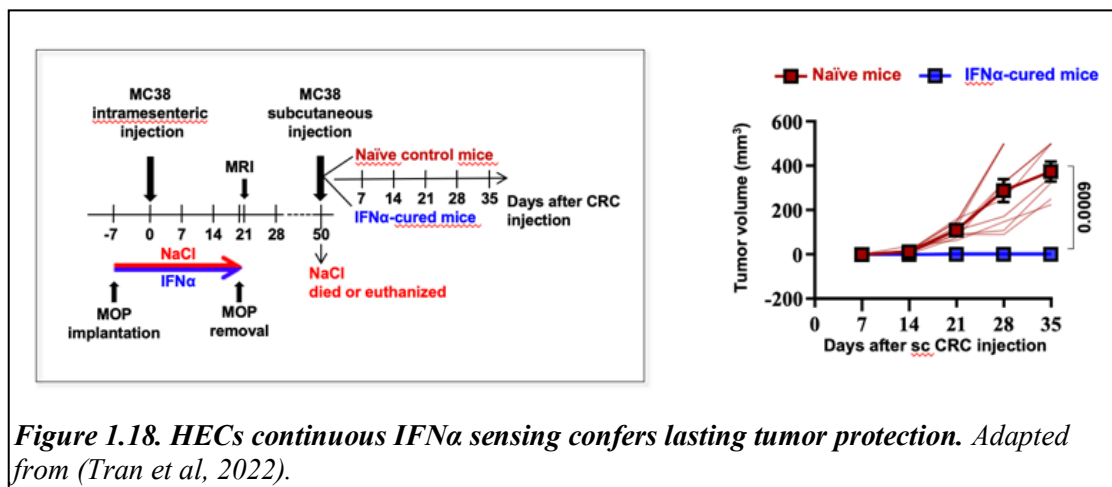
In contrast, depletion of *Ifnar1* on HECs allowed undisturbed growth of lesions (Fig. 1.17). Indeed, *VeCadIfnar1*_ KO mice treated with either NaCl or IFN α showed very similar numbers and sizes of liver lesions or survival rates, suggesting that the antimetastatic properties of IFN α require *Ifnar1* signaling on HECs.



Furthermore, *VeCadIfnar1_KO* mice exhibited increased tumor burden and mortality rates compared with NaCl-treated *Ifnar1^{fl/fl}* mice, suggesting that hepatic endothelial *Ifnar1* signaling exerts significant antitumor activity even at physiological endogenous intrahepatic levels of type I interferons (Fig.1.17).

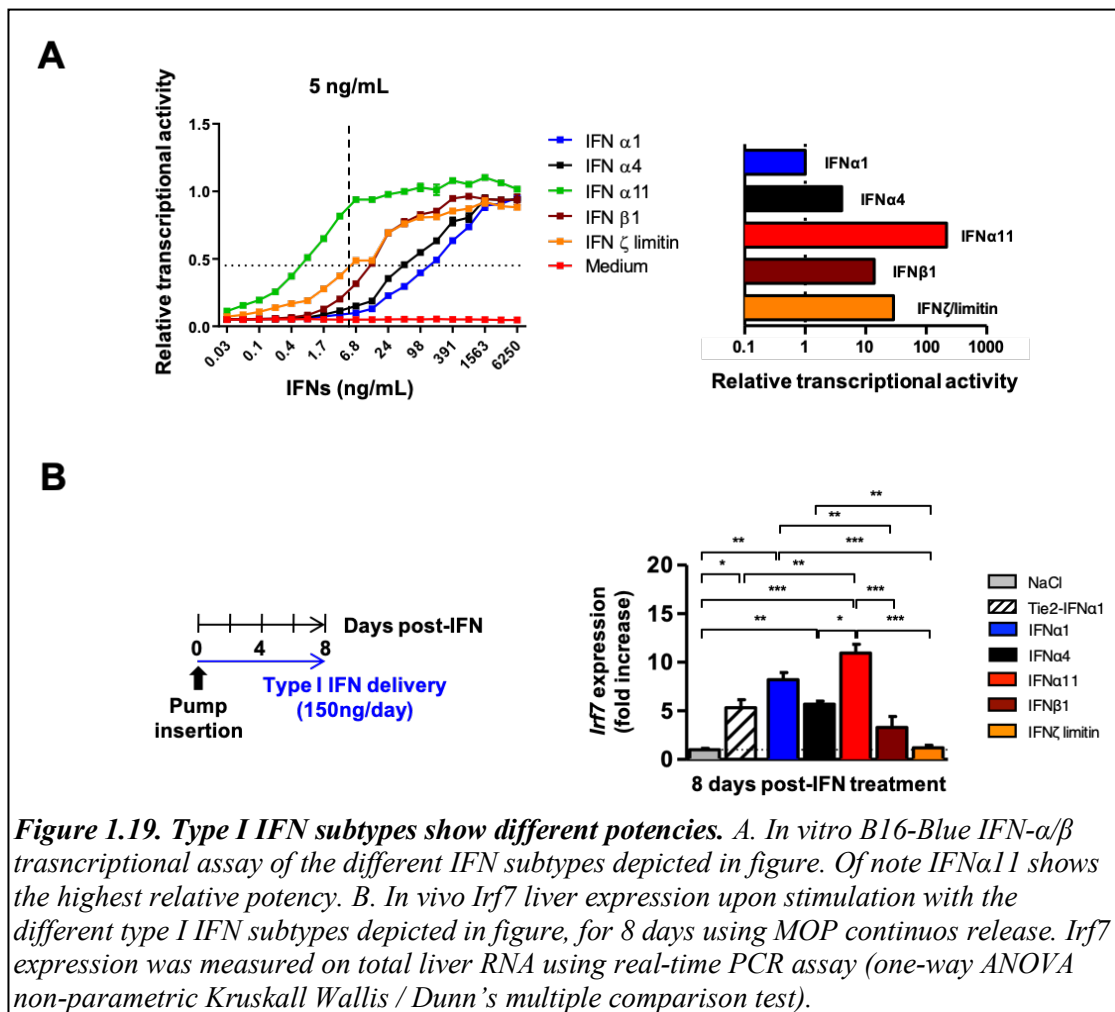
1.5.3 Continuous IFN α sensing improves immunostimulatory properties of HECs to provide lasting tumor protection

In an attempt to define the specific activities of continuous IFN α administration on HECs that enable efficient tumor constrain, we performed a series of *in vitro* and *in vivo* experiments. We found that continuous IFN α administration induces a mild and reversible capillarization of hepatic sinusoids, leading to the containment of CRC cells in hepatic vasculature (Tran *et al*, 2022). We furthermore defined an increased ability to stimulate cross-priming of naive CD8⁺ T cells *in vitro* by IFN α stimulated HECs, and increased systemic memory responses against tumor antigens after *in vivo* IFN α continuous treatment, resulting in an increased adaptive immune response to secondary tumor challenge in continuous IFN α -treated cured mice, even after discontinuation of IFN α therapy (Fig.1.18), highlighting the immunostimulatory potential of IFN α treatment on HECs, including LSECs.



1.5.4 Type I Interferon subtypes display different *in vitro* and *in vivo* potencies

Murine type I IFNs is a family of related proteins (14 IFN α subtypes, IFN β , IFN ϵ , and IFN- ζ /limitin) that bind the same heterodimeric receptor consisting of IFNAR1 and IFNAR2 (IFN α/β receptor) (Pesch *et al*, 2004). Based on relative receptor binding strengths and dissociation rates, type I IFNs control signal generation, downstream gene expression, and biological activities (Piehler *et al*, 2012; Zhang *et al*, 2017). In an attempt to characterize the differential *in vitro* transcriptional potencies of different type I IFN subtypes, we performed a cell-based functional assay using the commercial B16-Blue IFN- α/β cell line (InvivoGen), stably transfected with a reporter gene under the control of the IFN- α/β -inducible ISG5. Specifically, IFN α 1, IFN α 4, IFN α 11, IFN β , and IFN- ζ /limitin were used to stimulate the B16-Blue IFN- α/β cell line and test IFN subtypes relative potencies in stimulating transcriptional activity. As shown in Fig. 1.19 A, among the different subtypes analyzed, IFN α 11 showed the highest potency to stimulate transcriptional activity, indicating that it is a prototypical IFN with high potency, whereas



IFN α 1 showed the lowest potency to stimulate transcriptional activity, indicating that it is a prototypical IFN with low potency. We then tested the same group of type I IFN subtypes for their ability to induce expression of intrahepatic ISGs *in vivo* after eight days of continuous release by MOP (Fig. 1.19 B). The data obtained confirmed that prolonged release of IFN α 11 triggered the strongest intrahepatic ISG induction (Fig.1.19 B), suggesting that type I IFNs with high potency may enhance antitumor efficacy even in a deregulated tumor microenvironment (Katlinski et al., 2017).

1.6 Inactivation of Interferon receptor promotes the establishment of immune privileged tumor microenvironment

After assessing in a mouse models of CRC liver metastasis the efficacy of IFN α administration to curb liver metastases in a preventive setting, it is important to understand the partial effect of IFN α in the treatment of established CRC liver metastases. It is well known that solid tumors such as CRC evade control by the immune system by forming immune-privileged niches within the tumor microenvironment (Katlinski *et al*, 2017) Several cellular and acellular (e.g., oxygen and nutrient deprivation) elements of the tumor microenvironment reduce the proliferation, viability, or activity of CTLs, inhibiting their anti-tumor effector function (Katlinski *et al*, 2017). Indeed, decreased recruitment of CTLs within the CRC tumor microenvironment is associated with poor prognosis; conversely, increased accumulation of CTLs within the tumor microenvironment is associated with favorable outcome (Katlinski *et al*, 2017). As mentioned previously, IFN α supports the expansion and viability of CTLs within the tumor compartment. The level of IFNAR1 at the cell surface is critical for IFN-dependent biological functions. The level of IFNAR1 expression is regulated by ubiquitination/degradation cycles following phosphorylation of IFNAR1 (Katlinski *et al*, 2017). A strong correlation is observed between IFNAR1 levels in CTLs and the ability of the CRC tumor microenvironment to evade the immune system and thus acquire resistance to immunotherapies. Global expression profiling in hypoxic areas of colorectal tumors shows a decrease in expression of ISGs compared to the "non-cancerous mucosa" (Fig.1.20 A) (Katlinski *et al*, 2017), along with a marked decrease in nuclear phosphorylated STAT2 (Fig.1.20 B), a downstream effector of IFN α signaling, suggesting that IFN α signaling is inhibited in human CRC tumors. Although comparable mRNA expression of IFNAR1 is reported in CRC and normal colorectal tissues, dramatic differences in IFNAR1 protein levels can be observed by immunohistochemical staining for IFNAR1 (Fig.1.20 C) (Katlinski *et al*, 2017). IFNAR1 is more highly expressed in the stromal compartment of normal colorectal tissue, whereas all cell types in the CRC area show partial or complete loss of IFNAR1 (Fig.1.20 C). Moreover, downregulation of IFNAR1 in either the stromal or cancer cell compartment is associated with poor prognosis in CRC patients (Fig.1.20 D) (Katlinski *et al*, 2017). Interestingly,

downregulation appears to be dependent on tumor microenvironment (TME) stress, as IFNAR1-positive cells are spatially separated from tumor areas positive for GLUT1, a marker of TME stress (Fig. 1.20 D) (Katlinski *et al*, 2017). This finding suggests that TME stimuli may trigger IFNAR1 downregulation and suppress IFN α signaling.

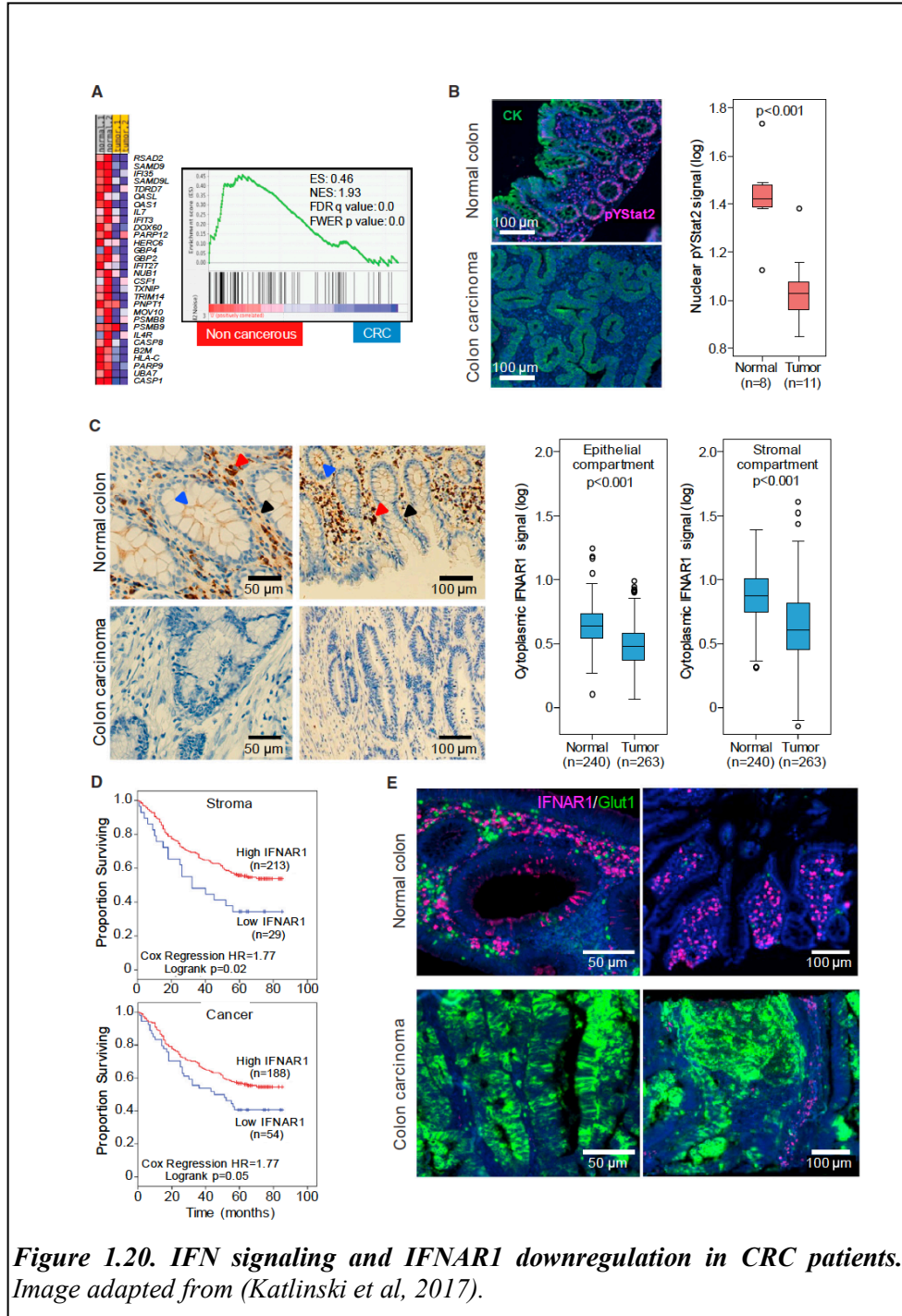


Figure 1.20. IFN signaling and IFNAR1 downregulation in CRC patients. Image adapted from (Katlinski *et al*, 2017).

Immunofluorescence is used to characterize IFNAR1-positive cells in human tissues: The majority of cells expressing high levels of IFNAR1 in normal human colon are CD3⁺

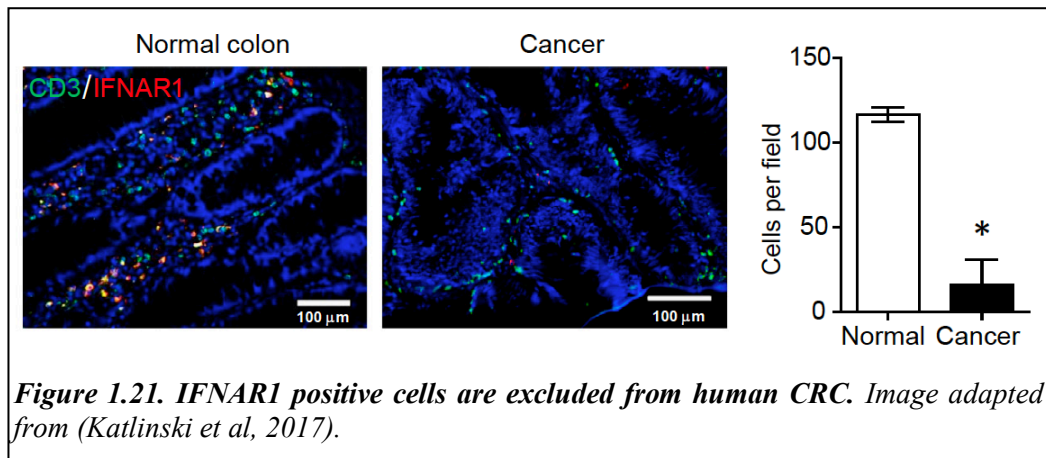


Figure 1.21. IFNAR1 positive cells are excluded from human CRC. Image adapted from (Katlinski *et al*, 2017).

cells (Fig. 1.21). Importantly, in human CRC tissues, most IFNAR1-positive T lymphocytes are localized in the periphery of the tumor and very few of them were found inside human tumors (Katlinski *et al*, 2017).

These results highlight the importance of IFNAR1 down-regulation in CTLs. Given the importance of these cells in anti-tumor immunity, it is likely that downregulation of IFNAR1 in the stromal compartment may stimulate cancer growth and progression (Katlinski *et al*, 2017). In summary, downregulation of IFNAR1 triggered by TME stress reduces the viability of intra-tumoral CTLs and causes the establishment of an immune-privileged niche in CRC tumors (Katlinski *et al*, 2017). According to these results, downregulation of IFNAR1 may determine the refractoriness of solid tumors to immunotherapies.

1.6.1 Inhibitors of stress-activated kinases for IFNAR1 stabilization

IFNAR1 levels at the cell surface are controlled by IFNAR1 ubiquitination and degradation after phosphorylation at Ser535 (Ser526 in mice) in the cytoplasmic tail of IFNAR1, as mentioned previously, and can be controlled by ligand-independent activities. Stimuli involved in phosphorylation of these serine residues can be triggered by signaling pathways such as unfolded protein response (UPR), hypoxia, nutrient deficit, vascular endothelial growth factor, and inflammatory cytokines, which represent a graded response to the stresses prevalent in the tumor microenvironment (Liu *et al*, 2009; Bhattacharya *et al*, 2013; Zheng *et al*, 2011; HuangFu *et al*, 2012). Key mediators of IFNAR1 phosphorylation are kinases involved in these integrated cellular stress responses, and these two important players include the p38 and PKD kinases, both of which are active in CRC tumors (Katlinski *et al*, 2017). p38 kinases are proline-directed serine/threonine kinases that belong to the mitogen-activated protein kinase (MAPK) family and are present in all eukaryotes. In contrast to the prototypical MAPKs ERK1 and ERK2, p38 kinases do not usually respond to mitogens but are activated by environmental stress and inflammatory signals (Canovas & Nebreda, 2021). The activities of p38 kinases integrate many types of signals and are involved in a wide range of biological responses, including environmental and intracellular damages, pathological processes such as infection or cancer, and physiological functions such as cell differentiation. Given the broad spectrum of processes involving p38 kinases, defects in this pathway have been associated with various diseases, implying that pharmacological modulation of p38 signaling could provide therapeutic improvements. The ability of p38 α to regulate the same process at different levels and with opposite effects also provides the opportunity to combine different inputs to modulate the result and balance the response in a way that is most appropriate for the context (Canovas & Nebreda, 2021). In this context, p38 α induces degradation of the IFN α / β receptor IFNAR1 but simultaneously stimulates transcription of interferon-stimulated genes (Joshi *et al*, 2010; Fuchs, 2012). In this way, cells can fine-tune the extent and duration of IFN α / β signaling. Unbalanced expression of these effects can lead to dysfunctional activities, such as in cancer progression. Accordingly, inhibition of p38 α stabilizes IFNAR1, which increases the viability of cytotoxic T lymphocytes and enhances their antitumor immune to CRC

tumors, induces the expression of chemokines that enable neutrophil infiltration in lung cancer, and helps block Treg adenosine-driven IFNAR1 downregulation, which in all cases suppresses tumor growth (Katlinski *et al*, 2017; Gui *et al*, 2020; Zhang *et al*, 2022). There is increasing evidence that p38 α functions as a non-oncogenic addictive factor in malignant cells, enabling the survival and proliferation of many cancer cell types through several means, which may explain why p38 α is not frequently mutated in tumors. Moreover, the role of p38 α is not limited to malignant cells but may also act in tumor stromal cells to promote tumor growth and spread (in part via pro-inflammatory signaling). In general, inhibition of p38 α may have antitumor effects by targeting this signaling pathway in different cell types of the tumor and its niche, increasing the efficacy of immunotherapies, and potentiating chemotherapies. However, considering the various effects of p38 α , its inhibition should be used with caution to avoid unexpected side effects. In this regard, long-term treatment, as required for chronic autoimmune or neurodegenerative diseases, is more likely to lead to side effects or adaptation and lack of efficacy than short-term treatment, as in oncological therapy. Importantly, some clinical trials have been conducted with the selective p38 α inhibitor ralimetinib (LY2228820), one, in particular, showing phase I adequate safety profile and partial activity in aromatase-refractory metastatic breast cancer (Patnaik *et al*, 2016), opening the way for a more in-depth investigation, possibly using a combinatorial treatment.

Protein kinase D2 (PKD2) is another important kinase involved in phosphorylation of IFNAR1 and active in CRC tumors (Katlinski *et al*, 2017). Protein kinase D (PKD) is a family of ubiquitous serine-threonine protein kinases belonging to the Ca²⁺/calmodulin-dependent protein kinase superfamily. PKD isoforms (PKD1/PKC μ , PKD2, and PKD3/PKC ν), which are homologous in structure and function, are extensively expressed in a variety of tissues. PKDs are activated by protein kinase Cs (PKCs) through phosphorylation of two conserved serine residues and exert their function in mediating mitogenic signaling (Tandon *et al*, 2015). Several studies have demonstrated the involvement of PKDs in key signaling pathways regulating tumor cell proliferation, such as β -catenin, androgen receptor, mTORC1-S6K1, and MAPK in various tumor cell models (Tandon *et al*, 2015). Also, the vascular endothelial growth factor (VEGF) transduction pathway, which is inhibited by type I IFN family cytokines, including IFN α and IFN β , is able to activate PKD2 kinase, which in turn phosphorylates IFNAR1, leading

to its downregulation (Zheng *et al*, 2011), in a negative feedback regulatory process. SD-208 is an ATP-competitive small PKD inhibitor molecule, that has been shown to significantly suppress prostate tumor cell proliferation by inducing G2/M cell cycle arrest via targeted inhibition of PKD and blocking cancer cell invasion (Tandon *et al*, 2015). SD-208 has also been reported as a TGF- β R1 inhibitor, raising questions about the specificity of PKD inhibition in reducing tumor cell invasion (Uhl *et al*, 2004; Mohammad *et al*, 2011). Nevertheless, SD -208 treatment administered in combination with ralimetinib showed the ability to stabilize IFNAR1 levels in CRC tumor-specific CTLs, which significantly increased their therapeutic index in an IFNAR1-dependent manner (Katlinski *et al*, 2017).

2. Aim of the work

The aim of this work is to define the role of the endogenous type I IFNs system in CRC liver metastases, and their relation to therapeutic outcomes, to rationally design IFN α adjuvant trials for CRC liver metastases and for clinical translation.

To this end, we will employ two independent and potentially synergistic strategies (i) use IFN isoforms with high *in vivo* potency that could be less dependent on IFNAR1 cell surface density, (ii) use pharmacological and genetic strategies to inhibit IFNAR1 protein degradation in the tumor microenvironment to develop effective combinatorial adjuvant IFN-based therapies to cure CRC metastatic patients. We pursued the following specific goals:

Aim 1: To determine whether colorectal tumors and liver CRC metastases express type I IFN molecules and specific IRGs and what is their role in IFNAR1 downregulation.

Aim 2: To determine the therapeutic potential of extended intraperitoneal release of type I IFN subtypes with high *in vivo* potency for the treatment of colorectal cancer metastases to the liver.

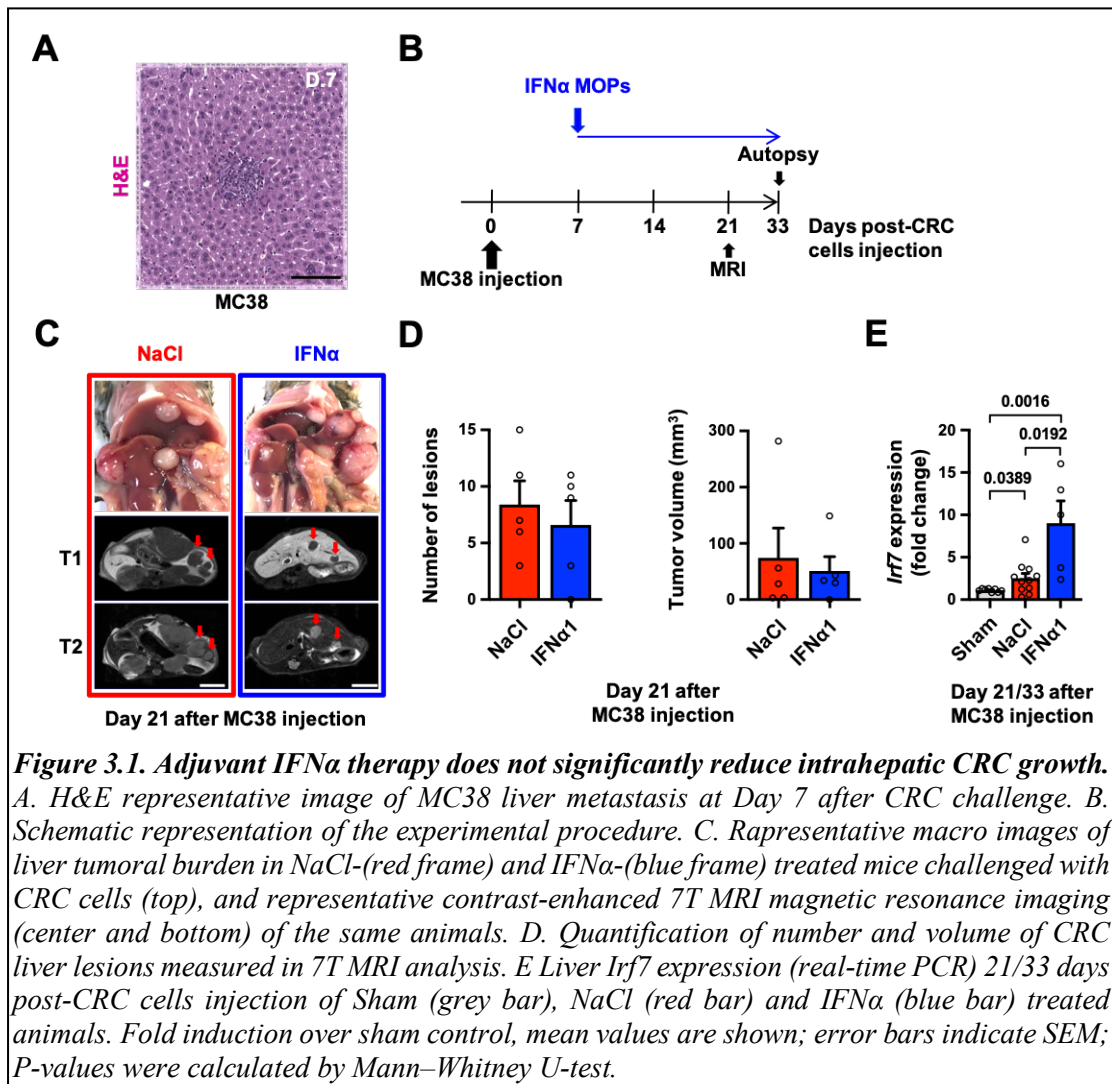
Aim 3: To determine the therapeutic potential of inhibitors of IFNAR1 downregulation for the treatment of established CRC liver metastases, both as monotherapy and in combination with adjuvant IFN-based therapies.

3. Results

3.1 Adjuvant IFN α therapy does not significantly reduce intrahepatic CRC growth

In the attempt to test the ability of continuous type I IFN treatment to impair liver metastases growth once CRC cell have already passed the liver vascular barrier and started to form micrometastatic lesions of about 100-150 μm^2 , as shown in hematoxylin and eosin (H&E) staining in Figure 3.1. A, a time point in which tumors begin to recruit neo-angiogenic vessels and immune-cells endowed with pro-tumoral properties (Catarinella *et al*, 2016), we tested the adjuvant capacity of type I IFN therapy. To this end, we set up a therapeutic IFN α 1 trial as described in Figure 3.1. B. As mentioned above, the use of IP-MOP that preventively release small quantities of IFN α 1 over time is able to induce IRGs in the liver without causing significant hematopoietic toxicity, reduce tumor burden and increase survival of treated mice (Tran *et al*, 2022).

To perform IFN α 1 therapeutic trial, H-2^{bx_d} F1 hybrids of C57BL/6 x BALB/c (CB6) mice, matched for sex and age, were injected with the microsatellite instable (MSI) MC38 CRC cell line (Corbett *et al*, 1975; Efremova *et al*, 2017), at the dose that induces tumors in more than 98% of mice with a survival time of about 40 days (Catarinella *et al*, 2016), and 7 days after tumor challenge were randomized to receive either IFN α 1 therapy or NaCl treatment as controls. Treated animals were implanted with MOP constantly releasing the IFN α 1 (Figure 1.14. Introduction and (Tran *et al*, 2022)) for 28 days, modified to be compatible with magnetic resonance imaging (MRI) analysis (Vousden *et al*, 2018). Control animals were implanted with MOP releasing NaCl vehicle as control (NaCl). The two groups of mice were followed and 21 days after tumor challenge underwent 7T MRI-based analyses (Figure 3.1. C lower panels) showing that both IFN α 1 and NaCl treated experimental animals developed multiple hepatic metastatic tumor lesions, that were comparable as mean of number (Figure 3.1. D left) or lesions overall volume (Figure 3.1. D right), with no mice displaying detectable tumors in other organs. Thirty-three days after tumor challenge mice were killed and tumor burden was evaluated macroscopically (Figure 3.1. C upper panel), demonstrating again no difference in liver



tumoral load between IFN α 1 and NaCl groups. In order to evaluate the effect on the liver microenvironment of therapeutic IFN α 1 delivered through the use of MOP, that at the time of necroscopy were still releasing IFN α 1, the intrahepatic expression of a prototypical Interferon Regulated Gene (IRG), like *Irf7* (Cheon *et al*, 2014), was monitored in IFN α 1 treated versus control NaCl mice. As depicted in Figure 3.1. E intrahepatic expression of *Irf7* was significantly increased in liver of tumor bearing mice continuously treated with IFN α 1 compared to both NaCl and Sham control mice. Interestingly as previously reported (Catarinella *et al*, 2016), also mice that did not receive therapeutic IFN α 1 therapy displayed a significantly increased intrahepatic level of *Irf7*, suggesting that, CRC metastases bearing livers, display an active interferon gene signature. These data suggest that mice displaying MC38 liver metastases, are resistant to IFN α 1 therapy, despite the significant upregulation of *Irf7* due to IFN α 1 treatment. Of

note, the presence of an endogenous type I IFN signature, detected in MC38 metastases bearing livers, raise the question of whether CRCs growing in the liver induce immune deregulation and/or develop resistance to IFN-based therapies. Notably, the endogenous type I IFN system - in addition to its pivotal role in immunity and cancer immune surveillance (Stark *et al*, 1998)- is emerging as a complex system that in certain circumstances may lead to immune deregulation (Chen *et al*, 2017).

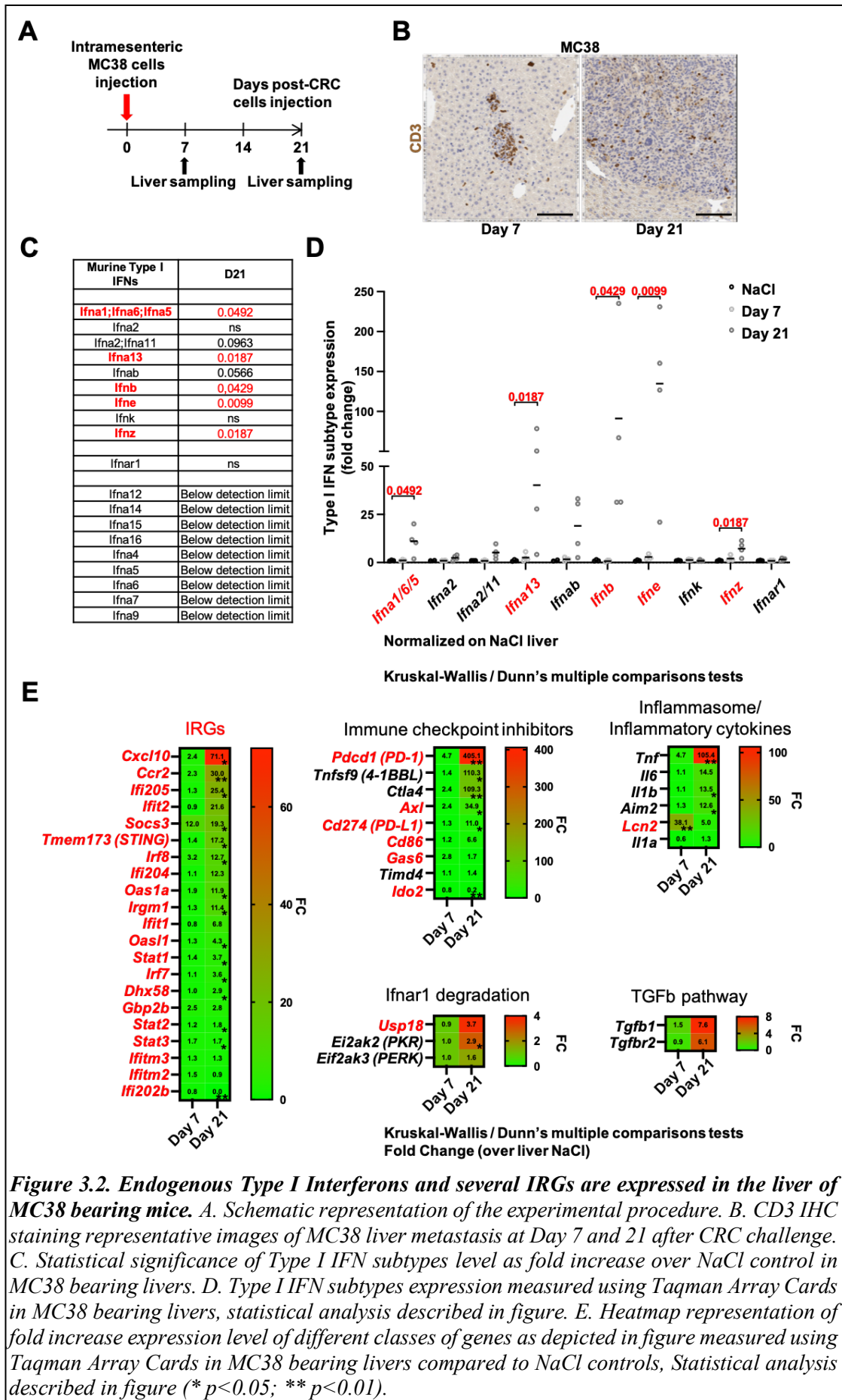
For instance, murine type I IFNs consist of a family of related proteins (14 IFN α subtypes, IFN β , IFN ϵ and IFN- ζ /limitin) that bind the same heterodimeric receptor composed of IFNAR1 and IFNAR2 (IFN α/β receptor) (Pesch *et al*, 2004). Due to relative receptor binding strengths and dissociation rates, type I IFNs control signal generation, downstream gene expression and biological activities (Piehler *et al*, 2012; Zhang *et al*, 2017). Thus, it is tempting to speculate that specific endogenous IFNs in the context of chronic stimulation, as in the TME, may lead to specific immune deregulations and a state of "refractoriness" of tumors to IFN-based therapies. Additionally, type I IFN receptor (IFNAR1) downregulation, a condition associated with the formation of immunosuppressive niches within CRCs (Katlinski *et al*, 2017), could represent an additional pathway of tumor refractoriness (Snell *et al*, 2017). A careful and functional characterization of endogenous IFNs and related IRGs as well as the expression pattern of IFNAR1 may be therefore beneficial to determine which patients will or will not respond to IFN therapies and define additional strategies counteracting the "adaptive resistance".

3.2 Endogenous Type I Interferons and several IRGs are expressed in the liver of MC38 bearing mice

To characterize the endogenous interferon signaling that we observed in mice bearing overt MC38 liver tumors we decided to perform a transcriptional analysis of CRC liver metastases of increasing dimensions (as described in Figure 3.2. A), to define the relation between tumor growth stage and the endogenous expression of all different murine type I interferon subtypes. Furthermore, we evaluated the expression of a panel of specific IRGs, immune checkpoint inhibitors genes, some of which are stimulated by interferon signaling (i.e. *Pdcd1* (PD-1), *Axl*, *Cd274* (PD-L1), *Cd86*, *Gas6*, *Ido2* (Snell *et al*, 2017), as well as genes involved in IFNAR1 degradation process (*Usp18*, *Ei2ak2* (PKR) and *Eif2ak3* (PERK) (Bhattacharya *et al*, 2013; Ivashkiv & Donlin, 2014), Inflammasome/Inflammation signaling and TGF β pathway (HuangFu *et al*, 2012), that have shown to play an important role in CRC tumor growth. In fact, metastases growing in the liver progressively attract pro-tumoral infiltrating immune cells and exclude T-cells, as shown in IHC staining for CD3 antigen in Figure 3.2. B, by mechanisms that relate to the production by cancer cells of TGF β (Munn & Bronte, 2016; Katlinski *et al*, 2017; Tauriello *et al*, 2018).

Upon analysis of transcriptional status of metastatic liver at 7 and 21 after tumor challenge, that was evaluated taking advantage of custom Taqman Array Cards assay (Applied Biosystem), we observed a significant upregulation of different type I interferon subtypes especially at the later timer point analyzed (in particular *IFNa1/6/5*, *IFNa13*, *IFNb*, *IFNe* and *Ifnz*) (Figure 3.2. C-D) among the different 18 members of the murine type I IFN family (Pesch *et al*, 2004). These data indicate that indeed several endogenous type I IFNs are expressed in the MC38 metastatic liver.

Accordingly, we observed that several IRGs were similarly upregulated at the same time point (Figure 3.2. E left). Actually, we observed the significant upregulation of prototypical IRGs like *Cxcl10*, *Tmem173* (Sting), *Oas1*, *Stat1*, *Stat2*, among others and importantly we confirmed the upregulation of *Irf7* as well. We also observed the upregulation of IRGs involved in negative feedback loop of IFN signaling like *Socs3*, *Oasl1* and *Usp18* (Figure 3.2. E left). Concomitantly, we observed the upregulation of genes involved in immune checkpoint inhibitory pathways, like *Pdcd1* (PD-1) *Tnfsf9*



(4-1BBL), *Ctla4*, *Axl*, *Cd274* (PD-L1) and *Gas6* among others (Figure 3.2. E upper center). Of note, some of these genes, like PD-1, PD-L1, *Axl* and *Gas6* are stimulated by IFN signaling (Snell *et al*, 2017), reinforcing the notion that MC38 metastases bearing livers, are characterized by an active expression of type I IFN interferon subtypes and of a prototypical type I IFN interferon signature.

In addition, we also observed at the same time point the upregulation of genes involved in the IFNAR1 degradation machinery, as the aforementioned *Usp18*, or kinases involved in Unfolded Protein Response (UPR) pathway like *Eif2ak2* (Pkr) and *Eif2ak3* (Perk) (Figure 3.2. E lower center), suggesting that type I IFN signaling may be further deregulated by a possible negative feedback mechanism, at least in some cells of the tumor microenvironment. Furthermore, UPR was demonstrated to be responsible of ligand-independent IFNAR1 degradation, alone or in combination with other pathways like hypoxia, nutrient deficit, vascular endothelial growth factor and inflammatory cytokines that form an intergraded response to the stresses that are prominent in the tumor microenvironment (Liu *et al*, 2009; Bhattacharya *et al*, 2013; Zheng *et al*, 2011; HuangFu *et al*, 2012). As mentioned above, inflammatory cytokines are involved in the regulation of IFNAR1 degradation, as a consequence of IFN responses (HuangFu *et al*, 2012), and importantly a high magnitude and significant upregulation of genes codifying inflammatory and inflammasome cytokines, like *Tnfa*, *Il6*, and *Il1b* among others, was observed (Figure 3.2. E upper right). The inflammatory phenotype observed in MC38 bearing livers was partially unexpected, as hepatic microenvironment is usually considered highly immunotolerant (Simone *et al*, 2021). Finally, we also observed an upregulation of genes codifying TGF β pathway proteins, like *TGF β 1* and *TGF β 2* (Figure 3.2. E lower right), as this pathway is prominently mutated in CRC tumors, contributing to cancer microenvironment shaping and T cells exclusion, as observed 21 days after MC38 tumor challenge (Figure 3.2. B) (Itatani *et al*, 2019; Tauriello *et al*, 2018). All in all, these results indicate that several type I endogenous IFNs subtypes are expressed in the livers of mice bearing CRC metastases, that are accompanied by a prominent IRGs signature, that comprises immune checkpoint inhibitors, inflammatory and IFNAR1 degradation genes, in the presence of Tgf β pathway activation, features that likely contribute to tumor growth and may lead to specific immune deregulations, a state of

"refractoriness" of tumors to IFN-based therapies and evasion from immune surveillance mechanisms.

3.3 CRC cell lines and tumor organoids express type I Interferon subtypes *in vitro*

After the evidence that in the hepatic metastatic microenvironment different type I IFN subtypes are expressed in association with an IRGs signature, we tested the hypothesis that murine CRCs directly produce specific endogenous type I IFNs subtypes as a way to deregulate the cell surface expression of IFNAR1 in the tumor microenvironment, thus representing a new way by which tumors deregulate a potentially anti-tumor pathway for their own growth. Accordingly, endogenous Type I IFN subtypes produced by CRC cells could potentially act on both tumor and innate and adaptive immune cells, thus defining an additional strategy of immune evasion by tumors (Aricò *et al*, 2019; Musella *et al*, 2017; Locquenghien *et al*, 2021). To directly test this hypothesis, and dissect the possible contribution of tumor cells on endogenous interferon production we performed transcriptional analysis of a panel of type I interferon subtypes that we found upregulated in CRC metastatic livers.

For this purpose, we selected a panel of murine CRC cell lines and tumor organoids, to which we added the murine pancreatic ductal adenocarcinoma (PDAC) Panc02 cell line, (H2^b restricted (Corbett *et al*, 1984), to compare an additional tumor type that frequently metastasize to the liver (Fig 3.3.1. A). In addition to the MC38 MSI CRC cell lines described before, we also analyzed the CT26 cell lines, that represent a bona fide microsatellite stable (MSS) cell line (Corbett *et al*, 1975; Castle *et al*, 2014) and a prototypical mouse MSS tumor organoids (MTO, H2^b restricted), that were obtained from the selection of liver metastatic tumors developed in transgenic mice harboring four key mutations that typify human CRCs such as *Apc*^{fl/fl}, *Kras*^{LSL-G12D}, *TGFβ2*^{fl/fl} and *Trp53*^{fl/fl} targeted to intestinal stem cells (ISCs) by means of the *Lgr5*^{eGFP-creERT2} driver (Tauriello *et al*, 2018). Finally, a primary cell population of Intestinal Crypts (IC) were obtained to compare non transformed epithelial cells with CRC cells. IC were collected from mouse colon as previously described (Sato *et al*, 2011), and analyzed for EpCAM expression, a marker of epithelial cells (Trzpis *et al*, 2007), using cytofluorimetric analysis. As shown in Figure 3.3.2. we used a physical gating strategy and the fluorescent minus one (FMO) controls for CD45 and EpCAM staining for this analysis. Indeed, IC showed a 90%

A

Cells	Tumor type	Strain	Description	Micro Satellite Status
IC	-	C57BL/6, H2 ^b	Intestinal crypts	-
MC38	CRC	C57BL/6, H2 ^b	grade III adenocarcinoma	MSI
CT26	CRC	BALB/c, H2 ^d	lower-crypt origin undifferentiated state	MSS
MTO ¹⁴⁰	CRC	C57BL/6, H2 ^b	<i>Lgr5^{eGFP-creERT2}-Apc^{fl/fl}-Kras^{LSL-G12D}-Tgfr2^{fl/fl}-Trp53^{fl/fl}</i>	MSS
Panc02	PDAC	C57BL/6, H2 ^b	3-methylcholanthrene-induced	-

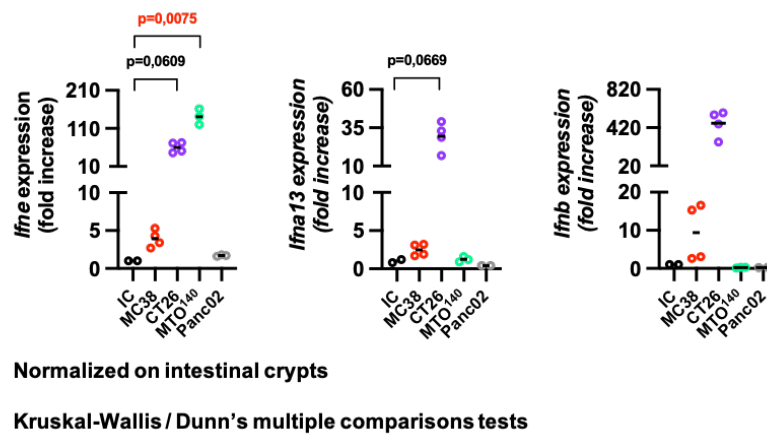
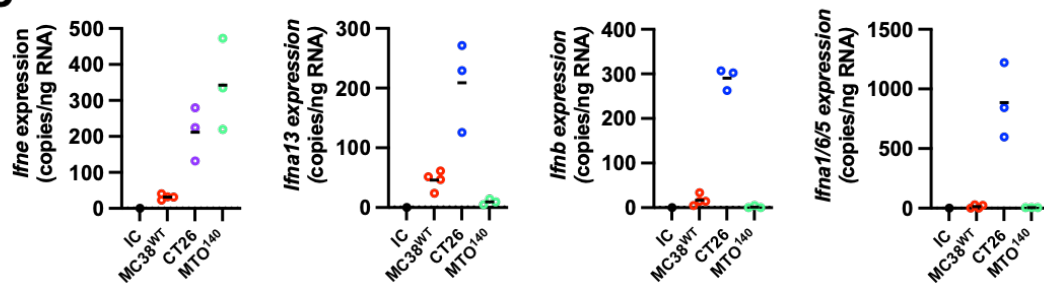
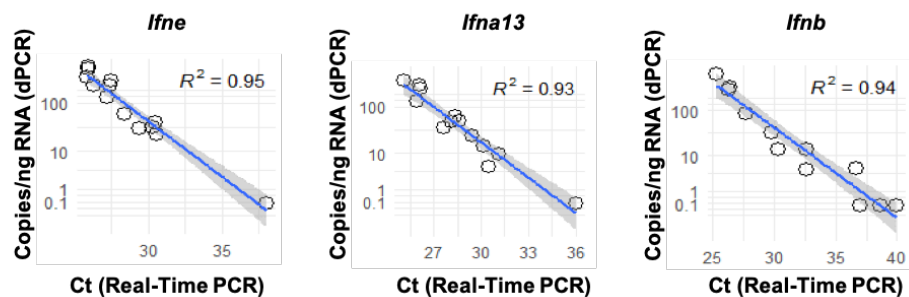
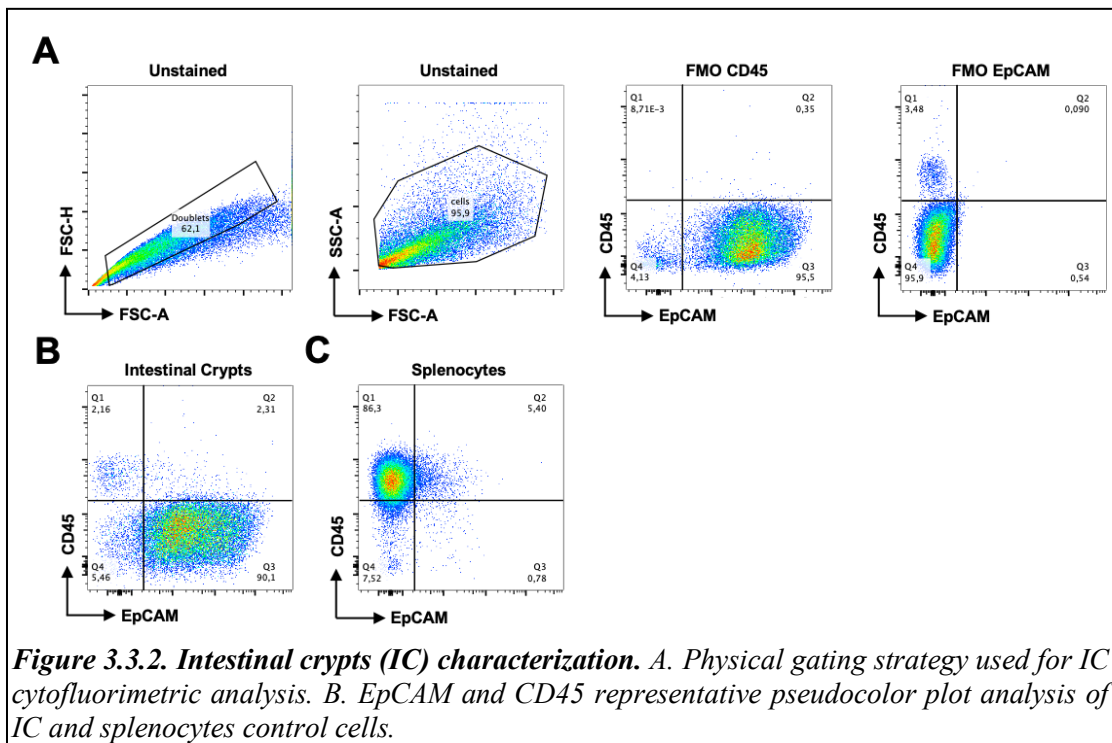
B**C****D**

Figure 3.3.1. CRC cell lines and tumor organoids express type I Interferon subtypes in vitro.
A. Description of cell lines, MTO, and primary cell used. **B.** Type I IFN subtypes expression relative to IC in different cell lines and MTO quantified by real-time PCR, statistical analysis and relative significance described in figure. **C.** Digital PCR analysis of absolute expression of depicted type I IFN subtypes on selected samples from B. **D.** Correlation analysis between real-time PCR and digital PCR results.

expression of epithelial marker (Figure 3.3.2. B), compared to splenocytes sample used as positive control for CD45 expression (Figure 3.3.2. C).

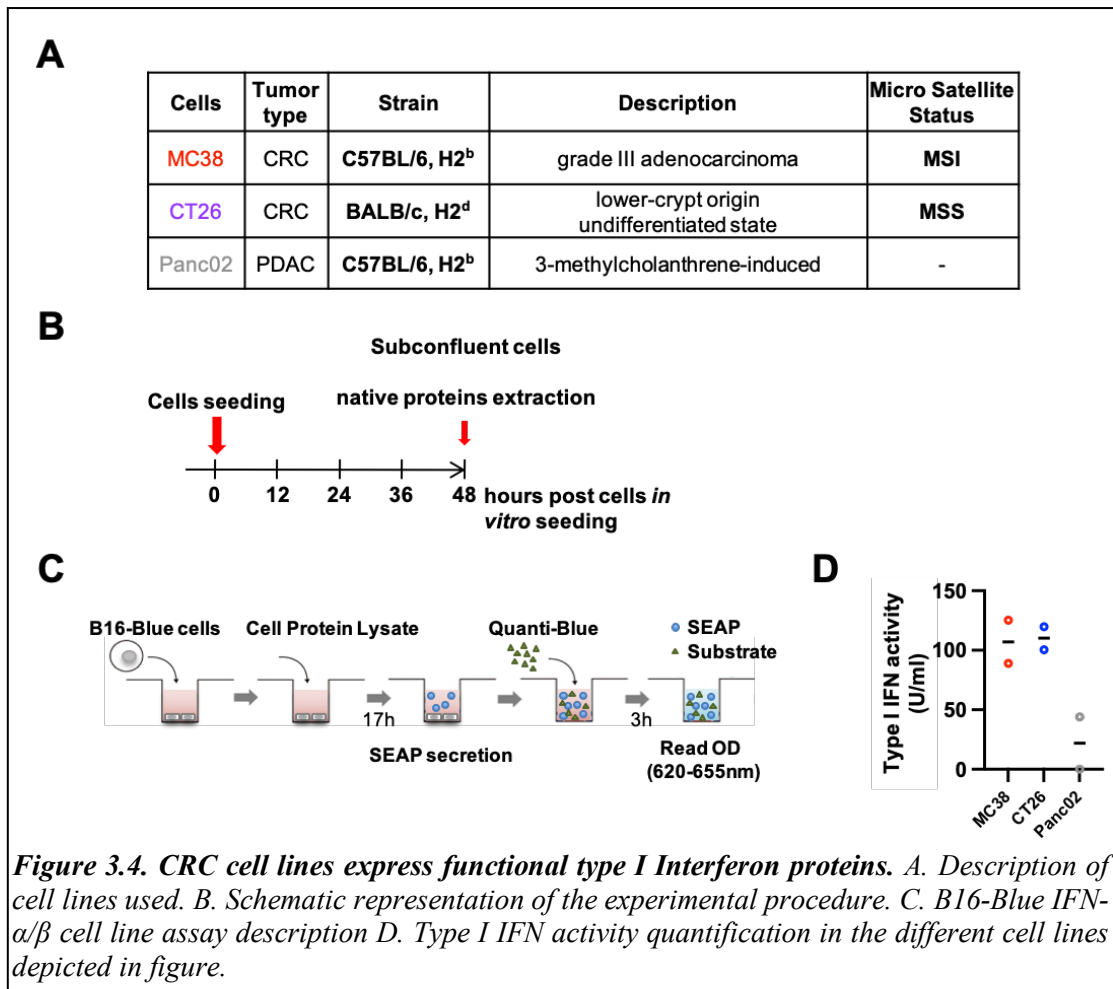
We then analyzed type I IFN subtypes expression in the different cells and organoids and we detected upregulation of *Ifne* transcript in all the three CRC cells, with significant and more marked levels in CT26 and MTO cells, whereas Panc02 cells did not show upregulation of this transcript (Figure 3.3.1. B left). Similar results were obtained for *Ifna13* and *Ifnb* transcripts levels, that showed upregulation in CT26 and MC38 CRC cells, and reduced expression in Panc02 PDAC cell line (Figure 3.3.1. B center, right). MTO did not display upregulation of these type I specific subtypes compared to the significant expression observed for *Ifne*. To validate these results using an independent, more sensible assay, able to quantify transcripts levels in an absolute way, we performed a Digital PCR (dPCR) analysis of a selection of the same samples. dPCR analysis similarly demonstrated an upregulation of different type I IFN subtypes in CRC cell lines and tumor organoids (Figure 3.3.1. C). Importantly, correlation analysis of real-time and dPCR results showed a direct proportion between the two (Figure 3.3.1. D), reinforcing the findings obtained with real-time PCR. These results demonstrate that CRC cell lines and organoids constitutively produce type I IFN subtypes *in vitro* and suggest that tumor cells contribute to the endogenous IFNs observed in metastatic liver. Furthermore, they



show that a prototypical PDAC mouse cell line capable of metastasizing to the liver does not have the same expression pattern, raising the question of whether this phenotype may contribute to sensitivity to exogenous type I IFN treatments.

3.4 CRC cell lines express functional type I Interferon proteins

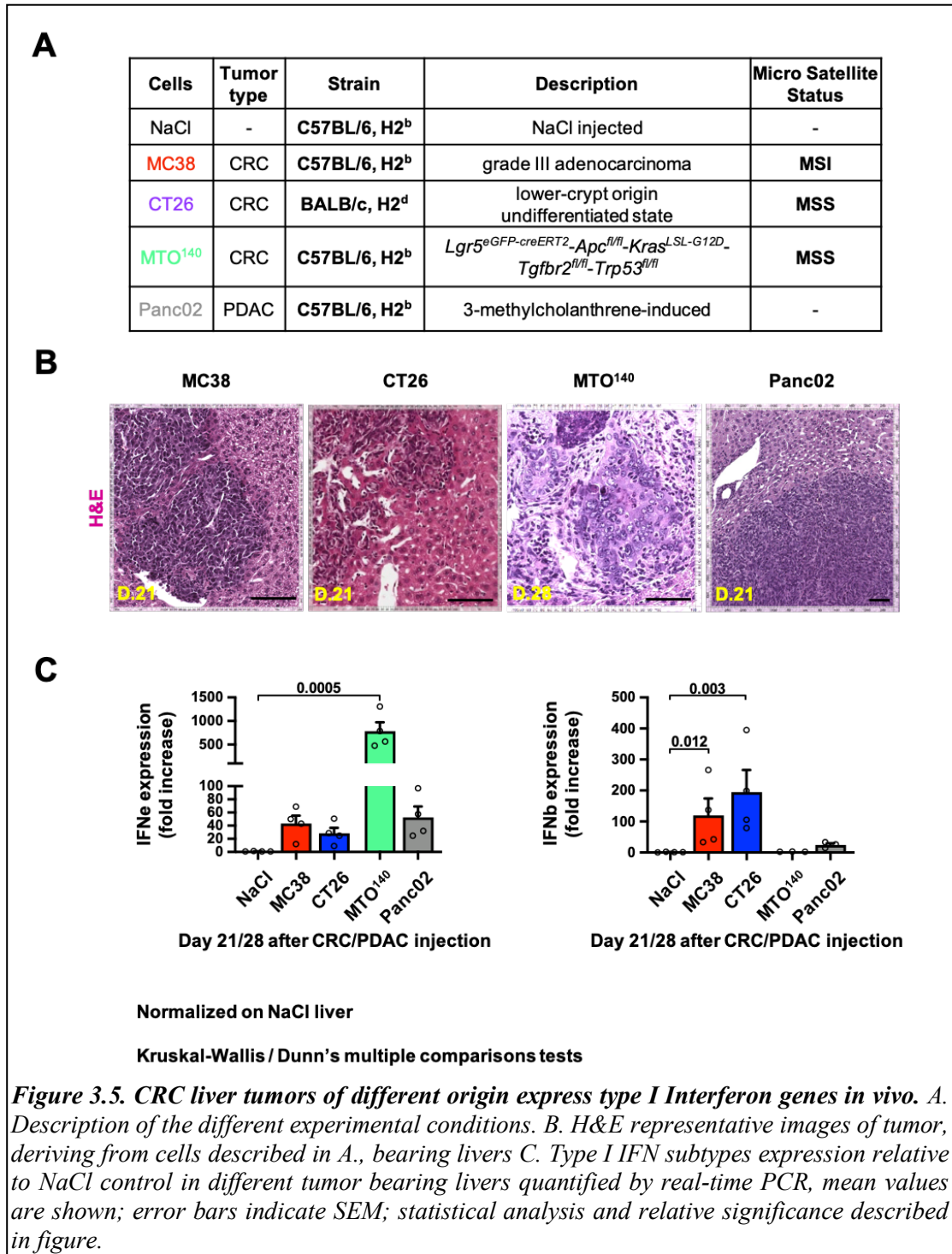
To determine whether the observed transcriptional activity of type I interferons correlates with the production of functional IFN proteins, we performed a functional assay using native protein extracts obtained from cell lines grown *in vitro*. To this end we analyzed type I IFN protein expression by MC38 and CT26 CRC cell lines grown *in vitro*, that we compared to the type I IFN non expressing Panc02 PDAC cells (Figure 3.4. A). Cell lines were seeded and 48 hours later, when they reached sub confluent condition, were harvested using a buffer that allow functional protein conservation (Figure 3.4. B). Native protein extracts were used to stimulate B16-Blue IFN- α/β cell line (InvivoGen) in exponential growth phase. This engineered commercial cell line was stably transfected



with a SEAP reporter gene under the control of the IFN- α/β -inducible ISG54 promoter enhanced by a multimeric ISRE. These cells, once stimulated with murine IFN- α or IFN- β were able to produce and release SEAP in the supernatant, the level of which can be determined using a SEAP detection medium (Figure 3.4. C). Using this assay to screen native protein extracts from MC38 and CT26 CRC cells and PANC02 controls, we showed that CRC cells do produce detectable levels of functional type I IFN proteins whereas Panc02 PDAC cells showed a 100-fold reduced type I IFN proteins expression, with levels on the edge of the detection level (Figure 3.4. D), compatible with the results obtained by qPCR. Again, these results confirm the ability of MC38 and CT26 CRC cell lines to express type I IFNs that retain the capacity to stimulate biological signals and functions, compared to Panc02 PDAC cells that show a very low expression of these cytokines, adding evidences of the possible contribution of CRC cells to endogenous type I IFNs expression in the tumor microenvironment. Finally, ongoing experiments will extend our observation to the other cell lines and tumor organoids.

3.5 CRC liver tumors of different origin express type I Interferon genes *in vivo*

To extend our *in vitro* observations, we next analyzed the livers of mice bearing metastases obtained with the same cell lines and MTOs analyzed above *in vitro*. To this end, we took advantage of the same panel of CRC cell lines, organoids and PDAC Panc02



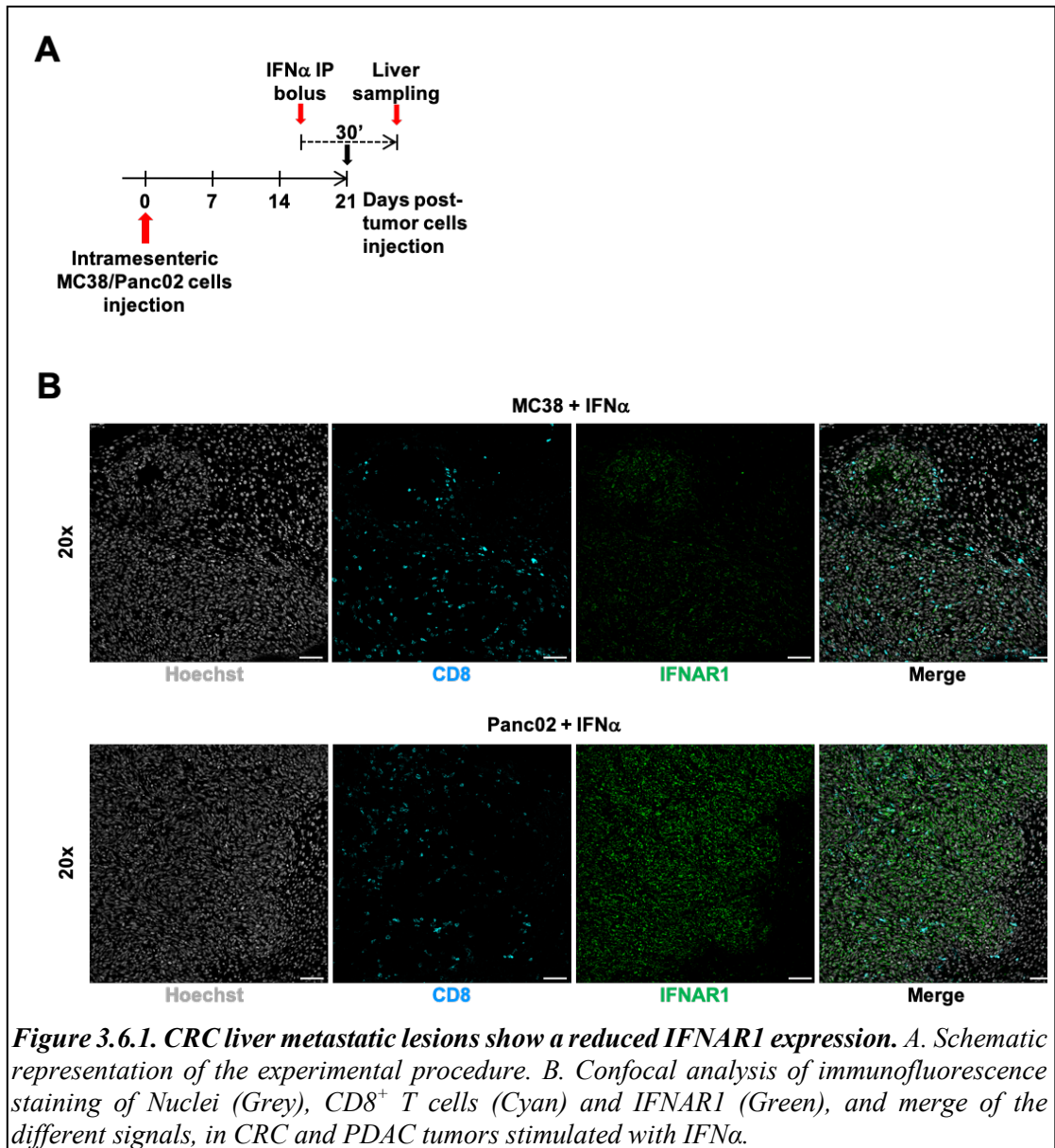
cells previously analyzed *in vitro*. Tumor lesions from different CRC and PDAC were collected at the time points when overt liver lesions were observed, as assessed by H&E staining (Figure 3.5. B).

In this setting IFNs transcriptional levels obtained in the different tumor types were normalized on the level obtained from saline injected control mice (Figure 3.5. A).

Analysis of the different metastatic lesions again revealed the presence of two type I IFN subtypes expressed in CRC cells (*Ifne* in MTO liver metastases and *Ifnb* in MC38 and CT26 liver metastases (Figure 3.5. C). Panc02 PDAC cells showed almost undetectable *Ifnb* expression, whereas *Ifne* expression appears to be more pronounced (Figure 3.5. C). The results again point to the peculiarity of CRC liver tumors to produce/induce the expression of endogenous type I IFN subtypes when growing in the hepatic microenvironment. Again, ongoing experiments will extend our observation to the other cell lines and tumor organoids.

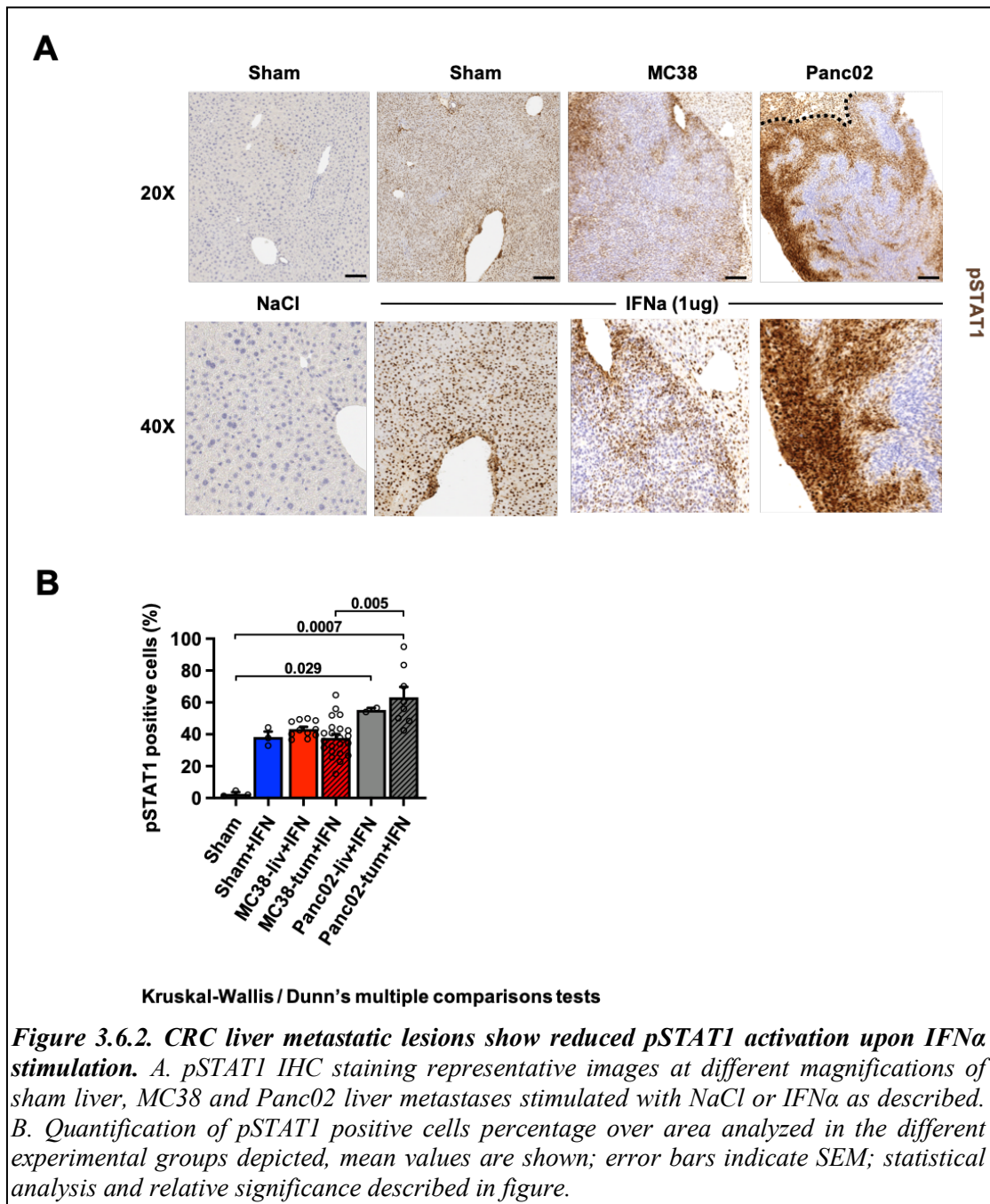
3.6 CRC liver metastatic lesions show a reduced IFNAR1 expression and IFN activation capacity

After observing that CRC cell lines and tumor organoids express type I IFNs *in vitro*, and that liver metastatic CRC tumors express type I interferons and IRGs, including checkpoint inhibitors, and that the tumor milieu is characterized by the expression of various inflammatory cytokines and genes related to IFNAR1 degradation, we investigated the status of the interferon receptor in CRC liver lesions. In this context, it has been reported that all of the above features can modulate the stability of IFNAR1 on the surface of cells that form the tumor inner and marginal edge compartments, thereby



affecting the ability of immune cells to respond to growing tumors and consequently inducing immune deregulation and/or develop resistance to IFN-based therapies (Katlinski *et al*, 2017; Snell *et al*, 2017; Locquenghien *et al*, 2021).

To characterize the status and the functional capacity of the Interferon $\alpha\beta$ -receptor and in particular of the IFNAR1 subunit in the liver of tumor metastases bearing mice, we perform an *in vivo* functional assay, to define the capacity of tumor components to respond to IFN α therapy as previously reported (Lin *et al*, 2016). Briefly, 21 days after



tumor challenge, when metastases were in their exponential phase of growth and were stably established in the liver, we treated mice with a high dose of IFN α (1 μ g) by intraperitoneal (IP) injection. To this end we used mice bearing MC38 (CRC) and Panc02 (PDAC) liver metastases (Figure 3.6.1. A). Thirty minutes after IFN administration, mice were killed and their livers collected for analysis. First, we performed immunofluorescence (IF) staining with antibodies specific for CD8 and IFNAR1 expression. Results showed a comparable low level of CD8⁺ in the tumor microenvironment of the two tumors and importantly a reduced expression of IFNAR1 in CRC liver lesions compared to PDAC (Figure 3.6.1. B).

Finally, we tested the ability of administered IFN α short term dose to activate the tumor microenvironment in this deregulated condition. To this end we performed an IHC staining for phosphorylated STAT1 (pSTAT1) protein, as a direct target that is phosphorylated after engagement of the Interferon $\alpha\beta$ -receptor by IFN α 1 (Lin *et al*, 2016). Consistent with the results described above, and as a consequence of the different densities of IFNAR1 surface expression in the tumor microenvironment, we observed a significant reduction of CRC tumors responding to IFN α 1, while livers with PDAC tumors (Figure 3.6.2. A) maintained a higher capacity to respond. Morphologically, CRC tumors endothelial cell lining hepatic vessel and some cells of the tumoral edge seem to retain the ability to respond to short term IFN α doses. Differently, PDAC tumor microenvironmental cells demonstrate a higher degree of pSTAT1 activation, with a broader responsive tumoral edge, that include also PDAC tumor inner mass (Figure 3.6.2. A lower panel). These observations reflect the significant increase of pSTAT1 positive cells percentage in PDAC compared to CRC tumor area obtained after the quantification of IHC staining (Figure 3.6.2. B).

The sum of these evidences corroborates the hypothesis that endogenous IFNs producing CRC tumors growing in the liver downregulate IFNAR1, inducing immune deregulation and acquiring resistance to IFN based therapies. Additional experiments aimed at defining the exact cell population/s responding to IFN α within the tumor microenvironment are ongoing and will represent a valuable indication of the cells capable to maintain surface expression of IFNAR1 in the different tumor types.

3.7 CRC and PDAC liver metastases show different sensibility to IFN based therapeutic approaches

To define the different response of CRC and PDAC cell lines to therapeutic continuous IFN treatment, and to define if the production of endogenous IFNs by tumors can correlate to IFN treatment response, we set up an IFN α trial comparing the two metastatic tumors. As we previously described, when administered to CRC tumor bearing mice, the IFN α therapeutic approaches, although inducing intrahepatic IRG induction, failed to induce significant anti-metastatic protection compared to control treated mice (Figure 3.1. C-E). To overcome the refractoriness of CRC metastatic tumors to IFN α therapy we planned to add to the trial a further treatment using a type I IFN subtype with high *in vivo* potency. As mentioned above, resistance mechanisms include, among others, the downregulation of IFNAR1 by CRC and components of the tumor microenvironment, including tumor infiltrating leukocytes and tumor specific T cells, and in this regards the use of IFN isoforms with high *in vivo* potency could be effective as consequence of less dependency on IFNAR1 cell surface densities. We chose IFN α 11 because in previous experiments we showed that between different murine type I IFN subtypes with distinctive *in vitro* potencies (IFN α 1, IFN α 4, IFN α 11, IFN β and IFN- ζ /limitin) IFN α 11 administered by prolonged intraperitoneal release stimulated the most potent intrahepatic IRGs induction (Figure 1.19. Introduction).

To perform the therapeutic trial, age and sex matched C57BL/6 mice were injected intra-mesenterically with MC38 or Panc02 cell lines, seven days after were randomized in the different experimental groups and were implanted with MOP containing either NaCl, IFN α 1 or IFN α 11 at a dose of 150 ng/day, for about 28 days. To determine if

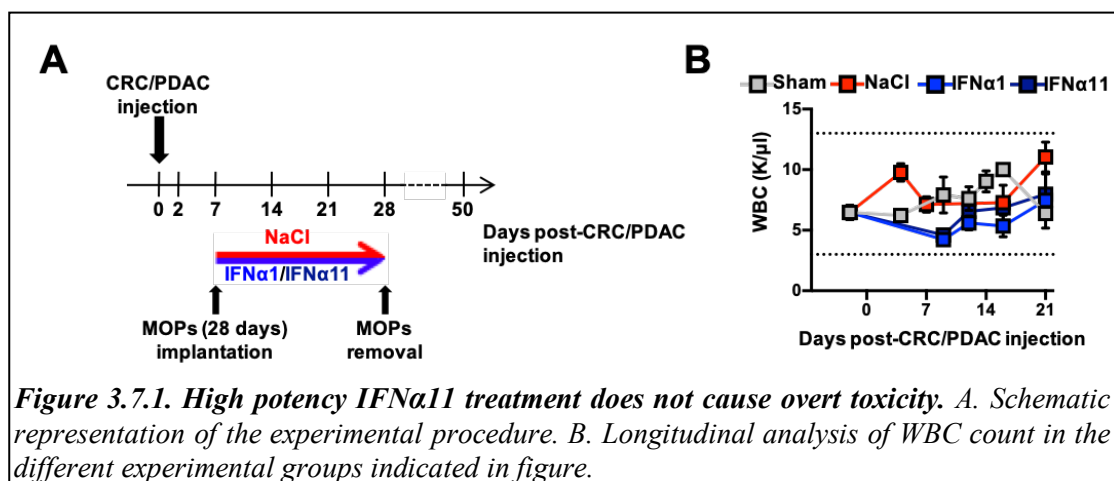
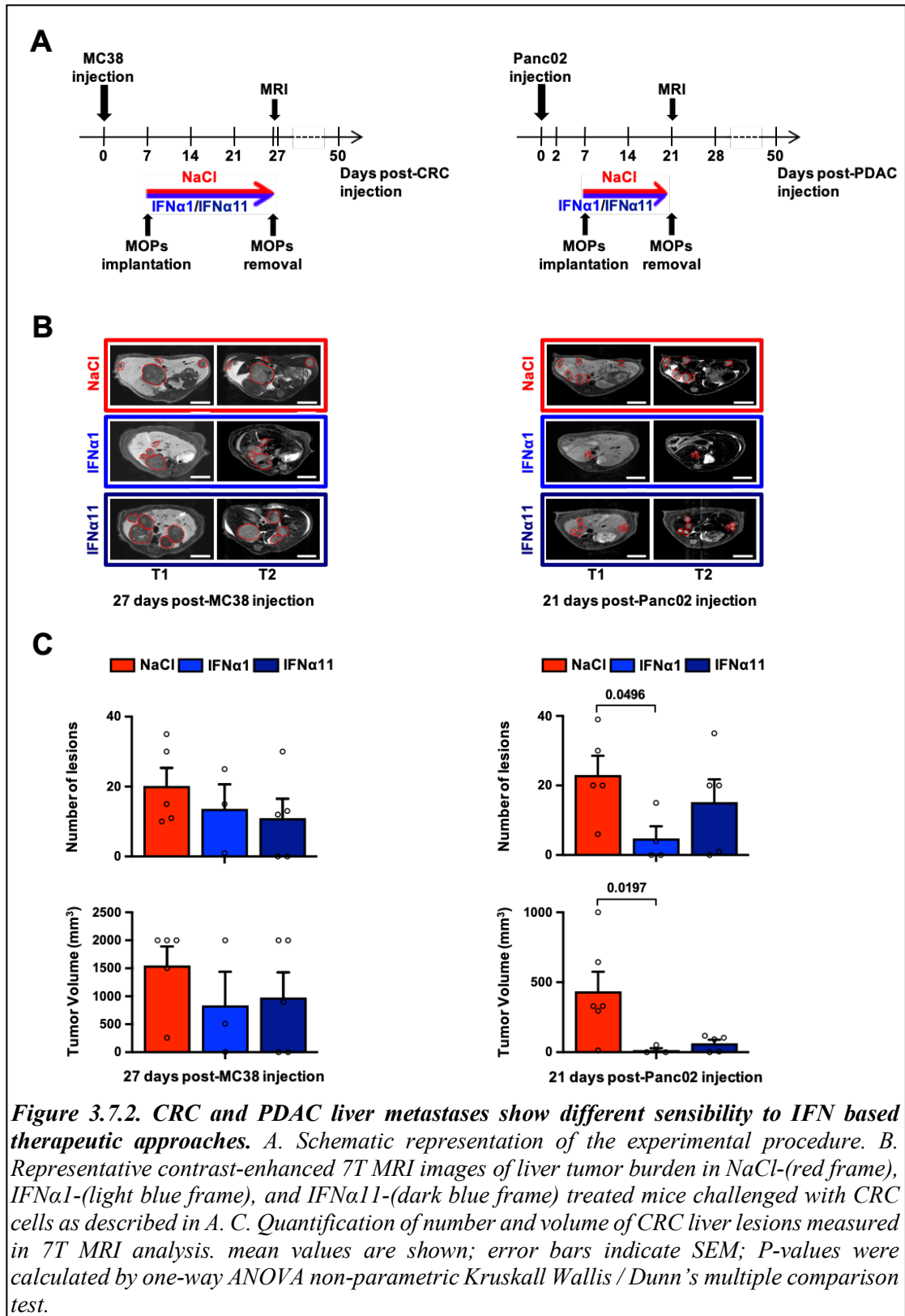


Figure 3.7.1. High potency IFN α 11 treatment does not cause overt toxicity. A. Schematic representation of the experimental procedure. B. Longitudinal analysis of WBC count in the different experimental groups indicated in figure.

continuous high potency IFN treatment can cause signs of hematopoietic toxicity all mice were followed and longitudinal peripheral blood analyses for the count of white blood



cell (WBC) were performed as indicated in Figure 3.7.1. A. The data depicted in Figure 3.7.1. B showed a reduction and a subsequent recovery in circulating WBC of both IFN α 1/11 treated animals, that returned to levels comparable to that of control groups afterwards. Importantly, the reduction observed in treated animals was still in the range of WBC normality, showing no overt toxicity for high potency IFN α 11 treatment.

To assess if IFN α 1 or IFN α 11 therapy resulted in a reduced tumor burden of treated mice 21 or 28 days after tumor challenge, depending on the considered tumor model (Figure 3.7.2. A), mice were analyzed by 7T MRI to quantify liver tumor burden. Neither low potency IFN α 1 or high potency IFN α 11 treatment showed the capacity to reduce tumor lesions number and volume in CRC bearing treated animals (Figure 3.7.2. B-C left), whereas prolonged low potency IFN α 1 therapeutic treatment showed a significant reduction of both metastatic lesions number and volume in Panc02 challenged animals (Figure 3.7.2. B-C right). Of note, in this setting high potency IFN α 11 interferon treatment resulted in a reduced tumor burden that however did not reach significant values, and in general did not demonstrate increased efficacy compared to low potency IFN α 1 (Figure 3.7.2. C right). These results demonstrate that in a deregulated microenvironment IFN subtype potency is not functional to treatment success, suggesting that availability of IFNAR1 in the tumor microenvironment controls success of therapy independently of IFN subtype potency. Moreover, results obtained in Panc02 model suggest that intrinsic tumor type features can dictate IFN therapeutic success, as the same IFN subtype (IFN α 1) treatment displayed profoundly different results based on the tumor type, no matter the potency of type I IFN subtype used.

3.8 CRC and PDAC cell lines display different cell autonomous susceptibility to IFN stimulation

In the attempt to clarify different possible cell autonomous susceptibility to type IFN stimulation between MC38 and Panc02 cells, we performed *in vitro* analysis on cell proliferation (a way to define the direct anti-proliferative capacity of IFN α (Piehler *et al*, 2012)) and IRGs upregulation in the presence of IFN α . As described in Figure 3.8. A (upper panel) MC38 and Panc02 cell line were grown in the presence of increasing doses of IFN α or in the presence of Vehicle as control. Both cell lines displayed a modest reduction of cell proliferation (ranging from near 5 to a maximum of 40 percent of proliferation inhibition) and only the highest dose of 10^5 pg/ml of IFN α resulted in a significant reduction of cell proliferation in Panc02 cell lines compared to Vehicle treated control (Figure 3.8. A). Importantly, the dose of 200 pg/ml of IFN α , that reflects the peak of IFN α blood concentration observed in mice treated with continuous releasing MOP (Figure 1.14. Introduction), did not influence the proliferation capacity of the two cell lines, suggesting that these IFN α doses did not directly affect anti-proliferation mechanisms. Seminal work from Schreiber and colleagues divide IFN activity on cells in two categories based on the relative receptor binding strengths and dissociation rates exerted by different cytokine concentration. In this light, ‘robust’ and ‘tunable’ IFN effects were described (Schreiber & Piehler, 2015), that possess different time of induction, biological functions and importantly different cell susceptibility. For example, antiviral state is the prototypic ‘robust’ activity of IFN, as is observed in all cell lines after few hours of activation using picomolar IFN concentration and is maintained even after subsequent removal of IFN. Differently, antiproliferative IFN activity is designed as ‘tunable’, describing activities that are cell-type specific, strongly dependent on the cellular context, requiring about 1000-fold higher IFN concentrations, continuous receptor activation over prolonged periods (days), and is susceptible to the concentration of cell surface receptors (Schreiber & Piehler, 2015).

Antiproliferative ‘tunable’ activity of IFN seems to be comparably reduced in the two cell lines, with the exception of the reduced proliferation observed in Panc02 cells at the highest IFN α concentration tested. To investigate the possible different susceptibility of MC38 and Panc02 cell lines to lower IFN α concentration, we analyzed the induction of

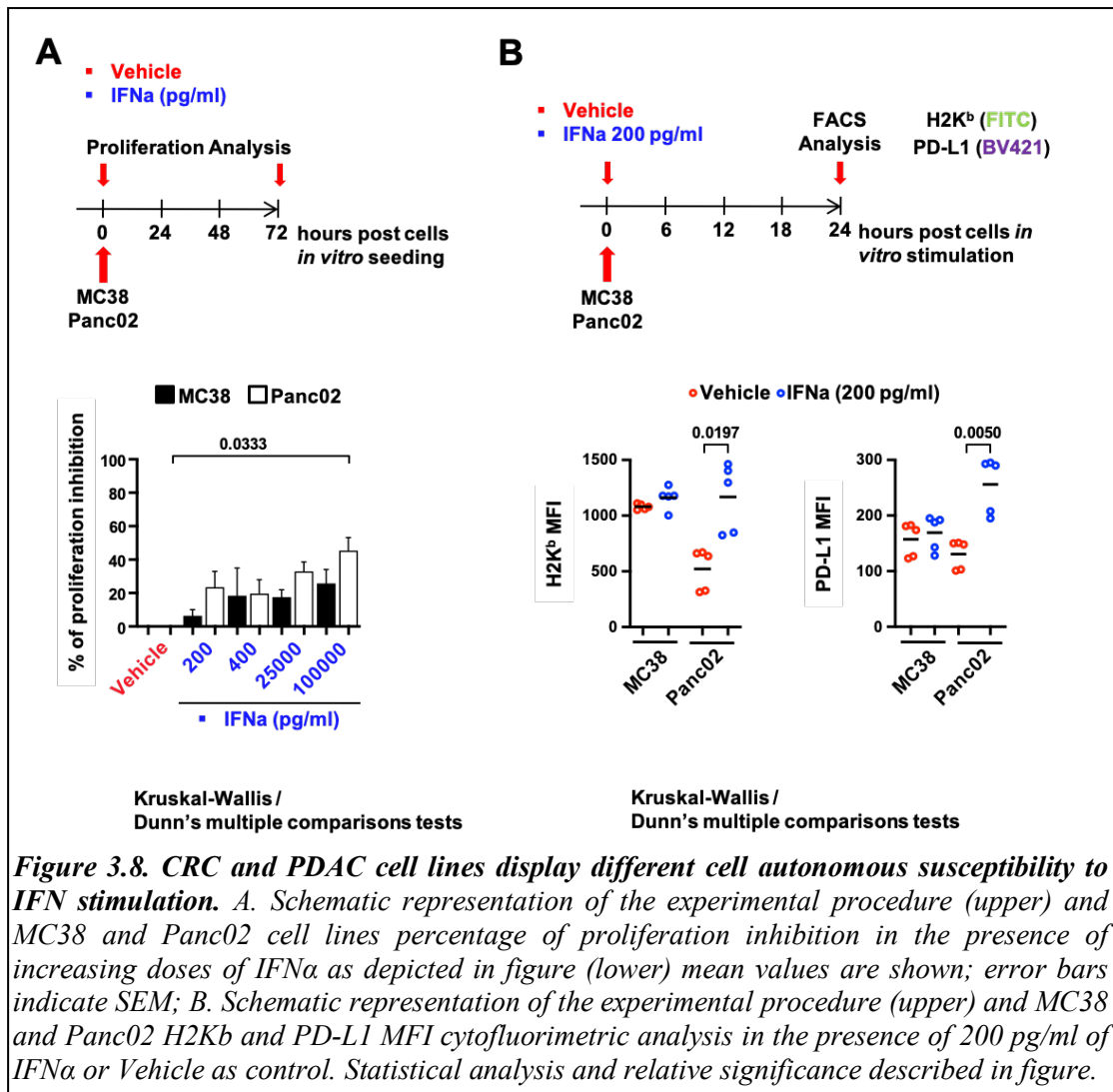


Figure 3.8. CRC and PDAC cell lines display different cell autonomous susceptibility to IFN stimulation. A. Schematic representation of the experimental procedure (upper) and MC38 and Panc02 cell lines percentage of proliferation inhibition in the presence of increasing doses of IFN α as depicted in figure (lower) mean values are shown; error bars indicate SEM; B. Schematic representation of the experimental procedure (upper) and MC38 and Panc02 H2K β and PD-L1 MFI cytofluorimetric analysis in the presence of 200 pg/ml of IFN α or Vehicle as control. Statistical analysis and relative significance described in figure.

two prototypical IRGs (H-2K/D β and PD-L1) by flow cytometry analysis in cells stimulated with 200 pg/ml IFN α for a short period of time (24 hours), activity that can be considered ‘robust’ (Figure 3.8. B). In this scenario stimulated MC38 cells did not show a different expression of the two IRGs in stimulated versus control samples. Differently, Panc02 cells stimulated with 200 pg/ml of IFN α upregulated significantly both surface proteins (Figure 3.8. B), suggesting a different cell autonomous ‘robust’ activity and capacity of these cells to respond to IFN α compared to the MC38 cell line.

In our view, the increased capacity of PDACs cells to respond to low IFN α doses compared to MC38 CRC cells, represent a proof of susceptibility to the ‘robust’ IFN effect on these cells, that could explain the differential efficacy of IFN therapy in Panc02 tumor liver bearing mice. Importantly the different IFN therapy and *in vitro* ‘robust’

activity susceptibility are associated with a different expression of type I endogenous IFN both *in vivo* and *in vitro* by MC38 and Panc02 tumors.

3.9 Pharmacological IFNAR1 degradation inhibitors reduce CRC metastases growth and improve survival

After the finding that CRC liver metastatic microenvironment is characterized by the production of endogenous type I IFNs, display a reduced expression of IFNAR1 and resistance to IFN-based therapies, we hypothesized that strategies targeting IFNAR1 downregulation using selected approaches can overcome IFN resistance, both in the context of endogenous IFN expression and exogenous IFN therapeutic treatment.

It has been reported that both pharmacological and genetic strategies able to counteract IFNAR1 downregulation, in particular in CD8⁺ tumor specific T cells, are effective in murine models of CRC tumors (Katlinski *et al*, 2017). To this end, we started to characterize the impact on CRC tumor growth of a combined pharmacological IFNAR1 stabilization strategy using p38 and PKD inhibitors, kinases responsible of ligand-dependent and independent IFNAR1 phosphorylation and subsequent degradation (Zheng *et al*, 2011; HuangFu *et al*, 2012; Katlinski *et al*, 2017). Indeed, these kinases were reported to be activated in CRC tumors (Zheng *et al*, 2011; HuangFu *et al*, 2012; Katlinski *et al*, 2017).

To this end we took advantage of the p38 inhibitor LY2228820 (LY) used in combination with the SD-208 (SD) PKD inhibitor (Katlinski *et al*, 2017). The use of pharmacological inhibitors of IFNAR1 degradation is useful to study the actual efficacy of combination therapy and thus its possible clinical application. We designed an experimental trial enrolling animals that have a wild-type expression of IFNAR1 receptor (both C57BL/6 and CB6 F1) (WT) in LY/SD treated or Vehicle treated control arms and two control arms (LY/SD combination treated or Vehicle control treated) using animals that are genetically knock out for IFNAR1 (IFNAR1-KO), in which the type I interferon receptor is constitutively deleted in all cells (Figure 3.9.1. A). These last two arms were used to control possible direct effects on IFNAR1 expressing CRC cells of the two drugs, as host tumor stroma resulting from IFNAR1-KO mice should not benefit of IFNAR1 stabilization and possible growth inhibitory effects would come from direct receptor stabilization and/or chemical induced toxicities on CRC cells. To perform the trial, age and sex matched WT and IFNAR1-KO mice were injected intra-mesenterically with MC38 cells and seven days after tumor challenge were randomized in the different

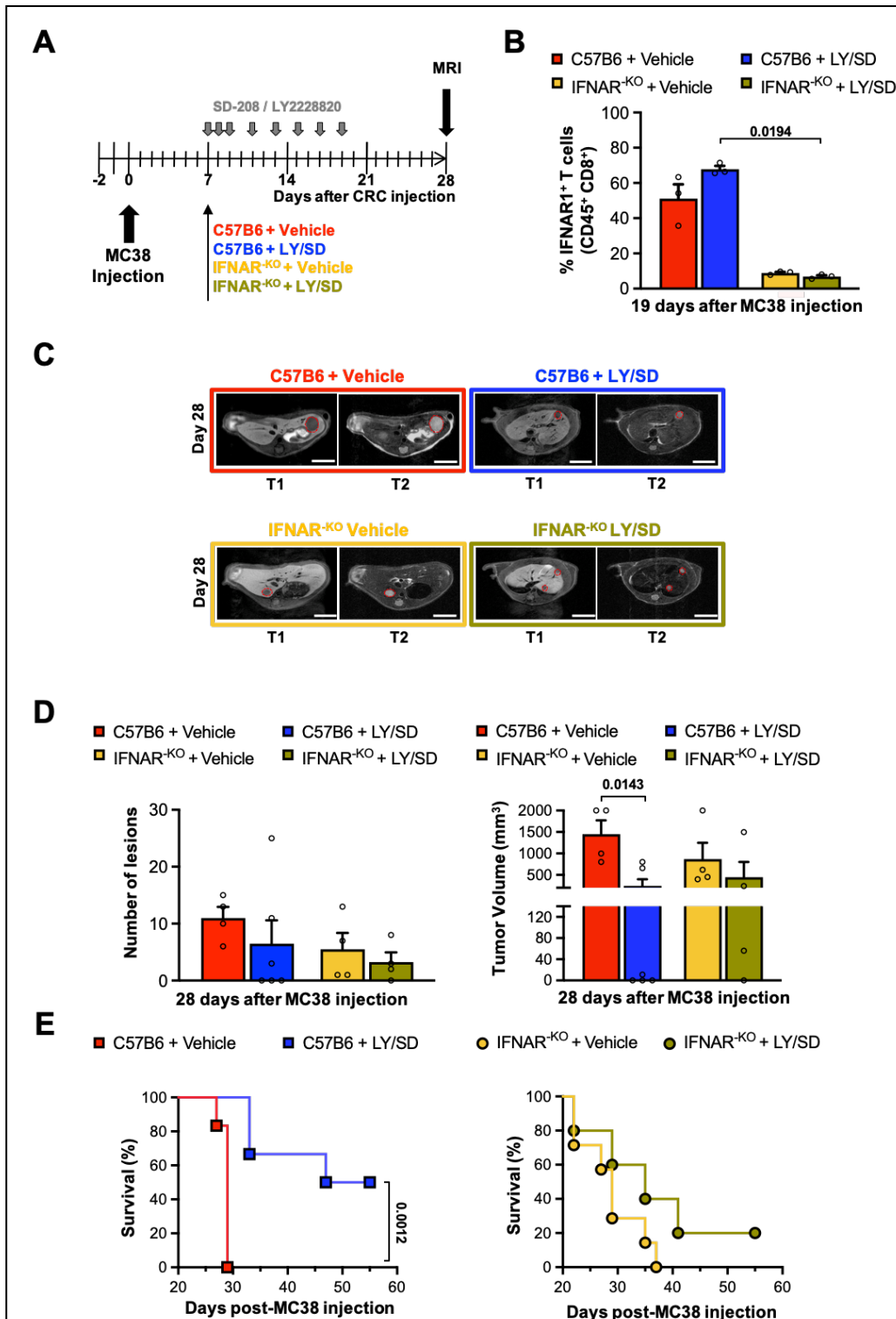
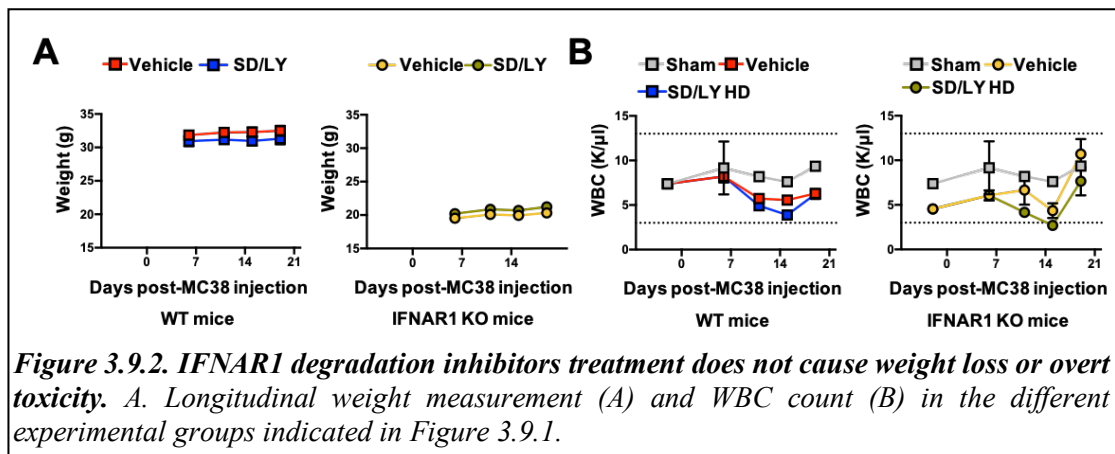


Figure 3.9.1. Pharmacological IFNAR1 degradation inhibitors reduce CRC metastases growth and improve survival. *A.* Schematic representation of the experimental procedure *B.* WBC counts 19 days after CRC challenge in the different experimental groups *C.* Representative contrast-enhanced 7T MRI images of liver tumoral burden in wild type NaCl- (red frame), LY/SD- (light blue frame) and IFNAR1-KO NaCl- (yellow frame), LY/SD- (green frame) treated mice challenged with CRC cells as described in *A.* *D.* Quantification of number and volume of CRC liver lesions measured in 7T MRI analysis. mean values are shown; error bars indicate SEM; *p*-values were calculated by one-way ANOVA non-parametric Kruskal Wallis / Dunn's multiple comparison test. *E.* Kaplan-Meier survival curves of the indicated groups of mice. *p*-values were calculated by log-rank/Mantel-Cox test.

experimental groups starting the experimental treatment. LY/SD and Vehicle (1% methylcellulose) were administered to experimental animals through oral gavage once a day for three consecutive days and then every other day until day 19 after tumor challenge (Figure 3.9.1. A). To assess possible toxic side effects of LY/SD therapy mice were followed, and longitudinal weight loss and peripheral blood analyses for the count of WBC were performed. No significant reduction of animal weight was observed during the treatment in both WT and IFNAR1-KO groups (Figure 3.9.2. A). WBC levels showed a temporary reduction in LY/SD treated groups after the beginning of the regimen, with a more marked decrease in IFNAR1-KO animals, that however did not exceed normal WBC range, at least in WT animals. WBC levels increased in treated animals over time and reached normal values 19 days after tumor challenge and 12 days after the start of treatment (Figure 3.9.2. B), demonstrating the lack of overt toxicity of LY/SD treatment. IFNAR1 levels on CD45⁺/CD8⁺ peripheral blood mononuclear cells (PBMCs) were analyzed in the last day of combinatorial treatment, to verify the ability of LY/SD regimen to increase IFNAR1 expression on circulating CD8⁺ T cells. Data demonstrated an increased level of expression of IFNAR1 on the surface of circulating cells obtained from WT LY/SD group compared to Vehicle treated group, increase that became significant comparing WT LY/SD to IFNAR1-KO treated groups (Figure 3.9.1. B). Twenty-eight days after tumor challenge, and ten days after SD/LY treatment termination, the four arms of the trial were examined for metastases number and volume using 7T MRI-based analyses (Figure 3.9.1. C). Data obtained from non-invasive MRI analysis showed a significant reduction of tumor volume in WT LY/SD treated animals compared to Vehicle control group, difference that was not observed in IFNAR1-KO treated versus control group, pointing out a significant effect of LY/SD drugs on the IFNAR1 competent WT



tumor microenvironment, even after 10 days after therapy discontinuation. The mild reduction observed in IFNAR1-KO treated group can implicate a partial direct effect on CRC cells, that however still appears to be of lesser amplitude than the direct effect on the tumor microenvironment (Figure 3.9.1. D). Future work using MC38^{IfnarKO} cells (Tran *et al*, 2022) will define the relative importance of direct inhibition of CRC proliferation by LY/SD therapy. Survival analysis of the four groups of animals reflected tumor burden quantification observed at 28 days after tumor challenge. WT treated animals survived significantly longer than control mice, whereas treatment of IFNAR1-KO group did not show a significant survival, albeit to a mild increase (Figure 3.9.1. E), that can denote a mixed effect of the drugs on tumor cells and microenvironment, but underscoring the primary role of stabilization on the latter.

These data underline the importance of stabilizing IFNAR1 receptor in the metastatic microenvironment in order to effectively counteract tumor growth, and again imply the presence of endogenous type I IFN subtypes in the tumor microenvironment.

3.10 OT-I^{SA} effector T cells ACT have an improved therapeutic index, survival/killing advantage and increases tumor CD3⁺ cell recruitment in combinatorial IFN α therapy

Among the various cells that compose the tumor microenvironment, tumor-specific cytotoxic T cells (CTL) have been shown to be highly susceptible to IFNAR1 downregulation, which strongly affects their ability to contain tumor growth (Katlinski *et al*, 2017). For this reason, we investigated the possible positive contribution of IFNAR1 stabilization to adoptive T cell therapy (ACT) strategies for liver CRC metastases in combination with IFN α adjuvant therapies. A panel of experimental trials were designed to dissect the properties and efficacy of IFNAR1 stabilized CTLs. In order to define the role of IFNAR1 stabilization on tumor specific T-cells we started to genetically modify the MC38 CRC cells using a lentiviral vector expressing NGFR-OVA (kindly provided by Prof. Naldini, Figure 3.10.1. A). We chose as experimental model the MC38 ovalbumin (MC38^{OVA}) expressing cells, as a target of effector CD8⁺ T cells specific for the immunodominant epitope of ovalbumin (SIINFEKL) (Figure 3.10.1. B). These cells were derived from transgenic C57BL/6-Tg(TcraTcrb)1100Mjb/J mice (OT-I mice), that contain transgenic inserts for mouse Tcra-V2 and Tcrb-V5 genes, designed to recognize ovalbumin peptide residues 257-264 (SIINFEKL - OVA₂₅₇₋₂₆₄) in the context of H2K^b, resulting in MHC class I-restricted, ovalbumin-specific, CD8⁺

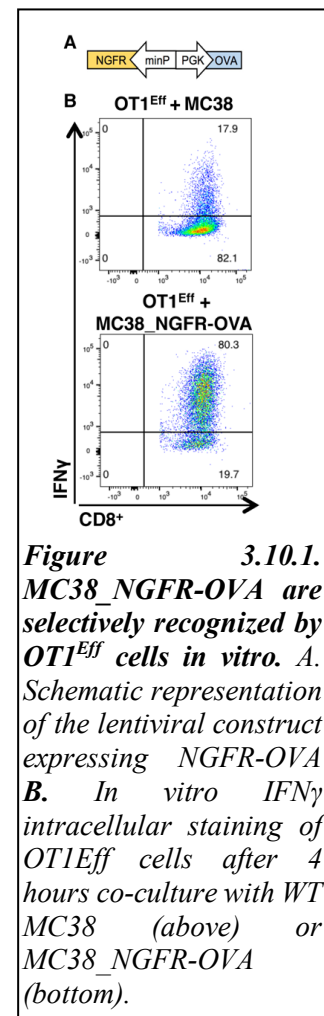
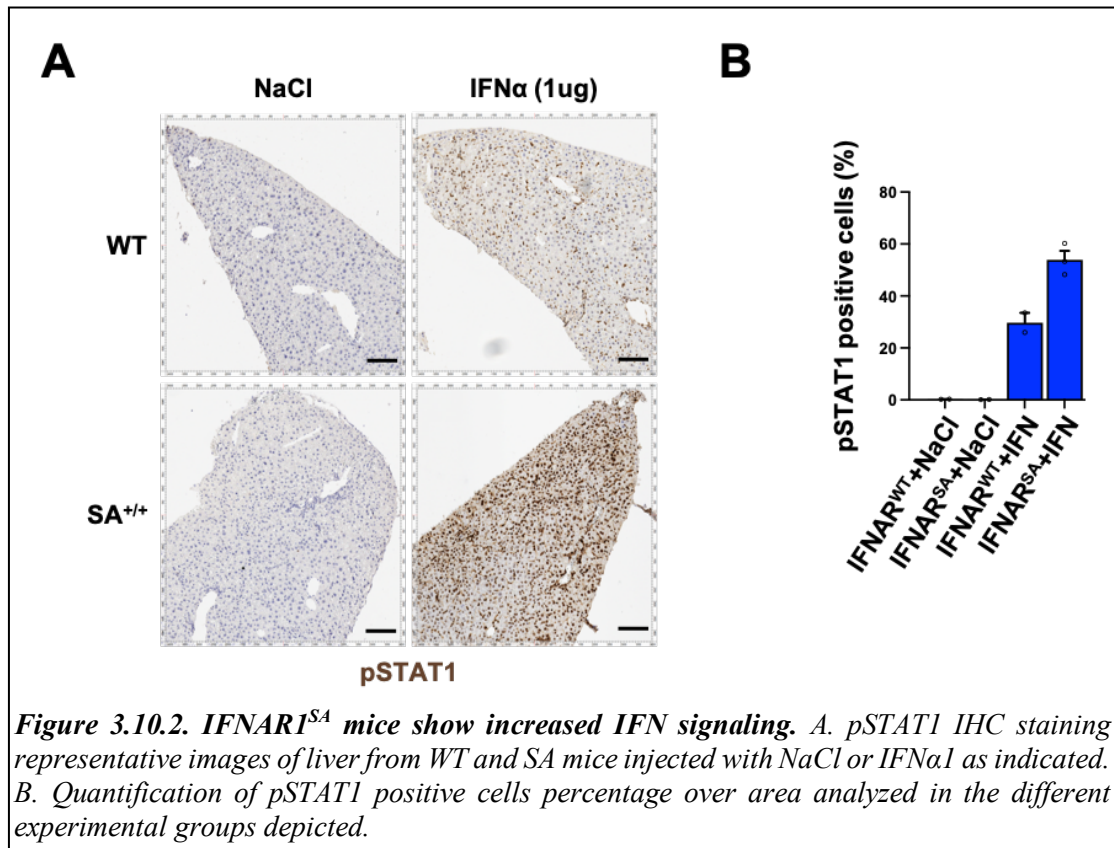


Figure 3.10.1. **MC38_NGFR-OVA are selectively recognized by OT1^{Eff} cells *in vitro*.** **A.** Schematic representation of the lentiviral construct expressing NGFR-OVA **B.** *In vitro* IFN γ intracellular staining of OT1^{Eff} cells after 4 hours co-culture with WT MC38 (above) or MC38_NGFR-OVA (bottom).

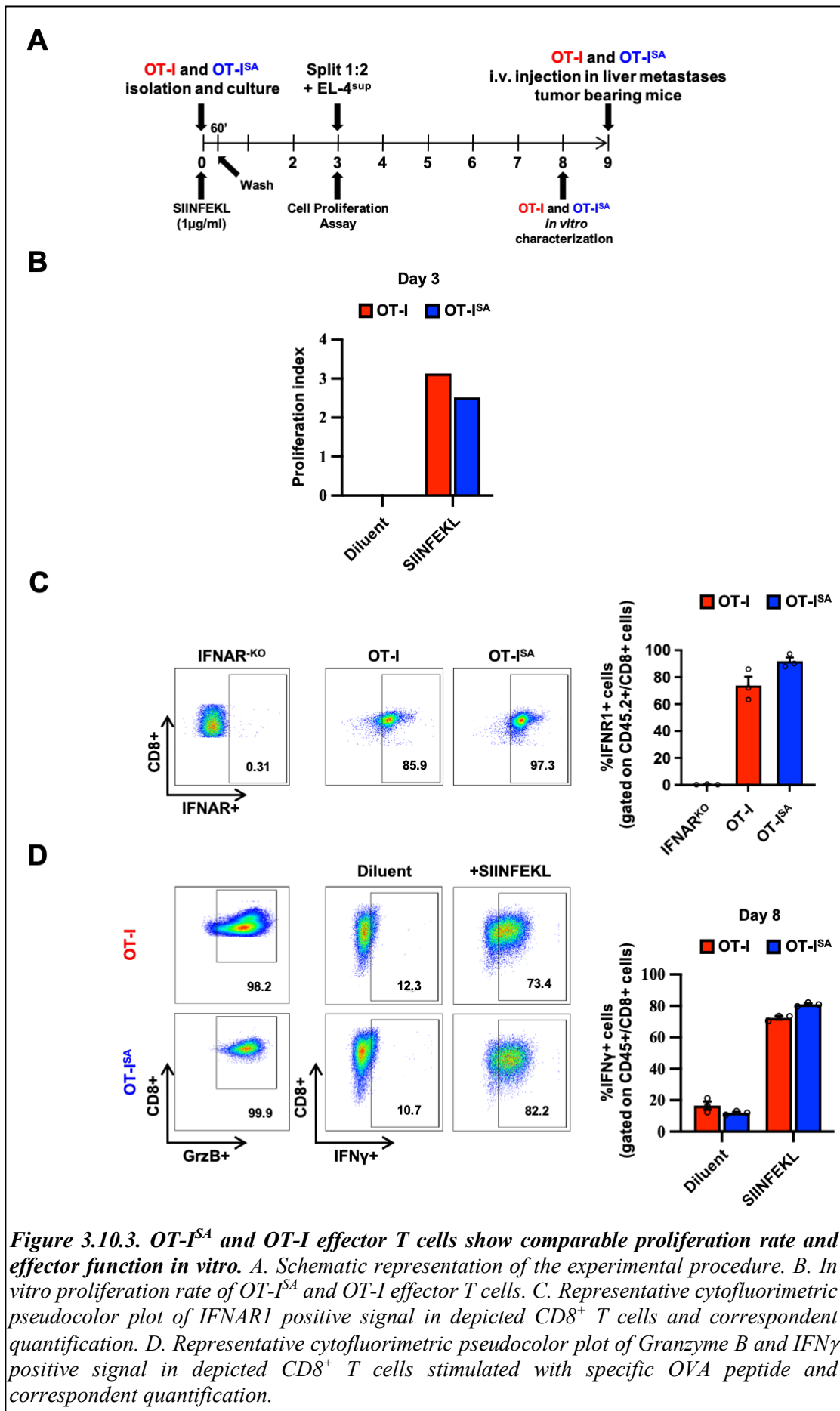
T cells (Hogquist *et al*, 1994). Naïve T cells obtained from OT-I donor splenocytes were subsequently differentiated *in vitro* by stimulation with the SIINFEKL peptide to produce effector T cells (Guidotti *et al*, 2015). In addition, to study the impact of stabilized IFNAR1 on T cells function we took advantage as T cell donor of OT-I IFNAR1^{S526A} (OT-I^{SA}) knock-in mice, that carry a serine to alanine (S526A) mutation in exon 11 of the interferon (alpha and beta) receptor 1 (*Ifnar1*) gene (kindly provided by Serge Fuchs,

Upenn) and originally described in (Bhattacharya *et al*, 2014). S526 is analogous to human Ser535, making this model a useful tool for translational studies. The genetic S526A alteration of the intracytoplasmic part of the IFNAR1 receptor renders it deficient in ubiquitination and degradation, and consequently non-degradable when stimulated with its own ligands. IFNAR^{SA} mice displayed an increased capacity to activate IFN pathway upon stimulation with IFN α , as demonstrated by the increased percentage of pSTAT1 liver positive cells in IFNAR^{SA} mice compared to IFNAR^{WT} mice after the



challenge with a short-term dose of IFN α (Figure 3.10.2).

OT-I and OT-I^{SA} effector CD8⁺ T cells differentiated *in vitro* were then characterized for their proliferation capacity, IFNAR1 membrane expression and activation level, through the measurement of IFN γ produced upon stimulation with target SIINFEKL peptide, as described in Figure 3.10.3. A. To determine whether the presence of nondegradable IFN α / β membrane receptor can cause differences in cell proliferation we analyzed cultured OT-I and OT-I^{SA} cells using commercial CellTrace™ Violet Cell Proliferation Kit (Molecular Probes). Three days of culture after SIINKFEL pulse of CD8⁺ T cells purified from donor splenocytes, cells were analyzed and proliferation index was calculated, showing a comparable proliferation capacity of the two cell types, with

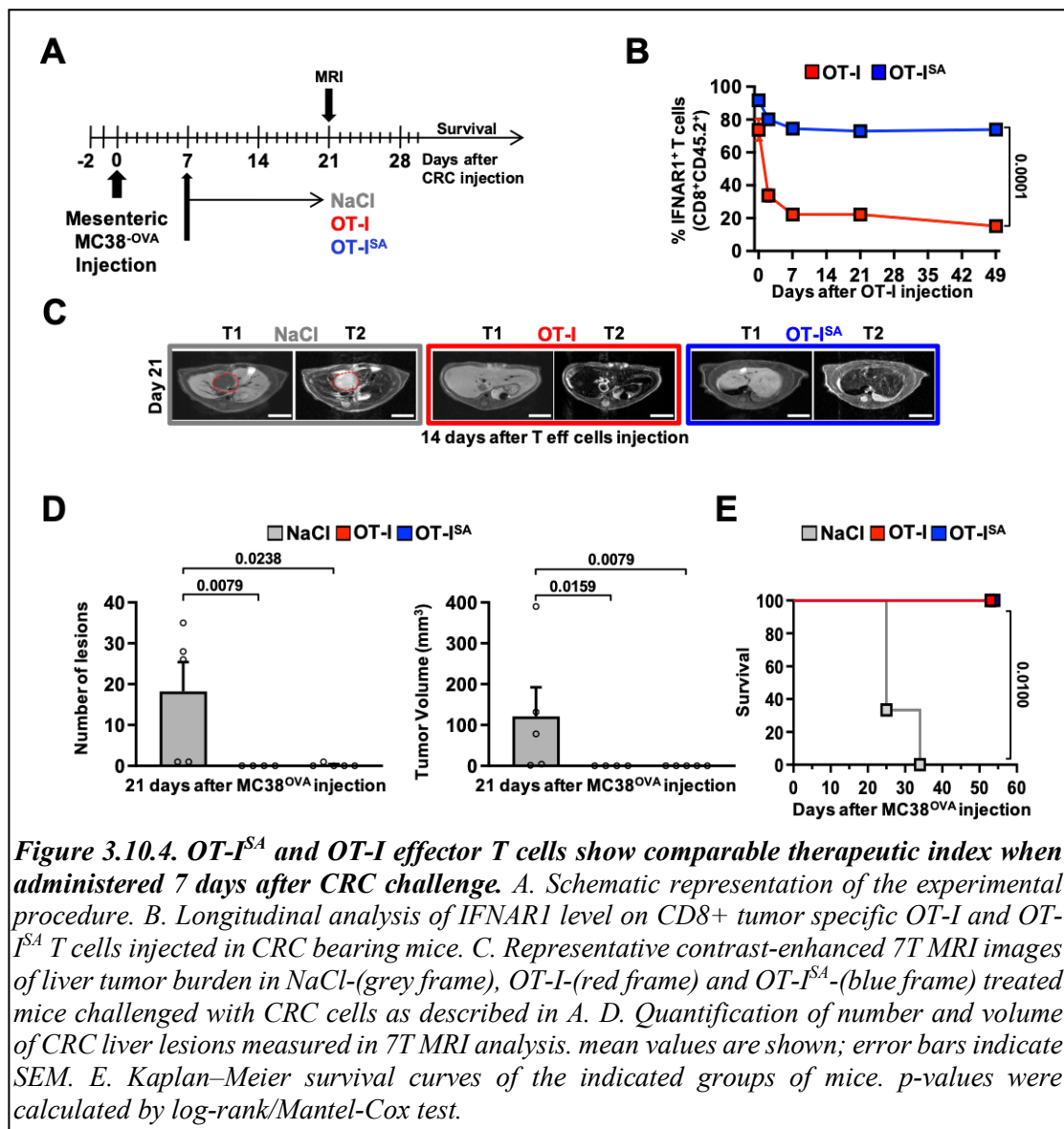


OT-I^{SA} cells displaying a lower but not significant proliferation index, denoting no overt proliferation defects in these cells (Figure 3.10.3. B). Cell membrane IFNAR1 expression levels eight days after *in vitro* differentiation and expansion were measured, showing a slight although not significantly increase in OT-I^{SA} cells (Figure 3.10.3 C). We finally evaluated the ability of OT-I and OT-I^{SA} cells to get activated upon the recognition of SIINKFEL specific peptide. IFN γ levels were measured after 4 hours of peptide stimulation at day 8 of differentiation process. Results from this analysis showed that near 70% of CD8⁺ OT -I cells produce IFN γ after stimulation, percentage that increases, albeit slightly, to near 80% in OT-I^{SA} cells (Figure 3.10.3 D). These characterization data demonstrate comparable *in vitro* properties in the two cell types.

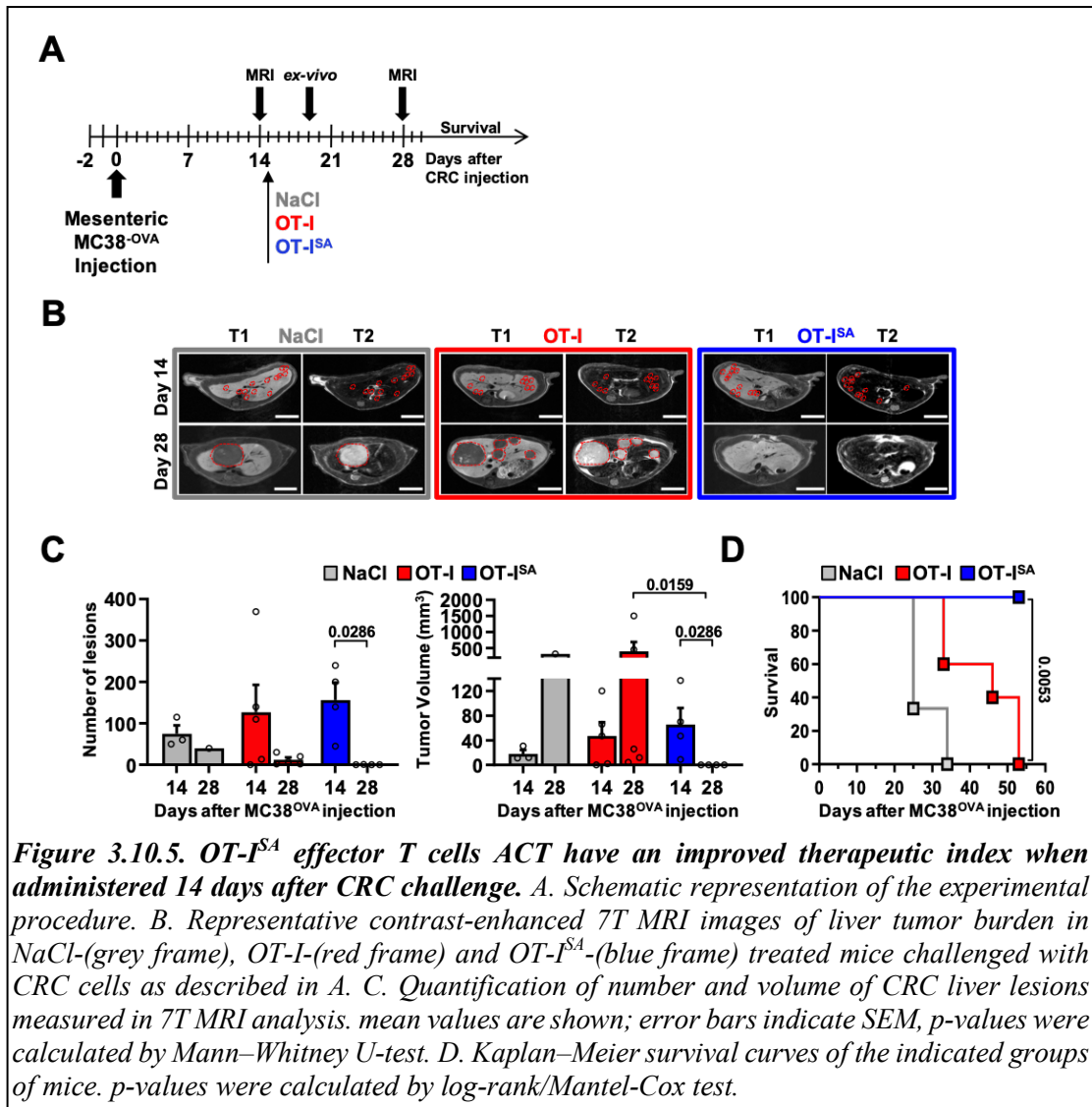
After *in vitro* characterization of OT-I and OT-I^{SA} effector T cells we performed a first experimental trial comparing the therapeutic capacity of the two cell lines on CRC liver lesions of increasing dimensions, infusing OVA specific CTLs at two different time points after CRC challenge (seven and fourteen days after tumor injection, i.e., when mice develop micrometastatic lesions of approximately 100-150 μ m and overt metastatic lesions of 2-4 mm, respectively), times when the tumors begin to recruit neoangiogenic vessels and immune cells with pro-tumoral properties.

For the first part of the trial we injected MC38^{OVA} cells in age and sex matched C57BL/6 Ly5.1.2 (CD45.1.2) mice, and seven days after we randomized mice in the different experimental groups. OT-I, OT-I^{SA} CTL (10^7 cells intravenously), or NaCl as control, were injected in the respective experimental groups (Figure 3.10.4. A). To evaluate IFNAR1 membrane expression on administered CTL, mice were followed and blood was periodically collected to perform cytofluorimetric staining. We took advantage of mismatch congenic markers to identify transferred cells (positive for CD45.2) in the blood of receiving animals (double positive for CD45.1 and CD45.2). We then check IFNAR1 positivity among CD8⁺ T positive circulating cells. About 80% of circulating transferred OT-I^{SA} T cells express IFNAR1, even after 50 days from ACT, whereas OT-I T cells displayed a progressive and significant reduction of IFNAR1 positive signal, that fell to levels below the 20% of total (Figure 3.10.4. B). This difference in receptor expression confirms the capacity of OT-I^{SA} cells to maintain a stable IFNAR1 expression, even in a deregulated microenvironment. Twenty-one days after CRC challenge, and fourteen days after CTL transfer, animal of the three experimental groups underwent 7T

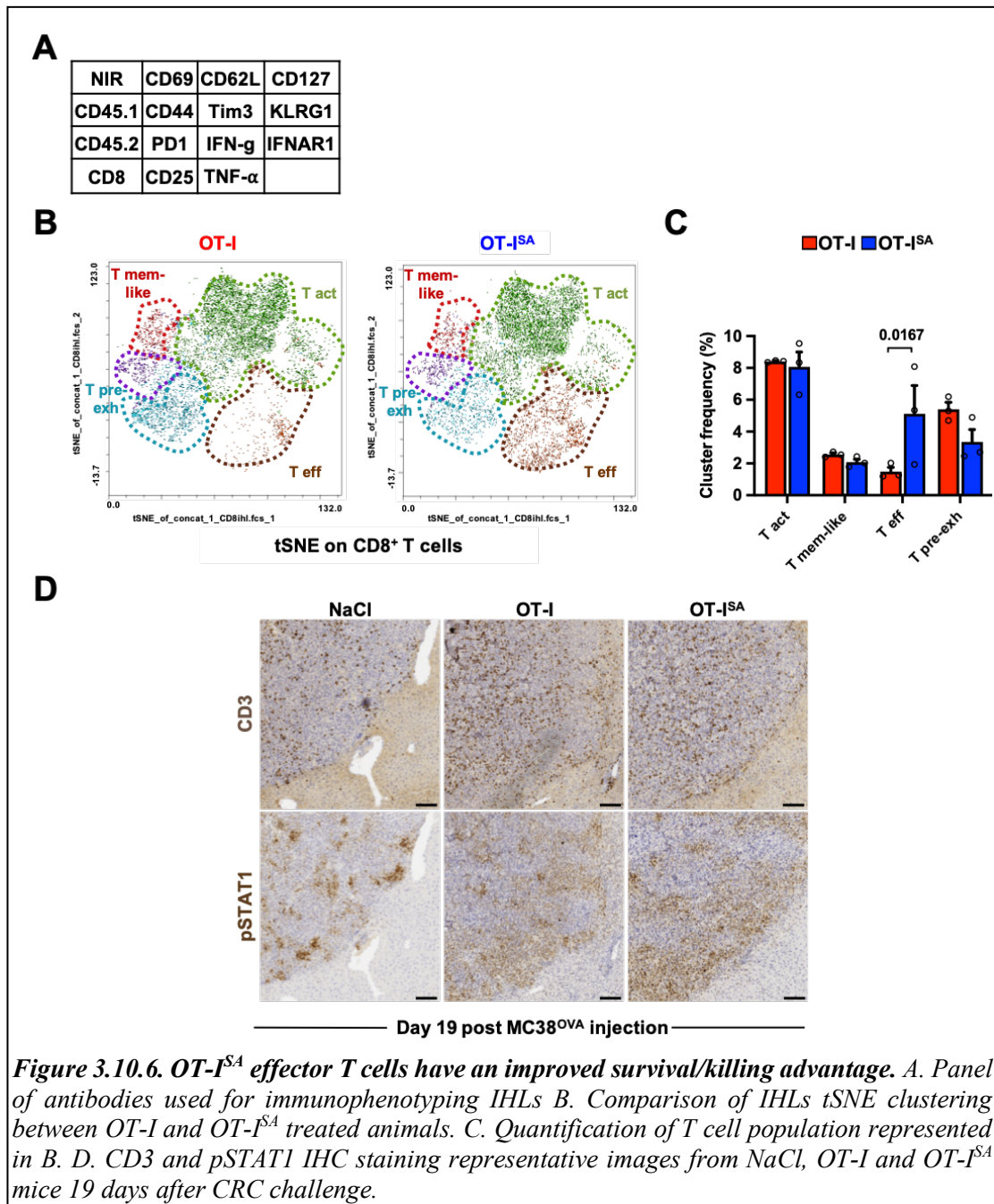
MRI analysis to assess liver tumor burden (Figure 3.10.4. C). MRI analysis showed the complete rejection of CRC liver metastases in both OT-I and OT-I^{SA} treated animals compared to mice injected with NaCl control that developed at this time point measurable liver lesions in the 60% of the cases (Figure 3.10.4. D). Animals were then followed to evaluate the survival rate of the different experimental treatments, and accordingly to MRI results all the NaCl injected control mice underwent humanitarian euthanasia protocols within 35 days from tumor challenge, whereas all OT-I and OT-I^{SA} treated animals resulted cured from CRC onset (Figure 3.10.4. E). These data show that both OT-I and OT-I^{SA} cells possess a high therapeutic index if ACT starts when the number and volume of metastases are still limited, succeeding in completely eradicating the tumor and curing treated animals.



To define the therapeutic index of the two cell types in a more stringent setting, we perform the second part of the trial starting ACT treatment fourteen days after tumor challenge. As, based on our previous experience, at this time point CRC liver metastases dimension is over the resolution capacity of 7T-MRI technique (Catarinella *et al*, 2016), we performed a pre-treatment screening to distribute experimental animals into homogeneous treatment groups based on number and volume of hepatic lesions. Groups were then treated as before with OT-I, OT-I^{SA} or NaCl as control. Twenty-eight days after tumor challenge, and fourteen days after ACT, we performed a second 7T-MRI analysis to verify therapy course (Figure 3.10.5. A-B). Data obtained showed an increase in volume lesions in NaCl and OT-I treated animals compared to the previous time point, whereas in marked contrast OT-I^{SA} receiving animals displayed a decreased lesion volume compared to previous time point, demonstrating disease remission. Importantly,



tumor volume of OT-I^{SA} treated animals at this time point is significantly reduced compared to the previous one, and conversely also compared to OT-I treated animals tumor volume at the same time point (Figure 3.10.5. C). These results also reflect the different survival capacity of the three groups, with OT-I^{SA} treated mice showing a significantly increased survival time compared to OT-I treated (Figure 3.10.5. D), thanks to the complete remission of liver metastases observed in MRI analysis. The data obtained show that OT-I^{SA} effector T cells were able to counteract the growth of metastases, even



14 days after the injection of tumor cells and in the presence of overt metastatic lesions of 2-4 mm. These results highlight a better therapeutic potential for these cells when the masses are larger and in greater numbers, compared to IFNAR1 wild type effector T cells, in which a pathological degradation of membrane receptor occur. This suggests that the presence of a stabilized IFNAR1 on cell membrane is fundamental for an effective ACT against liver CRC metastases.

Next, to investigate the features of the differently observed immune responses, a selected number of animals from the three experimental groups were killed nineteen days after tumor challenge, and 4 days after ACT treatment, at a time point when the anti-tumor immune response is in its active phase. To define the possible differences in exogenous lymphocyte populations that were transferred we performed an intra hepatic leukocytes (IHLs) preparation with a subsequent cytofluorimetric analysis using a selected panel of conjugated antibodies (Figure 3.10.6. A) in CD45.2⁺/ CD8⁺ cells, to investigate how cell therapy with OT-I^{SA} specific T cells could enhance the immune response and contribute to tumor eradication. IHLs preparations obtained were stimulated for 4 hours with SIINFEKL peptide in the presence of brefeldin, in order to evaluate also the production of IFN γ , and thus activity as cytotoxic effector cells. After peptide stimulation, cells were labeled with Near IR antibody (ThermoFisher), to distinguish live cell population, labeled with surface antibodies and, after membrane permeabilization, with intracellular markers, such as IFN γ . After data acquisition, FlowSOM algorithm (Bioconductor) was used to cluster and visualize bidimensionally the combination of high-dimensional flow cytometric data obtained, based on the different expression of the proteins recognized by the antibodies used. Data were then visualized as a t-distributed stochastic neighbor embedding (tSNE) plot (Figure 3.10.6. B left) and cluster frequencies for the different samples were calculated (Figure 3.10.6. C right). The populations identified were then matched to previous evidences and are the following:

- i. Activated T cells: characterized by the expression of CD25 and CD44 markers (Shipkova & Wieland, 2012).
- ii. Memory-like T cells: characterized by the expression of CD25, CD44 markers in combination with CD62L marker (Martin & Badovinac, 2018).
- iii. Effector T cells: cells characterized by the expression of CD25, TNF α , CD44 markers and IFN γ producing (Shipkova & Wieland, 2012).

iv. Pre-exhausted T cells: characterized by the expression of low CD25, CD44, and of inhibitory PD1 and Tim3 markers (Guo *et al*, 2018).

Quantification of cluster frequencies demonstrated a significant increase in Effector T cells (T eff) population in OT-I^{SA} compared to OT-I treated groups (Figure 3.10.6. C), reflecting a higher tumor response of OT-I^{SA} transferred cells, that four days after ACT are performing their functional cytotoxic function producing antiproliferative, proapoptotic, and antitumoral IFN γ in combination with the expression of CD25 and CD44 activation markers. Furthermore, a trend in decreased of Pre-exhausted T cells (T pre-exh) population is observed in OT-I^{SA} treated compared to OT-I treated groups (Figure 3.10.6. C), denoting cells characterized by progressive loss of effector functions due to the expression of immune checkpoint inhibitory molecules that blunt their tumor response. No evident differences were observed between OT-I^{SA} and OT-I treated groups concerning the frequency of clusters describing Activated T cells (T act) and Memory-like T cells (T mem-like) (Figure 3.10.6. C). Samples from NaCl, OT-I and OT-I^{SA} treated groups were also IHC stained for CD3 and pSTAT1 expression analysis. Data demonstrated an increased CD3⁺ T cells infiltration within tumor mass in animals treated with OT-I antigen specific T cells compared to NaCl treated animals. This phenotype is associated with an increased and more diffuse IFN pathway activation, as reported by pSTAT1 expression in mice that received OT-I^{SA} effector T cells, reflecting a higher degree of signaling through a stabilized IFNAR1 receptor (Figure 3.10.6. D).

From these data, it can be concluded that OT-I^{SA} ACT, in which type I interferon receptor is stabilized, significantly improves the efficacy T cell response to the tumor, maintaining a longer and effective T lymphocytes activity.

Considering the high therapeutic index of OT-I^{SA} ACT treatment using 10^7 effector cells, that is able to cure the totality of treated mice within fourteen days from therapy begin (Figure 3.10.5. C-D), and in the attempt to find a dose of OT-I^{SA} effector T cells that allow a therapeutic window to test IFN α combinatorial treatment efficacy, we performed a titration experiment using three different OT-I^{SA} effector T cells doses (1×10^7 , 5×10^6 , 1×10^6 and NaCl as control) to find the dose suitable to be used in combinatorial experiments. Survival of treated groups showed a still significant survival time of mice treated with 5×10^6 cells, that however died in 80% of the cases, compared

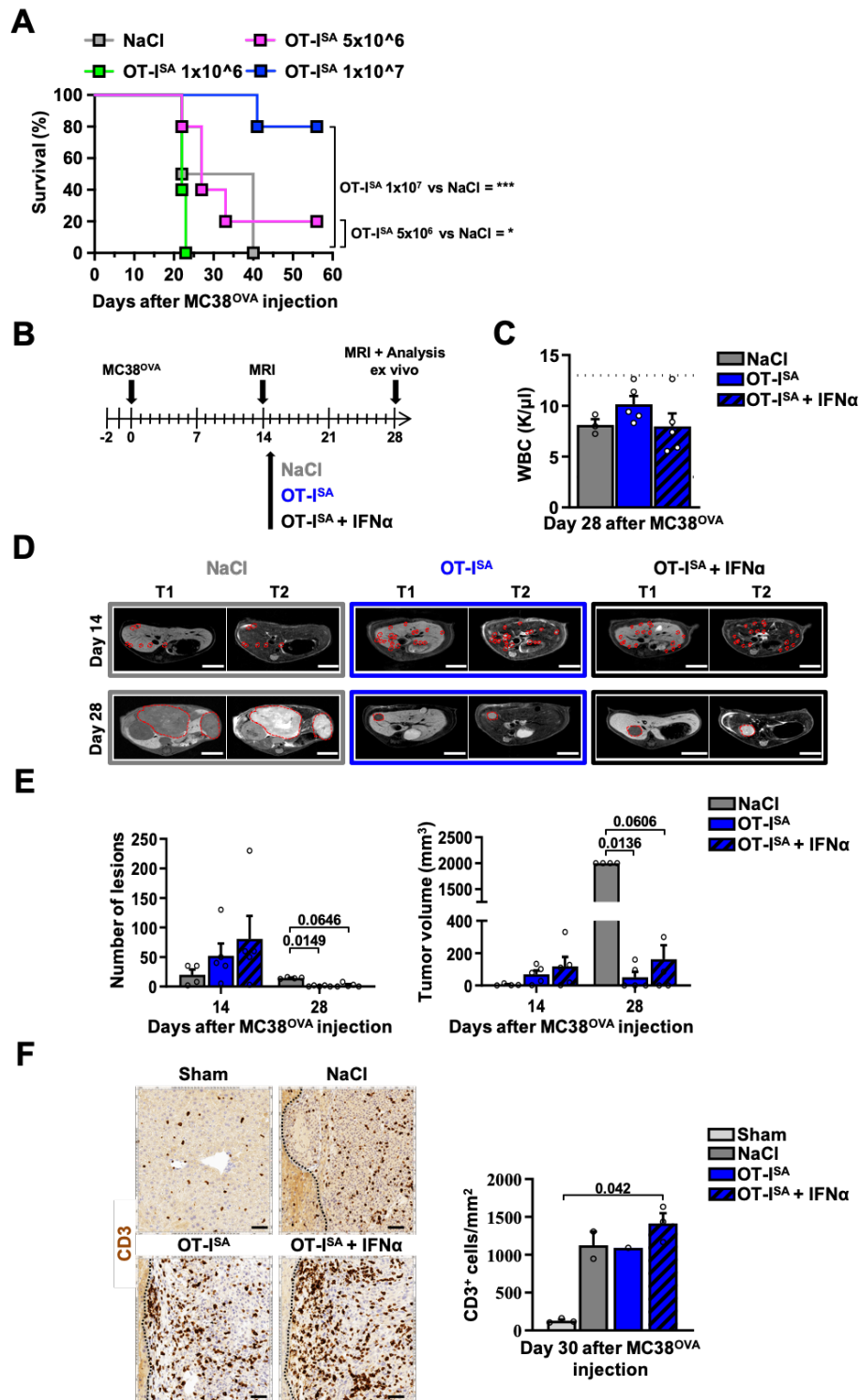


Figure 3.10.7. IFN α therapy in combination with OT-I^{SA} ACT increases CD3⁺ cell recruitment in the tumor reducing tumor growth. A. OT-I^{SA} effector T cell in vivo titration. B. Schematic representation of the experimental procedure. C WBC counts 19 days after CRC challenge in the different experimental groups. D. Representative contrast-enhanced 7T MRI images of liver tumor burden in NaCl-(grey frame), OT-ISA-(blue frame) and OT-I^{SA}+IFN α -(black frame) treated mice challenged with CRC cells as described in B. E. Quantification of number and volume of CRC liver lesions measured in 7T MRI analysis. mean values are shown; error bars indicate SEM, p-values were calculated by Mann-Whitney U-test. F. CD3 IHC staining representative images of Sham, NaCl, OT-I^{SA} and OT-I^{SA}+IFN α treated mice 30 days after CRC challenge and corresponding quantification. mean values are shown; error bars indicate SEM; p-values were calculated by one-way ANOVA non-parametric Kruskal Wallis/Dunn's multiple comparison test.

to NaCl treated control, open the path for a possible IFN α adjuvant effect (Figure 3.10.7. A). In this experimental setting 1×10^7 OT-ISA treatment as expected resulted in the significant survival of 80% of the animals, whereas the treatment with 1×10^6 effector T cells seemed not be sufficient to confer protection to experimental animals, that showed a survival time similar or even worse to that of NaCl treated control, effect that need further investigation (Figure 3.10.7. A).

After finding out what dose was compatible with combinatorial IFN treatment, we performed the experimental trial to evaluate the potential benefit of OT-ISA and IFN α combination strategy. Again, MC38^{OVA} cells were injected in age and sex matched C57BL/6 Ly5.1.2 (CD45.1.2) mice, and after fourteen days a 7T-MRI pre-treatment screening was performed to distribute experimental animals into homogeneous treatment groups based on number and volume of hepatic lesions. Subsequently groups were treated with OT-ISA, OT-ISA in combination with IFN α -MOP adjuvant treatment, and NaCl as control (Figure 3.10.7. B). Twenty-eight days after tumor challenge, and fourteen days after ACT, we performed a second 7T-MRI analysis to verify therapy course (Figure 3.10.7. D) and experimental groups were sacrificed to perform functional characterization. WBC count in the three group did not display significant toxicity in combinatorial treatment compared to OT-ISA mono-therapy or NaCl control (Figure 3.10.7. C). Quantification of tumor burden demonstrate a comparable therapeutic effect of OT-ISA-IFN α combinatorial therapy and OT-ISA mono-therapy in comparison to NaCl treated control (Figure 3.10.7. E). Importantly, when we quantified, using IHC staining, the burden of intratumoral CD3⁺ T cells in the different conditions we found that IFN α adjuvant therapy in combination with OT-ISA treatment significantly increased the recruitment of tumor infiltrating CD3⁺ T cells in liver CRC lesions, possibly contributing to increase OT-ISA therapeutic index (Figure 3.10.7. F).

All in all, these results demonstrate that IFNAR-stabilized ACT in combination with adjuvant IFN α therapy confers the advantage of using a cell product with increased IFN signaling capacity in the presence of exogenous IFN.

3.11 IRF7 increased expression correlates with worse prognosis in patients with primary CRC tumors, and IFNAR1 is downregulated in CRC tumors and synchronous liver metastases

Following the findings from animal models demonstrating a deregulated IFN-producing liver CRC microenvironment, that is refractory to adjuvant IFN therapy and that can be successfully overcome by IFNAR1 stabilization strategies, we performed a RNAseq meta-analysis of The Cancer Genome Atlas (TCGA) database for the expression of IRF7 in patients with CRC primary tumor. The analysis was made using a standard processing pipeline, taking advantage of the Gene Expression Profiling Interactive Analysis 2 (GEPIA 2) system (Tang *et al*, 2019). We chose IRF7 gene expression as a prototypical IRG that can be considered a proxy for the activation state of the IFN pathway (Cheon *et al*, 2014). To this end, levels of IRF7 expression as measured in RNAseq data collected in TCGA database from 269 individuals with colon adenocarcinoma were ranked, and used to subdivide patients in high versus low IRF7 expressing groups (135 vs 134 patients respectively). This clustering was then used to verify overall survival of the two groups. The results obtained from data stratification demonstrated a significant higher overall survival in patients with low versus high IRF7 expression (Cox Regression Hazard Ratio=1.8; Logrank p=0.019) (Figure 3.11. A), showing: i. the presence of an active IFN signature in CRC primary tumors and ii. that IFN pathway activation correlates with worse prognosis in primary CRC patients, suggesting the presence of a deregulated tumor microenvironment. Importantly, when the same analysis was performed in PDAC affected patients, no significant difference was observed between high and low IRF7 expressing patients (Cox Regression Hazard Ratio=1; Logrank p=0.82) (Figure 3.11. B), in accordance to the experimental results obtained in animal models that did not find endogenous IFN expression and consequent deregulation in PDAC tumor microenvironment. Finally, as positive control we repeated again overall survival analysis based on IRF7 expression in breast cancer patients, that displayed an opposing effect of IRF7 upregulation, as breast cancer patients with high IRF7 expression show a better overall survival compared to low expressing patients (Cox Regression Hazard Ratio=0.77; Logrank p=0.11) (Figure 3.11. C), in accordance with

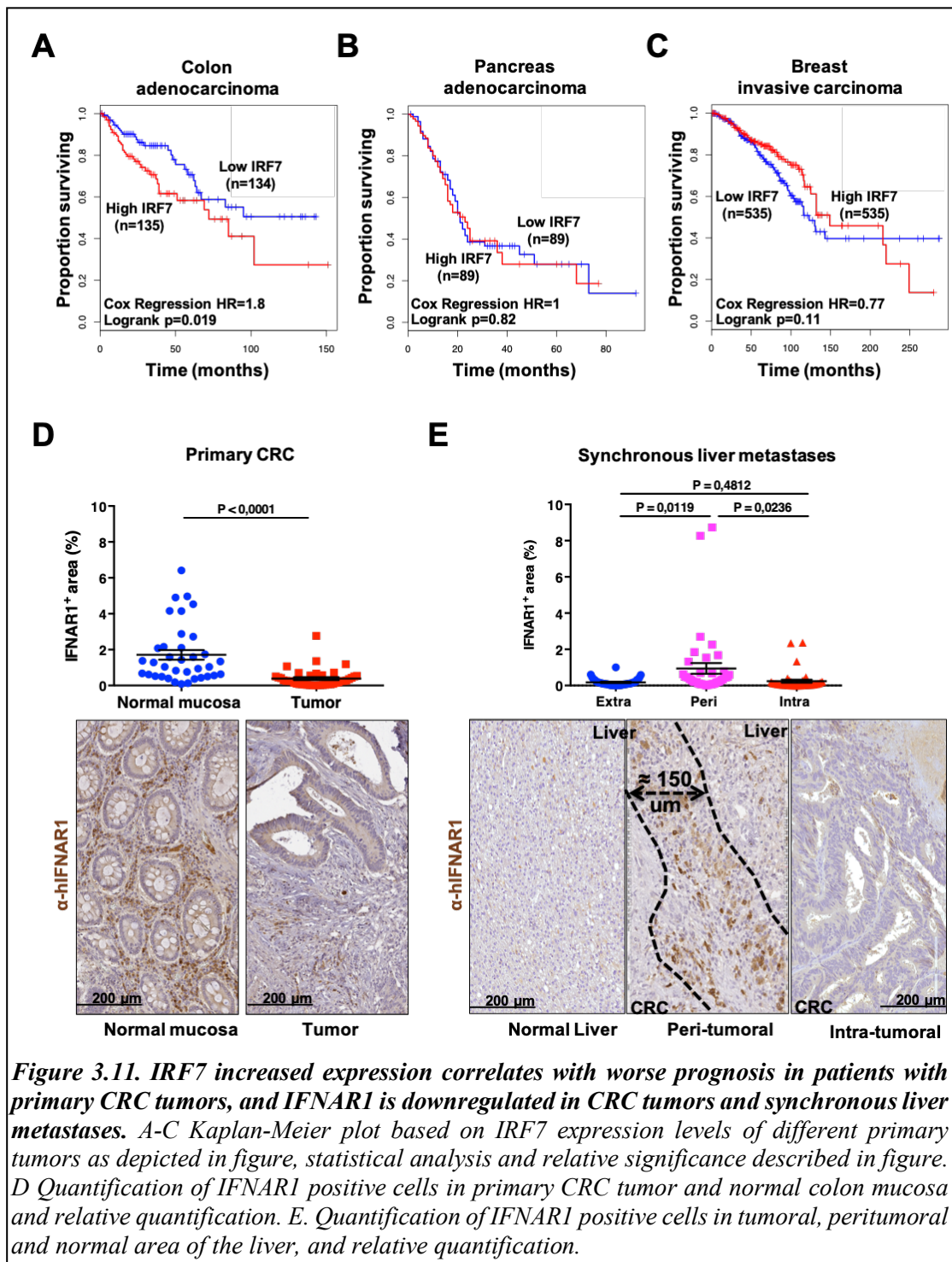


Figure 3.11. IRF7 increased expression correlates with worse prognosis in patients with primary CRC tumors, and IFNAR1 is downregulated in CRC tumors and synchronous liver metastases. A-C Kaplan-Meier plot based on IRF7 expression levels of different primary tumors as depicted in figure, statistical analysis and relative significance described in figure. D Quantification of IFNAR1 positive cells in primary CRC tumor and normal colon mucosa and relative quantification. E. Quantification of IFNAR1 positive cells in tumoral, peritumoral and normal area of the liver, and relative quantification.

evidence from the group of Parker, that demonstrated a protecting effect of IRF7 expression from bone metastatization process of breast cancer (Bidwell *et al*, 2012).

After demonstrating the presence of an active IFN signature in CRC primary tumor, that negatively contribute to patient survival, we performed a retrospective study in a selected cohort of patients with diagnosis of CRC and synchronous liver metastases who

underwent resective surgery and for which hepatic and colic tissues were quantitatively and qualitatively adequate for IHC staining of IFNAR1 protein. We confirmed the reduced expression of IFNAR1 in primary CRC tumor compared to normal colic mucosa (Figure 3.11. D), as previously demonstrated by the group of Fuchs (Katlinski *et al*, 2017).

Importantly, in the analysis of synchronous liver metastases, we demonstrated for the first time a significant downregulation of IFNAR1 in the inner CRC liver lesions and an associated increase in IFNAR1 expression at the leading edge of the liver tumors (Figure 3.11. D), which is often associated with immune cell accumulation (Halama *et al*, 2011). These results demonstrate the presence of an active IFN signature in human CRC tumors that correlates with poorer patient prognosis and is associated with IFNAR1 downregulation in primary and metastatic tumors, suggesting the presence of a refractory microenvironment and potentially raising the importance for future translational application of experimental results obtained in animal models with IFNAR1 stabilization strategies and IFN adjuvant therapy combinations.

4. Discussion

In this work, we demonstrated that stabilization of IFNAR1 in the liver CRC metastatic microenvironment significantly reduces tumor burden, leading to a better outcome in experimentally treated animals.

Thus, we presented significant data linking IFNAR1 downregulation in the microenvironment of CRC liver metastases to the production of several (IFN α 1, IFN α 13, IFN β , IFN ϵ) endogenous type I subtypes by CRC cells, leading to IFN signature activation in the liver and consequent reduced IFNAR1 expression and IFN stimulatory capacity. This IFN-refractory phenotype is associated with a reduced or absent response to adjuvant IFN therapy of CRC liver metastases already established in the hepatic parenchyma (once CRC cells have already crossed the vascular barrier of the liver and started to form micrometastatic lesions of approximately 100-150 μ m²). In this refractory system producing endogenous type I subtypes, we tested two different therapeutic strategies to increase IFN signaling through a deregulated microenvironment.

The first strategy, but with little success in this complex scenario, involved the use of IFN subtypes with high *in vivo* potency to increase signaling capacity through a lowly expressed IFNAR1 in the refractory tumor microenvironment. All IFN subtypes bind to the same heterodimeric receptor (IFN $\alpha\beta$ receptor, consisting of IFNAR1 and IFNAR2 subunits). The different IFN subtypes show varying potency in their ability to signal downstream of the receptor based on relative binding strength and dissociation rate. In particular, we have shown in previous experiments that IFN α 11 has the highest *in vitro* and *in vivo* potency among the different IFN subtypes, whereas IFN α 1 is shown to be a prototypical IFN with low potency. Therefore, we performed a study comparing the ability of adjuvant IFN α 11 treatment versus IFN α 1 treatment to reduce tumor burden in treated mice. We also included a pancreatic ductal adenocarcinoma cell line (PDAC) in the study because we have shown in the previous description of endogenous IFN production by various CRC cell lines and the associated IFNAR1 downregulation and reduced IFN signaling, that a PDAC cell line (Panc02 cells), which is also capable of metastasizing to the liver, exhibits reduced or no production of endogenous type I IFNs and accordingly shows higher IFNAR1 expression and increased ability to signal through the receptor.

The results of the study showed that neither IFN α 11 nor IFN α 1 were able to reduce tumor burden in CRC bearing livers, whereas in PDAC bearing animals low potency IFN α 1 showed significant ability to reduce tumor burden, while with high potency IFN α 11 showed no increased efficacy compared to IFN1, suggesting that in a deregulated microenvironment the potency of the IFN subtype is not functional for treatment success, and that the availability of IFNAR1 in the tumor microenvironment controls treatment success. This demonstrate also that intrinsic characteristics of the tumor type may dictate IFN therapeutic success, as treatment with the same IFN subtype (IFN α 1) showed completely different results depending on the tumor type, regardless of the potency of the type I IFN subtype used. In an attempt to investigate the possible different cell autonomous properties of CRC and PDAC cells that may affect their ability to respond to adjuvant IFN therapy, we also showed that the antiproliferative activity of IFN did not affect tumor growth, at least in the range of IFN doses of our treatment, in agreement with our previously published data (Catarinella *et al*, 2016; Tran *et al*, 2022). Interestingly, CRC and PDAC cells showed different behavior in terms of upregulation of ISG molecules in the presence of low IFN α 1 concentration, compatible with the levels we achieve with MOP treatment.

This difference reflects differential cell autonomous "robust" activity and capacity of the CRC and PDAC cell lines we analyzed (Piehler *et al*, 2012), and further ongoing experiments are needed to clarify whether these phenotypes also occur in other CRC and PDAC cell lines.

Because we found that in a deregulated microenvironment with low IFNAR1 availability, the use of high potency IFN did not improve outcome, we used a second strategy aimed at stabilizing the IFNAR1 receptor either generally in the CRC tumor microenvironment by pharmacological IFNAR1 stabilization or more specifically in CRC specific genetically modified CTLs used to perform ACT approaches. The latter approach was also tested in combination with adjuvant IFN α therapy, demonstrating a functional increase in T cells.

For pharmacological inhibition of IFNAR1 downregulation, we treated established CRC tumors with two small molecules capable of inhibiting two different kinases stimulated by stress mechanisms in the tumor microenvironment and capable of phosphorylating the intracytoplasmic tail of IFNAR1, leading to IFNAR1

downregulation. Importantly, one of these molecules, the p38a inhibitor LY2228820 (ralimetinib), is already in clinical trials (Patnaik *et al*, 2016), which increases the translational relevance of our study.

Combined treatment with the two molecules resulted in a significant reduction in CRC tumor burden and thus increased survival of treated animals. Importantly, a group of mice genetically lacking IFNAR1 (IFNAR1-KO mice) was used as control and demonstrated the significant dependence of IFNAR1 expression in the host tumor microenvironment for the efficacy of kinase inhibitor treatment. Even if we cannot completely exclude additional off-target effects on CRC tumor cells, these results indicated that pharmacological treatment of p38 and PKD kinases exerted their function mainly in an IFNAR1-dependent manner. One of the possible off-target effects that may contribute in a small way to the obtained results derives from the ability of the PKD inhibitor used (SD-208) to inhibit TGF- β R1 activity (Uhl *et al*, 2004), thus affecting the ability of CRC cells to shape the tumoral microenvironment and influencing their invasive phenotype (Mohammad *et al*, 2011; Tauriello *et al*, 2018). The results we obtained also strengthen the notion that CRC metastatic microenvironment is endowed with endogenous type I IFN, since the stabilization of IFNAR1 and the resulting enhanced IFN signaling should rely on the presence of IFN ligand to exert its function. Despite the described efficacy of monotherapy with kinase inhibitors in CRC liver metastases, ongoing experiments with this pharmacological treatment in combination with adjuvant IFN therapy will define the potential enhanced effect of exogenous IFN in the context of IFNAR1 stabilization, also with a view to clinical translation of these findings, which may be based on a pharmacological treatment that has not shown overt toxicity in experimental animals and is already in clinical use with an acceptable safety profile for at least one of the two small molecules (Patnaik *et al*, 2016).

The genetic stabilization strategy we specifically applied to tumor-specific CTLs ACT showed even greater efficacy in containing CRC liver tumors. For genetic stabilization of tumor-specific T cells, we used an amino acid substitution in the intracytoplasmic tail of IFNAR1 (S526A, SA) that prevents phosphorylation of the receptor and subsequent ubiquitination by a specific E3 ligase that binds to phosphorylated Ser526, thereby blocking degradation of IFNAR1 at the cell surface (Katlinski *et al*, 2017). Tumor-specific CD8⁺ effector T cells with this genetic modification were then used in an ACT

experimental protocol to treat CRC liver tumors of increasing dimension (i.e., at different, increasing time points after CRC cell challenge) and showed significantly better ability to cure CRC liver metastases compared with the wild-type T cell counterpart. When we titrated down the cell dose to perform a combinatorial experimental strategy with adjuvant IFN α therapy, the combination of genetically stabilized IFNAR1 ACT with IFN α treatment significantly increased T cell infiltration of CRC liver metastases implying a better overall response to CRC tumors using receptor stabilization in the presence of exogenous IFN.

Furthermore, genetic stabilization of IFNAR1 resulted in increased expression of effector phenotype T cells and decreased presence of the exhaustion marker in IFNAR1 stabilized cells compared to IFNAR1 wild-type tumor-specific T cells.

Finally, when analyzing patient data and samples, we found a close correlation with the results in our experimental models, again highlighting the translational relevance of our findings. We demonstrated a direct correlation between IRF7 ISG expression and significantly reduced overall survival in patients with primary colon adenocarcinoma by analyzing data from The Cancer Genome Atlas Database. Importantly, this correlation was not found in patients with adenocarcinoma of the pancreas, a tumor that did not produce type I IFN molecules in our experimental models and had increased sensitivity to adjuvant IFN α therapies, compared with IFN-producing CRC liver tumors that were refractory to adjuvant IFN α therapy and had reduced IFNAR1 expression.

In this context, we performed a retrospective study of IFNAR1 expression in patients undergoing resection for primary CRC and synchronous CRC liver metastases. The results showed significant downregulation of IFNR1 in primary tumors compared with normal colon mucosa, confirming previously published data (Katlinski *et al*, 2017). Importantly, we showed that human CRC liver metastases also exhibited decreased IFNAR1 expression in the inner tumor region compared with increased expression at the tumor margin, mirroring data obtained in mouse models. Additional analyses on the possible expression of the IFN signature also in this deregulated metastatic microenvironment and of the presence of human endogenous IFN subtypes in liver metastases from CRC patients will increase the power of these results and are currently being performed in the laboratory.

The results of this work demonstrate that a type I IFNs producing deregulated microenvironment is present in CRC liver metastases and that strategies aimed at stabilizing IFNAR1 on cells of the tumor microenvironment are successful in treating this malignancy. More broadly, these results also suggest that different tumor types, or even different patients of the same tumor type, metastasizing to the liver, may have a different ability to produce/induce type I IFN signaling, and that potentially IFN signaling activation markers may predict the ability of patients to respond to IFNAR1 stabilization and IFN adjuvant therapies.

Some pieces of information are still missing from this work, and we are in the process of filling in the knowledge gaps, such as the precise characterization of the cell types that downregulate IFNAR1 expression in the tumor microenvironment and whether cell types other than CRC, as expected, produce type I IFN subtypes in the tumor milieu and what their identity and function are. Finally, we are aware that mechanistic experiments are required to unequivocally prove the protumoral effect of endogenous IFN produced by CRC cells, using strategies that can selectively block IFN production from CRC cells/tumor microenvironment, and we are actively working on the design of these experiments.

5. Materials and Methods

5.1 Animal studies

Eight to ten-week old C57BL/6 J, BALB/c, C57BL/6J-IFNARKO, C57BL/6-Tg(TcraTcrb)1100Mgb/Crl, JAX:003831 (OT-I) mice were obtained from the Charles River Laboratory in Calco (Italy). CB6 mice were obtained by crossing male inbred C57BL/6 J (H-2b-restricted) with inbred BALB/c female mice (H-2d-restricted) to produce H-2bxd-F1 hybrids. CD45.1.2/B6J (LY5.1.2) were obtained crossing male LY 5.1 male mice (obtained from Charles River Laboratory) with female inbred C57BL/6 J (LY 5.2) to produce CD45.1.2/B6J (LY5.1.2) F1 hybrids. Tg (TcraTcrb) C57BL/6 IfnarSA (OT-ISA) were kindly provided by Serge Y. Fuchs from University of Pennsylvania School of Veterinary Medicine (PennVet) in Philadelphia (PA). OT -I and OT-ISA mice possess a restricted transgenic T cell receptor for the murine MHC H2kb allele and can recognize the immunodominant epitope of ovalbumin (SIINFEKL) at residues 257-264 (OVA257-264). IFNa/bR^{-/-} mice in C57BL/6 background (obtained through the Swiss Immunological Mutant Mouse Repository, Zurich, Switzerland). All experiments performed were approved by the Animal Care and Use Committee of the San Raffaele Scientific Institute and were conducted in a specific pathogen-free facility (SPF), in isolated cages and under 12-hour light-dark cycles with free access to water and a standard diet.

5.2 Tumor cell lines and organoids.

MC38 (H-2b, C57BL/6-derived) cell line (Corbett et al, 1975; Catarinella et al, 2016; Efremova et al, 2017; Tran et al, 2022) derived from mouse colon adenocarcinoma was kindly donated by P. Berraondo López from the Centro de Investigación Médica Aplicada (CIMA) in Pamplona (Spain). CT26 (H-2d, BALB/c- derived) cell line was purchased from ATCC. Mouse tumor organoids (MTO) (Apcfl/fl, KrasLSL-G12D, Tgfbr2fl/fl and Trp53fl/fl targeted gene recombination to intestinal stem cells (ISCs) by means of the Lgr5eGFP-creERT2, H-2b, C57BL/6-derived) (Tauriello et al, 2018) were kindly donated by E. Batlle from Institute for Research in Biomedicine (IRB) in Barcelona

(Spain). Panc02 (H-2b, C57BL/6-derived) cell line (Corbett et al, 1984) was kindly donated by L. Piemonti from Diabetese Research Institute (DRI) at HSR in Milan (Italy). MC38OVA expressing ovalbumin peptide (OVA), cloned and selected by FACS to detect the presence of the OVA transgene (NGFR-OVA viral vector kindly donated by L. Naldini from TIGET at HSR in Milan (Italy). Cell lines were grown in DMEM/RPMI GlutaMAX medium (Gibco) containing 10% FBS (Lonza) and 1% W/S (Gibco) in an incubator at 37 ° C (5% CO₂). MTOs were grown in DMEM Advance/F12 medium supplemented with B-27supplement, rhEGF 50 ng/ml, rhNOGGIN 100 ng/ml and Galunisertib 1uM within drops of Matrigel+Advanced DMEM/F12 medium (2:1).

MC38 cells were injected at a dose of 7×10^4 /mouse in all the *in vivo* experiments in this work, except for experiments where the final time point was day 7 after CRC challenge in which were injected at the dose of 7×10^5 /mouse. CT26 cells were injected at a dose of 5×10^3 /mouse in all the *in vivo* experiments in this work. MTO were detached and prepared as a single cell suspension before injection of $2,5 \times 10^5$ cells/mouse. Panc02 cells were injected at the dose of 1×10^5 /mouse in all the *in vivo* experiments in this work.

5.3 Mouse models of liver metastases.

Eight- to ten-week-old sex- and age-matched mice were injected with the aforementioned cell lines and organoids by injections into the superior mesenteric vein as previously described (Bij *et al*, 2010). For injections into the plenum or superior mesenteric vein, deep anesthesia was induced by isoflurane inhalation (5% for induction and 2% for maintenance at 2 l/min oxygen). The indicated number of CRC/PDAC cells/organoids was injected into the superior mesenteric vein with a 29G needle. To prevent excessive bleeding, the venipuncture was compressed with a sterile and absorbable hemostatic gauze (TABOTAMP®). The peritoneum and skin were sutured with 4.0- and 7-mm silk wound staples, as described (Catarinella et al., 2016). This experimental setting may mimic the vascular spread of CRC cells during primary tumor resection, allowing therapeutic IFN α infusion to be considered as an adjuvant treatment.

5.4 Recombinant Mouse IFN α therapy.

Continuous intraperitoneal IFN α delivery (IFN α 1 carrier-free, Biolegend, San Diego, CA, USA) was achieved by intraperitoneal implantation of mini-osmotic pumps (MOP, ALZET, Cupertino, CA, USA) capable of delivering 150 ng IFN α per day for 14 or 28 days. NaCl-containing MOP were used as controls. MOP filling, priming, and implantation into the peritoneum were performed according to the manufacturer's instructions. To avoid MRI artifacts due to metallic components in MOP, MOP was modified to be compatible with magnetic resonance imaging (MRI) analysis as previously reported (Vousden et al, 2018). To directly examine the responsiveness of liver cells to IFN α , signaling downstream of the *Ifnar1* receptor was assessed by measuring pSTAT1 by IHC 30 minutes after an ip injection of NaCl or 1 μ g IFN α , a dose that can synchronize pSTAT1 expression in all *Ifnar1*-expressing cells (Lin *et al*, 2016).

5.5 Magnetic resonance imaging (MRI).

All MRI studies were performed at the Experimental Imaging Center of SRSI on a preclinical 7 Tesla scanner MR (Bruker, BioSpec 70/30 USR, Paravision 6.0.1, Germany) equipped with 450/675 mT/m gradients (slew rate: 3400/4500 T/m/s; rise time 140 μ s) and coupled to a dedicated 4-channel volume coil for mice. All images were acquired *in vivo* under inhalation anesthesia (isoflurane, 3% for induction and 2% for maintenance in 1 l/min of oxygen) with the mice lying prone on the examination table. A dedicated temperature control system was used to prevent hypothermia; respiratory rate and body temperature were continuously monitored throughout the MRI examination (SA Instruments, Inc., Stony Brook, NY, USA). An intravenous injection of gadoxetic acid (Gd- EOB-DTPA; Primovist, Bayer Schering Pharma) at a dose of 0.05 μ mol/g body weight was administered via the tail vein before the mice were placed on the scanner table. As previously described (Sitia *et al*, 2012), MRI studies relied on an axial fat-saturated T2-weighted sequence (TurboRARE-T2: TR =3394ms, TE =33ms, voxel size=0.125x0.09x0.8mm, mean=3) acquired immediately after Gd- EOB-DTPA injection and an axial fat-saturated T1-weighted scan (RARE -T1: TR =581ms, TE =8.6ms, voxel size=0.125x0.07x0.8mm, mean=4) subsequently acquired during the hepatobiliary phase

(HBP) of contrast excretion (starting 10 minutes after Gd-EOB-DTPA injection). Two board-certified radiologists with experience in clinical and preclinical abdominal MR imaging, blinded to all other information, reviewed all MRI studies using open-source image visualization and quantification software (Mipav, 5.3.4 and later versions, Biomedical Imaging Research Services Section, ISL, CIT, National Institute of Health, USA). Liver metastases were identified as focal lesions that exhibited mild hyperintensity on T2-weighted images and concomitant hypointensity on contrast-enhanced T1-weighted HBP images. Liver metastases were segmented by manually drawing regions of interest (ROIs) on each slice, resulting in volumes of interest (VOIs; lesion area x slice thickness) for the entire sequence. The total CRC metastasis mass was determined by summing the volumes of all individual VOIs, which were provided semi-automatically by the software.

5.6 Peripheral blood analyses.

At the indicated time points after IFN α or LY/SD administration, anticoagulated whole blood was collected from mice from the retro-orbital plexus of anesthetized animals (isoflurane, 5% for induction and 2% for maintenance at 2 l/minute oxygen) using Na-heparin-coated capillaries (Hirschmann Laborgeraete GmbH, Germany) and vials (Microvette, Sarstedt, Germany). Hematological parameters were determined using an automated cell counter (ProCyt Dx, IDEXX Laboratories, USA).

5.7 B16-BlueTM IFN- α / β assay on cell protein extracts.

B16-BlueIFN α / β TM cells were purchased from InvivoGen (SanDiego, CA) and grown in RPMI GlutaMAX medium (Gibco) containing 10% FBS (Lonza) and 1% W/S (Gibco) in an incubator at 37 ° C (5% CO₂) with the addition of 100 μ g/ml Zeocin (InvivoGen), the selection agent for the SEAP transgene expressed by the cells. As previously described,(Rees & Lowy, 2018), B16-BlueTM cells were plated at 7,5x10⁴ cells/well in 96 well multiwell plates (Corning Costar) 24 h prior to the start of the experiment. For IFN standard curve 0,1 U/ml to 50,000 U/ml of IFN α 1 (IFN α 1 carrier-free, Biolegend, San Diego, CA, USA) was added to the cells. Native Protein extracts were obtained from subconfluent cells placed on an ice plate, using mechanical disruption followed by four

cycles of freeze and thaw, to avoid any chemical protein denaturation. Native Protein lysates were quantified using Bicinchoninic acid (BCA) assay (Thermo Fisher) following manufacturer's recommendation and subsequently 6 μ g of protein lysate were added to B16-Blue™ cells. Cells were then incubated with IFN and native protein extracts for 17 h, at 37 °C, 5% CO₂, in a humidity-controlled incubator. To determine SEAP production 20 μ l of supernatants from B16-Blue cells were removed and placed in new 96 well plates and QuantiBlue SEAP detection solution (InvivoGen) was added to samples to a final volume of 200 μ l and the mixture incubated at 37° C for 3hours. SEAP levels were determined using a spectrophotometer at 650 nm. The IFN α activity in the samples was determined by plotting the optical density (OD) subtracted from blank OD to eliminate background, using a 4-parameter logistic fit for the standard curve by using Prism v8 (GraphPad).

5.8 RNA extraction and quantitative real-time PCR gene expression analyses.

Total RNA was isolated from liver homogenates or from *in vitro* cell pellets using the ReliaPrep™ RNA Tissue or Cell Kit Miniprep System (Promega) and subsequently treated with DNase TURBO (Thermo Fisher Scientific) according to the manufacturer's recommendations. The extracted RNA was subsequently retro-transcribed into cDNA using SuperScript™ IV VILO™ Master Mix (Invitrogen), according to producer's protocol. For experiments performed using custom pre-spotted TaqMan Array Cards (Applied Biosystems), cDNA was pre-amplified using a custom pool of primers specific for the genes included in the assay using the TaqMan PreAmp Master Mix (Applied Biosystems) following manufacturer protocol. Quantitative real-time PCR analysis was performed utilizing the ViiA7 or QuantStudio 12Flex Fast Real-Time PCR System (Applied Biosystems). For single probe IFN subtypes screening and quantification *in vivo* and *in vitro* were used the following FAM-MGB labeled TaqMan gene expression assays (Applied Biosystems): GAPDH (Mm99999915_g1), Ifn ϵ (Mm00616542_s1), Ifn α 13 (Mm01731013_s1), IFN β (Mm00439552_s1), IFN α 1-6-5 (Mm03030145_gH). Gene expression was determined as the difference between the threshold cycle (Ct) of the gene of interest (Goi) and the Ct of the housekeeping gene (Gapdh) of the same sample (Δ Ct).

Fold-change expression of each *Goi* was calculated in comparison to its basal expression in the control sample using the formula $2^{-\Delta\Delta Ct}$ as described (Sitia *et al.*, 2012).

5.9 Digital PCR gene expression analyses.

Absolute expression of mouse interferon genes in cDNA was quantified using the QIAcuity Digital PCR (dPCR) system (QIAGEN, Hilden, Germany) and the corresponding Taqman gene expression assays (*ifna1*: Mm03030145_gH, *ifnb*: Mm00439552_s1, *ifna13*: Mm01731013_s1, and *ifne*: Mm00616542_s1, Life Technologies, Carlsbad, USA). The optimal amount of cDNA for quantification by dPCR was determined in preliminary dilution experiments and corresponded to 1ng of cDNA for each gene. A 12ul mix containing the 20X Taqman gene expression assay, the 4X master mix from the QIAcuity Probe PCR Kit (Qiagen), and the established amount of cDNA was prepared and transferred to a well of a Nanoplate 8.5K 96-well (Qiagen). The plate was then loaded into a QIAcuity One instrument (Qiagen), which processed the samples as follows

1. a standard priming step (i.e. sample partitioning);
2. a thermal cycling step (95°C for 2 minutes, followed by 40 cycles at 95°C for 15 seconds plus 60°C for 30 seconds);
3. an imaging step (i.e. acquiring the FAM emission from single partitions for 500 ms).

The number of positive partitions measured for each target using the QIAcuity software suite (Qiagen) was converted to copies per reaction and normalized to the ng of cDNA inputs.

5.10 Isolation of splenocytes and Generation of Effector CD8⁺ T Cells.

Spleens were obtained from OT -I or OT-I^{SA} mice and placed in a 70- μ m cell strainer on a Petri dish containing 10 ml of plain RPMI, crushed with a syringe plunger to obtain a cell suspension, and washed three times with plain RPMI as previously described (Sitia *et al.*, 2012). The cell suspension was centrifuged at 400 g for 5 min at room temperature, and the resuspended pellet was incubated with ACK lysis buffer for 30 sec and neutralized

with RPMI. The resulting splenocytes were processed for generation of effector CD8⁺ T cells basically as described in (Manjunath *et al*, 2001). Briefly, the obtained splenocytes were counted and 2.5x10⁵ cells / well plated in 24-well plates. Cells were then stimulated for 1 hour with SIINFEKL peptide (OVA 257-264, Proimmune) 1µg / ml in complete RPMI 1640 medium, washed and incubated at 37 ° C (5% CO₂) for 9 days for cell expansion. Three days after plating, the proliferation index was examined; after eight days of expansion, the expression of membrane cell activation (IFN γ production) were calculated for both cell types. In all *in vivo* experiments described, except where noted, each mouse was injected with 1x10⁷ OT -I or OT-I^{SA} effector T cells.

5.11 Cell proliferation assays

In vitro cell proliferation was evaluated using the Cell Titer-Glo Luminescent Cell Viability Assay (Promega G7571) following manufacturer's recommendation. Briefly, cells were seeded in 96-well flat bottom plates at 2,5x10³ cells/well in the presence of increasing concentration of IFN α 1 or vehicle, wells of complete medium without cells were included as baseline control. At the settled time points, generally every 24h, the viability assay was performed. Cell Titer Substrate was resuspended in 10 ml Cell Titer Buffer at room temperature creating Cell Titer Reagent. Plate was placed at room temperature 30 minutes before the assay is performed; then, 100 µl of Cell Titer Reagent was added to each well. Samples were then mixed on an orbital shaker for 2 minutes, and incubated in the dark at room temperature for 10 minutes. Finally, the mix was transferred in a OptiPlate-96 Black (PerkinElmer) and luminescent signal was read using a Victor3 luminometer (PerkinElmer).

The commercial CellTrace™ Violet Cell Proliferation Kit for Flow Cytometry (ThermoFisher) was used to calculate the proliferation index of OT -I and OT-I^{SA} effector T cells. Splenocytes isolated from mouse spleens, as described above, were plated in PBS in 96-well plates and stained with the reagents included in the kit.

Cells were then covered and incubated at room temperature for 20 minutes. To stop the staining reaction, 150 µl of complete medium was added to each well and the cells were incubated for 5 minutes. Cells were then removed, centrifuged, and washed to remove the residual unbound dye, and then placed back into complete RPMI-1640

medium. After three days of plating, they were collected, centrifuged at 1200 rpm for 3 minutes, and resuspended in FACS buffer for flow cytometer analysis.

Analysis was performed using FlowJo software (BD Biosciences) using the "Proliferation modeling" tool.

5.12 Immunofluorescence and confocal microscopy.

Livers were perfused with PBS, harvested and fixed 1 hour at room temperature in Antigenfix solution (DiaPath), equilibrated in 30% sucrose in PBS overnight at 4 °C before embedding in OCT (Bio-Optica) and freezing at -80 °C. 30 µm thick cryosections were mounted on Superfrost Plus slides (Thermo Scientific). For immunofluorescence staining, sections were blocked and permeabilized with PBS containing 5% FBS and 0.1% Triton X-100 (Sigma-Aldrich) for 30 minutes at room temperature and then incubated with 10% donkey serum (DS; Sigma-Aldrich) in PBS for 30-60 minutes at room temperature. Staining with primary and secondary antibodies was performed with staining buffer (PBS containing 1.5% DS, 0.2% Triton X-100 and 1% BSA) using the following antibodies and dilutions: Hoechst (Invitrogen) 1:5000 for 3min at room temperature, anti-CD8 (dilution 1:100, clone 4SM16, eBioscience) + anti-rat AF549 (dilution 1:200, Thermo Fisher Scientific); anti-IFNAR1 (1:50, rabbit polyclonal, Sino Biological) + anti-rabbit AF488 (dilution 1:100, Thermo Fisher Scientific). Confocal images were acquired using a Leica SP8 confocal system (Leica Microsystems) available from the SRSI Advanced Light and Electron Microscopy BioImaging Center (ALEMBIC). 15-20 µm z-stacks were projected in 2D and processed using Fiji image processing software (Schindelin *et al*, 2012).

5.13 Isolation of intra hepatic leukocytes (IHLs).

Mice were sacrificed under anesthesia with cervical dislocation, and the abdomen was rapidly opened. Livers were retrogradely perfused with 10 ml of D-PBS (Gibco, Invitrogen). The needle (26 G x ½") of a 10-ml syringe was inserted into the inferior vena cava, the portal vein was cut, and the liver was slowly perfused with PBS to remove circulating lymphocytes. Mouse livers were weighed at the time of autopsy, and

intrahepatic leukocytes were isolated from two liver lobes of known weight (one half of the liver) placed in 10 ml of cold RPMI 1640 medium (Gibco, Invitrogen). The two lobes were cut into small pieces with scissors and homogenized with the plunger of a 1-ml syringe. The single liver cell suspension was passed through a 70- μ m cell strainer and centrifuged at 489 g for 5 min. The pellet was resuspended in the digestion medium containing 10 ml RPMI 1640 medium (Gibco, Invitrogen), 25 μ l DNAase I (2000 kunits/ml, Sigma), and 2 mg collagenase IV (Sigma). The suspension was digested for 40 minutes at 37°C, shaking the tube every 10 minutes. Cells were centrifuged at 489 g for 5 minutes and resuspended in 25 ml of ice-cold RPMI. They were then centrifuged at 17 g for 3 minutes to precipitate the connective tissue. The supernatant was transferred to another 50 ml Falcon tube and centrifuged at 489 g for 5 minutes. The pellet was resuspended in 4 ml of Percoll 1131 (Sigma)/RPMI/PBS gradient and was centrifuged at 769 g for 20 minutes without stopping. The pellet of leukocytes was recovered, RBC were lysed using ACK lysis buffer. ACK was neutralized using 10ml of RPMI 1640 medium, cells were washed, and resuspended in 10 ml RPMI 1640 medium. 20 μ l of the isolated IHLs were diluted with 20 μ l of trypan blue (Sigma) and counted in a Burker counting chamber. The obtained number of cells was doubled to obtain the total number of IHLs.

5.14 Flow cytometry.

For IHLs multi-color staining cells were resuspended in PBS and LIVE/DEAD Fixable Near-IR dead cell dyes (Thermo Fisher Scientific) and incubated for 15 minutes at RT in the dark to determine cell viability. Cells were then blocked with FACS buffer (PBS containing 2% FBS)/BV buffer (Biolegend), containing InVivo Mab anti-mouse CD16/CD32 (BioXCell) and stained at 4 °C in the dark for 30 minutes for surface markers using the following antibodies:

anti-CD45.1 (clone A20, BD Biosciences), anti-CD45.2 (clone 104, Biolegend), anti-mouse CD8a (clone 53-6.7, Biolegend), anti-CD69 (clone H1.2F3, Biolegend), anti-CD44 (clone IM7, BD Biosciences), anti-CD279 (PD-1) (clone RMP1-30, BD Biosciences), anti-CD25 (clone PC61, BD Biosciences), anti-CD62L (clone MEL-14, Biolegend), anti-CD366 (Tim-3) (clone RMT3-23, Biolegend), anti-CD127 (clone SB/199, BD Biosciences), anti-KLRG1 (MAFA) (clone 2F1/KLRG1, Biolegend) and anti-IFNAR-1 (clone MAR1-5A3, Biolegend).

For intracellular TNF α and IFN γ staining (anti-TNF α (clone MP6-XT22, Biolegend) and anti-IFN γ (clone XMG1.2, BD Biosciences), cells were then fixed, permeabilized, and stained according to the manufacturer's guidelines for the Foxp3/transcription factor staining buffer set (Thermo Fisher Scientific). Samples were read using FACS Symphony (BD Biosciences) and analysis was performed using Flowjo software (BD biosciences) and FlowSOM plug-in (Bioconductor).

The induction of interferon stimulated genes (ISGs) on MC38 and Panc02 cell lines was analyzed by flow cytometry. 5×10^5 cells were seeded in 6-multiwell plates and then stimulated with IFN α 1 diluted in RPMI complete medium at 200 pg/ml. 24 hours later cells were detached, transferred in FACS tubes and stained in FACS Buffer with the antibodies of interest. Staining was performed at 4°C for 20 minutes; the antibodies used are: anti-H-2Kb/H-2Db (clone 28-8-6, Biolegend), anti-CD274 (PD-L1) (clone 10F.9G2, Biolegend). Shortly before reading, samples were stained with 7-AAD viability staining solution (Biolegend). Samples were read using FACS Canto II (BD Biosciences) and data were processed using FlowJo software (BD Biosciences).

5.15 Kinase inhibitors preparation

For pharmacological stabilization of IFNAR1, the combination of p38 and PKD inhibitors (SD -208 PKD inhibitor 25mg and LY2228820 P38 inhibitor 5mg (Sellkem)), as previously described (Katlinski *et al*, 2017). SD -208 was resuspended in 1% methylcellulose at a concentration of 7.8 mg / mL and administered at a concentration of 3 mg/kg. LY2228820 was resuspended in NaCl at a concentration of 30 mg/mL and administered at a concentration of 1 mg/kg- The combination of drugs was administered to the animals for 8 days via a 300- μ l oral gavage according to the schedule depicted in Figure.3.9.1.

5.16 Patients

In collaboration with Dr. Federica Cipriani and Prof. Luca Aldrighetti (Hepatobiliary Surgery Unit, OSR) and Dr. Ugo Elmore and Prof. Riccardo Rosati (Gastroenterology Surgery Unit, OSR) and Dr. Federica Pedica and Prof. Claudio Doglioni (Pathology Dept., OSR), we evaluated the expression pattern of IFNAR1 protein in the colon and liver of patients undergoing CRC surgery for primary and secondary tumors. Between the 205 patients that underwent resective surgery at Hepatobiliary Surgery Unit, San Raffaele Hospital between 2007 and June 2017 we recruited 50 patients with synchronous primary and liver CRCs metastases for which we had quantitatively, and qualitatively adequate formalin-fixed paraffin embedded (FFPE) colon and hepatic tissues (approved by OSR Ethical Committee; IFNAR1_CE 05/04/2018). After IFNAR1 staining, slides were acquired using Aperio ImageScope. A certified pathologist, identified ROIs of normal colon mucosa and tumoral tissue that were then utilized for IFNAR1 quantification using dedicated macros on Aperio ImageScope. For each slide we analysed an area of colon e liver tissue that ranged from 1.23 mm² to 9,86 mm² per section). None of the patients selected was HIV or HBV/HCV positive or had hepatobiliary diseases.

5.17 Immunohistochemistry.

At time of autopsy for each mouse, livers were perfused with PBS, harvested and different pieces were sampled, fixed in zinc-formalin, processed and embedded in paraffin for histological and immunohistochemical analysis, as previously described (Sitia *et al*, 2012). Immunohistochemical staining using a Bond RX Automated Immunohistochemistry (Leica Microsystems GmbH, Wetzlar, Germany) was performed on 3- μ m-thick sections. For image acquisition and analysis eSlide Manager (Aperio Leica Biosystems) was used.

Immunohistochemistry (IHC) for IFNAR1, using rabbit polyclonal α -hIFNAR1 antibody (Sigma HPA018015) [84], has been performed by the Pathology Department of San Raffaele Hospital using the protocol “Jolly Umap Rb Tit 40+20 Univer (03/05/2017)” with Discovery ULTRA Staining Module by Ventana Medical Systems, Inc.

All images were acquired using the Aperio AT2 system (Leica Biosystems). Quantifications were performed by automated image analysis software through dedicated macros of the ImageScope program, customized following manufacturer’s instructions (Leica Biosystems). The images shown were identified as representative area of interest within the total area of the specimen analyzed and exported as ImageScope snapshots.

5.18 Statistical analysis.

In all experiments values are expressed as mean values \pm SEM. Statistical significance was estimated by two-tailed non-parametric Mann-Whitney test (e.g. to evaluate differences generated as a consequence of tumor growth) or by non-parametric one-way ANOVA Kruskal Wallis test with Dunn’s Multiple comparison test when more than two groups were analyzed. Statistical significance of survival experiments was calculated by log-rank/Mantel-Cox test. All statistical analyses were performed with Prism 8 (GraphPad Software) and were reported in Figure legends. P-values <0.05 were considered statistically significant and reported on graphs. If not mentioned, differences were not statistically significant.

6. References

- Adam R, Gramont A de, Figueras J, Kokudo N, Kunstlinger F, Loyer E, Poston G, Rougier P, Rubbia-Brandt L, Sobrero A, *et al* (2015) Managing synchronous liver metastases from colorectal cancer: A multidisciplinary international consensus. *Cancer Treat Rev* 41: 729–741
- Aghili M, IZADI S, MADANI H & MORTAZAVI H (2010) Clinical and pathological evaluation of patients with early and late recurrence of colorectal cancer. *Asia Pac J Clin Oncol* 6: 35–41
- André T, Boni C, Navarro M, Tabernero J, Hickish T, Topham C, Bonetti A, Clingan P, Bridgewater J, Rivera F, *et al* (2009) Improved Overall Survival With Oxaliplatin, Fluorouracil, and Leucovorin As Adjuvant Treatment in Stage II or III Colon Cancer in the MOSAIC Trial. *J Clin Oncol* 27: 3109–3116
- Aricò E, Castiello L, Capone I, Gabriele L & Belardelli F (2019) Type I Interferons and Cancer: An Evolving Story Demanding Novel Clinical Applications. *Cancers* 11: 1943
- Armaghany T, Wilson JD, Chu Q & Mills G (2011) Genetic alterations in colorectal cancer. *Gastrointest Cancer Res Gcr* 5: 19–27
- Benson ABI, Schrag D, Somerfield MR, Cohen AM, Figueredo AT, Flynn PJ, Krzyzanowska MK, Maroun J, McAllister P, Cutsem EV, *et al* (2004) American Society of Clinical Oncology Recommendations on Adjuvant Chemotherapy for Stage II Colon Cancer. *J Clin Oncol* 22: 3408–3419
- Bhattacharya S, HuangFu W-C, Dong G, Qian J, Baker DP, Karar J, Koumenis C, Diehl JA & Fuchs SY (2013) Anti-tumorigenic effects of Type 1 interferon are subdued by integrated stress responses. *Oncogene* 32: 4214–4221
- Bhattacharya S, Katlinski KV, Reichert M, Takano S, Brice A, Zhao B, Yu Q, Zheng H, Carbone CJ, Katlinskaya YV, *et al* (2014) Triggering ubiquitination of IFNAR1 protects tissues from inflammatory injury. *EMBO Mol Med* 6: 384–397
- Bian J, Dannappel M, Wan C & Firestein R (2020) Transcriptional Regulation of Wnt/ β -Catenin Pathway in Colorectal Cancer. *Cells* 9: 2125
- Bidwell BN, Slaney CY, Withana NP, Forster S, Cao Y, Loi S, Andrews D, Mikeska T, Mangan NE, Samarajiwa SA, *et al* (2012) Silencing of Irf7 pathways in breast cancer cells promotes bone metastasis through immune escape. *Nat Med* 18: 1224–1231

- Bij GJ van der, Bögels M, Otten MA, Oosterling SJ, Kuppen PJ, Meijer S, Beelen RHJ & Egmond M van (2010) Experimentally induced liver metastases from colorectal cancer can be prevented by mononuclear phagocyte-mediated monoclonal antibody therapy. *J Hepatol* 53: 677–685
- Bocci V (1994) Pharmacology and side-effects of interferons. *Antivir Res* 24: 111–119
- Boland CR, Thibodeau SN, Hamilton SR, Sidransky D, Eshleman JR, Burt RW, Meltzer SJ, Rodriguez-Bigas MA, Fodde R, Ranzani GN, *et al* (1998) A National Cancer Institute Workshop on Microsatellite Instability for cancer detection and familial predisposition: development of international criteria for the determination of microsatellite instability in colorectal cancer. *Cancer Res* 58: 5248–57
- Borden EC (2019) Interferons α and β in cancer: therapeutic opportunities from new insights. *Nat Rev Drug Discov* 18: 219–234
- Bork U, Grützmann R, Rahbari NN, Schülich S, Distler M, Reissfelder C, Koch M & Weitz J (2014) Prognostic relevance of minimal residual disease in colorectal cancer. *World J Gastroentero* 20: 10296–10304
- Bracci L, Proietti E & Belardelli F (2007) IFN- α and Novel Strategies of Combination Therapy for Cancer. *Ann Ny Acad Sci* 1112: 256–268
- Brenner H, Kloor M & Pox CP (2014) Colorectal cancer. *Lancet* 383: 1490–1502
- Canovas B & Nebreda AR (2021) Diversity and versatility of p38 kinase signalling in health and disease. *Nat Rev Mol Cell Bio* 22: 346–366
- Castle JC, Loewer M, Boegel S, Graaf J de, Bender C, Tadmor AD, Boisguerin V, Bukur T, Sorn P, Paret C, *et al* (2014) Immunomic, genomic and transcriptomic characterization of CT26 colorectal carcinoma. *BMC Genomics* 15: 190
- Catarinella M, Monestiroli A, Escobar G, Fiocchi A, Tran NL, Aiolfi R, Marra P, Esposito A, Cipriani F, Aldrighetti L, *et al* (2016) IFN α gene/cell therapy curbs colorectal cancer colonization of the liver by acting on the hepatic microenvironment. *EMBO Mol Med* 8: 155–170
- Cella M, Jarrossay D, Facchetti F, Alebardi O, Nakajima H, Lanzavecchia A & Colonna M (1999) Plasmacytoid monocytes migrate to inflamed lymph nodes and produce large amounts of type I interferon. *Nat Med* 5: 919–923
- Chen K, Collins G, Wang H & Toh JWT (2021) Pathological Features and Prognostication in Colorectal Cancer. *Curr Oncol* 28: 5356–5383
- Chen K, Liu J & Cao X (2017) Regulation of type I interferon signaling in immunity and inflammation: A comprehensive review. *J Autoimmun* 83: 1–11

- Cheon H, Borden EC & Stark GR (2014) Interferons and their stimulated genes in the tumor microenvironment. *Semin Oncol* 41: 156–173
- Clinton SK, Giovannucci EL & Hursting SD (2019) The World Cancer Research Fund/American Institute for Cancer Research Third Expert Report on Diet, Nutrition, Physical Activity, and Cancer: Impact and Future Directions. *J Nutrition* 150: 663–671
- Compton CC (2003) Colorectal Carcinoma: Diagnostic, Prognostic, and Molecular Features. *Modern Pathol* 16: 376–388
- Compton CC & Greene FL (2004) The Staging of Colorectal Cancer: 2004 and Beyond. *Ca Cancer J Clin* 54: 295–308
- Corbett TH, Griswold DP, Roberts BJ, Peckham JC & Schabel FM (1975) Tumor induction relationships in development of transplantable cancers of the colon in mice for chemotherapy assays, with a note on carcinogen structure. *Cancer Res* 35: 2434–2439
- Corbett TH, Roberts BJ, Leopold WR, Peckham JC, Wilkoff LJ, Griswold DP & Schabel FM (1984) Induction and chemotherapeutic response of two transplantable ductal adenocarcinomas of the pancreas in C57BL/6 mice. *Cancer Res* 44: 717–26
- Cremolini C, Loupakis F, Antoniotti C, Lupi C, Sensi E, Lonardi S, Mezi S, Tomasello G, Ronzoni M, Zaniboni A, *et al* (2015) FOLFOXIRI plus bevacizumab versus FOLFIRI plus bevacizumab as first-line treatment of patients with metastatic colorectal cancer: updated overall survival and molecular subgroup analyses of the open-label, phase 3 TRIBE study. *Lancet Oncol* 16: 1306–1315
- Curtsinger JM, Gerner MY, Lins DC & Mescher MF (2007) Signal 3 Availability Limits the CD8 T Cell Response to a Solid Tumor. *J Immunol* 178: 6752–6760
- Curtsinger JM, Valenzuela JO, Agarwal P, Lins D & Mescher MF (2005) Cutting Edge: Type I IFNs Provide a Third Signal to CD8 T Cells to Stimulate Clonal Expansion and Differentiation. *J Immunol* 174: 4465–4469
- Demaria O, Gassart AD, Coso S, Gestermann N, Domizio JD, Flatz L, Gaide O, Michielin O, Hwu P, Petrova TV, *et al* (2015) STING activation of tumor endothelial cells initiates spontaneous and therapeutic antitumor immunity. *Proc Natl Acad Sci USA* 112: 15408–15413
- Denève E, Riethdorf S, Ramos J, Nocca D, Coffy A, Daurès J-P, Maudelonde T, Fabre J-M, Pantel K & Alix-Panabières C (2013) Capture of Viable Circulating Tumor Cells in the Liver of Colorectal Cancer Patients. *Clin Chem* 59: 1384–1392
- Dunlop MG, Tenesa A, Farrington SM, Ballereau S, Brewster DH, Koessler T, Pharoah P, Schafmayer C, Hampe J, Völzke H, *et al* (2013) Cumulative impact of common

genetic variants and other risk factors on colorectal cancer risk in 42 103 individuals. *Gut* 62: 871

- Duong CPM, Yong CSM, Kershaw MH, Slaney CY & Darcy PK (2015) Cancer immunotherapy utilizing gene-modified T cells: From the bench to the clinic. *Mol Immunol* 67: 46–57
- Efremova M, Rieder D, Klepsch V, Charoentong P, Finotello F, Hackl H, Hermann-Kleiter N, Löwer M, Baier G, Krogsdam A, *et al* (2017) Targeting immune checkpoints potentiates immunoediting and changes the dynamics of tumor evolution. *Nature Communications*: 1–13
- Esteller M, Sparks A, Toyota M, Sanchez-Cespedes M, Capella G, Peinado MA, Gonzalez S, Tarafa G, Sidransky D, Meltzer SJ, *et al* (2000) Analysis of adenomatous polyposis coli promoter hypermethylation in human cancer. *Cancer Res* 60: 4366–71
- Fidler MM, Soerjomataram I & Bray F (2016) A global view on cancer incidence and national levels of the human development index. *Int J Cancer* 139: 2436–2446
- Fiorentini G, Sarti D, Aliberti C, Carandina R, Mambrini A & Guadagni S (2017) Multidisciplinary approach of colorectal cancer liver metastases. *World J Clin Oncol* 8: 190–202
- Forcet C, Ye X, Granger L, Corset V, Shin H, Bredesen DE & Mehlen P (2001) The dependence receptor DCC (deleted in colorectal cancer) defines an alternative mechanism for caspase activation. *Proc National Acad Sci* 98: 3416–3421
- Fuchs SY (2012) Ubiquitination-mediated regulation of interferon responses. *Growth Factors* 30: 141–148
- Geiersbach KB & Samowitz WS (2011) Microsatellite Instability and Colorectal Cancer. *Archives Pathology Amp Laboratory Medicine* 135: 1269–1277
- González-Navajas JM, Lee J, David M & Raz E (2012) Immunomodulatory functions of type I interferons. *Nat Rev Immunol* 12: 125–135
- Grigore AD, Jolly MK, Jia D, Farach-Carson MC & Levine H (2016) Tumor Budding: The Name is EMT. Partial EMT. *J Clin Medicine* 5: 51
- Gui J, Zahedi F, Ortiz A, Cho C, Katlinski KV, Alicea-Torres K, Li J, Todd L, Zhang H, Beiting DP, *et al* (2020) Activation of p38 α stress-activated protein kinase drives the formation of the pre-metastatic niche in the lungs. *Nat Cancer* 1: 603–619
- Guidotti LG, Inverso D, Sironi L, Di Lucia P, Fioravanti J, Ganzer L, Fiocchi A, Vacca M, Aiolfi R, Sammiceli S, *et al* (2015) Immunosurveillance of the Liver by Intravascular Effector CD8⁺ T Cells. *Cell* 161: 486–500

- Guo X, Zhang Y, Zheng L, Zheng C, Song J, Zhang Q, Kang B, Liu Z, Jin L, Xing R, *et al* (2018) Global characterization of T cells in non-small-cell lung cancer by single-cell sequencing. *Nat Med* 24: 978–985
- Hafner A, Bulyk ML, Jambhekar A & Lahav G (2019) The multiple mechanisms that regulate p53 activity and cell fate. *Nat Rev Mol Cell Bio* 20: 199–210
- Halama N, Michel S, Kloor M, Zoernig I, Benner A, Spille A, Pommerencke T, Knebel DM von, Folprecht G, Lubber B, *et al* (2011) Localization and Density of Immune Cells in the Invasive Margin of Human Colorectal Cancer Liver Metastases Are Prognostic for Response to Chemotherapy. *Cancer Res* 71: 5670–5677
- Hanahan D & Weinberg RA (2000) The Hallmarks of Cancer. *Cell* 100: 57–70
- Hanahan D & Weinberg RA (2011) Hallmarks of Cancer: The Next Generation. *Cell* 144: 646–674
- Hogquist KA, Jameson SC, Heath WR, Howard JL, Bevan MJ & Carbone FR (1994) T cell receptor antagonist peptides induce positive selection. *Cell* 76: 17–27
- Horowitz M, Neeman E, Sharon E & Ben-Eliyahu S (2015) Exploiting the critical perioperative period to improve long-term cancer outcomes. *Nat Rev Clin Oncol* 12: 213–226
- HuangFu W-C, Qian J, Liu C, Liu J, Lokshin AE, Baker DP, Rui H & Fuchs SY (2012) Inflammatory signaling compromises cell responses to interferon alpha. *Oncogene* 31: 161–172
- Indraccolo S (2010) Interferon- α as angiogenesis inhibitor: Learning from tumor models. *Autoimmunity* 43: 244–247
- Itatani Y, Kawada K & Sakai Y (2019) Transforming Growth Factor- β Signaling Pathway in Colorectal Cancer and Its Tumor Microenvironment. *Int J Mol Sci* 20: 5822
- Ivashkiv LB & Donlin LT (2014) Regulation of type I interferon responses. *Nat Rev Immunol* 14: 36–49
- Jiang X, Xu J, Liu M, Xing H, Wang Z, Huang L, Mellor AL, Wang W & Wu S (2019) Adoptive CD8⁺ T cell therapy against cancer: Challenges and opportunities. *Cancer Lett* 462: 23–32
- John SKP, George S, Primrose JN & Fozard JBJ (2011) Symptoms and signs in patients with colorectal cancer. *Colorectal Dis* 13: 17–25
- Joshi S, Kaur S, Kroczyńska B & Plataniias LC (2010) Mechanisms of mRNA translation of interferon stimulated genes. *Cytokine* 52: 123–127

- Kalbasi A & Ribas A (2020) Tumour-intrinsic resistance to immune checkpoint blockade. *Nat Rev Immunol* 20: 25–39
- Kaplan RN, Riba RD, Zacharoulis S, Bramley AH, Vincent L, Costa C, MacDonald DD, Jin DK, Shido K, Kerns SA, *et al* (2005) VEGFR1-positive haematopoietic bone marrow progenitors initiate the pre-metastatic niche. *Nature* 438: 820–827
- Katlinski KV, Gui J, Katlinskaya YV, Ortiz A, Chakraborty R, Bhattacharya S, Carbone CJ, Beiting DP, Gironde MA, Peck AR, *et al* (2017) Inactivation of Interferon Receptor Promotes the Establishment of Immune Privileged Tumor Microenvironment. *Cancer Cell* 31: 194–207
- Kelly RJ, Kemeny NE & Leonard GD (2005) Current Strategies Using Hepatic Arterial Infusion Chemotherapy for the Treatment of Colorectal Cancer. *Clin Colorectal Canc* 5: 166–174
- Kinzler KW & Vogelstein B (1996) Lessons from Hereditary Colorectal Cancer. *Cell* 87: 159–170
- Kirby JA, Bone M, Robertson H, Hudson M & Jones DEJ (2003) The number of intraepithelial T cells decreases from ascending colon to rectum. *J Clin Pathol* 56: 158
- Kirtane K, Elmariah H, Chung CH & Abate-Daga D (2021) Adoptive cellular therapy in solid tumor malignancies: review of the literature and challenges ahead. *J Immunother Cancer* 9: e002723
- Koopman M, Antonini NF, Douma J, Wals J, Honkoop AH, Erdkamp FL, Jong RS de, Rodenburg CJ, Vreugdenhil G, Loosveld OJ, *et al* (2007) Sequential versus combination chemotherapy with capecitabine, irinotecan, and oxaliplatin in advanced colorectal cancer (CAIRO): a phase III randomised controlled trial. *Lancet* 370: 135–142
- Kotenko SV, Gallagher G, Baurin VV, Lewis-Antes A, Shen M, Shah NK, Langer JA, Sheikh F, Dickensheets H & Donnelly RP (2003) IFN- λ s mediate antiviral protection through a distinct class II cytokine receptor complex. *Nat Immunol* 4: 69–77
- Kow AWC (2019) Hepatic metastasis from colorectal cancer. *J Gastrointest Oncol* 10: 1274–1298
- Krasinskas AM (2011) EGFR Signaling in Colorectal Carcinoma. *Pathology Res Int* 2011: 932932
- Lee GH, Malietzis G, Askari A, Bernardo D, Al-Hassi HO & Clark SK (2015) Is right-sided colon cancer different to left-sided colorectal cancer? – A systematic review. *European J Surg Oncol Ejs* 41: 300–308

- Li J, Ma X, Chakravarti D, Shalapour S & DePinho RA (2021) Genetic and biological hallmarks of colorectal cancer. *Gene Dev* 35: 787–820
- Lim DR, Kuk JK, Kim T & Shin EJ (2017) Comparison of oncological outcomes of right-sided colon cancer versus left-sided colon cancer after curative resection. *Medicine* 96: e8241
- Lin J-D, Feng N, Sen A, Balan M, Tseng H-C, McElrath C, Smirnov SV, Peng J, Yasukawa LL, Durbin RK, *et al* (2016) Distinct Roles of Type I and Type III Interferons in Intestinal Immunity to Homologous and Heterologous Rotavirus Infections. *Plos Pathog* 12: e1005600
- Liu J, HuangFu W-C, Kumar KGS, Qian J, Casey JP, Hamanaka RB, Grigoriadou C, Aldabe R, Diehl JA & Fuchs SY (2009) Virus-Induced Unfolded Protein Response Attenuates Antiviral Defenses via Phosphorylation-Dependent Degradation of the Type I Interferon Receptor. *Cell Host Microbe* 5: 72–83
- Locquenghien M von, Rozalén C & Celià-Terrassa T (2021) Interferons in cancer immunoediting: sculpting metastasis and immunotherapy response. *J Clin Invest* 131: e143296
- Majumdar SR, Fletcher RH & Evans AT (1999) How Does Colorectal Cancer Present? Symptoms, Duration, and Clues to Location. *Am J Gastroenterol* 94: 3039–3045
- Manjunath N, Shankar P, Wan J, Weninger W, Crowley MA, Hieshima K, Springer TA, Fan X, Shen H, Lieberman J, *et al* (2001) Effector differentiation is not prerequisite for generation of memory cytotoxic T lymphocytes. *J Clin Invest* 108: 871–878
- Martin MD & Badovinac VP (2018) Defining Memory CD8 T Cell. *Front Immunol* 9: 2692
- Michor F, Iwasa Y, Vogelstein B, Lengauer C & Nowak MA (2005) Can chromosomal instability initiate tumorigenesis? *Semin Cancer Biol* 15: 43–49
- Millette S, Sicklick JK, Lowy AM & Brodt P (2017) Molecular Pathways: Targeting the Microenvironment of Liver Metastases. *Clin Cancer Res* 23: 6390–6399
- Mimori K, Tanaka F, Shibata K & Mori M (2012) Review: single nucleotide polymorphisms associated with the oncogenesis of colorectal cancer. *Surg Today* 42: 215–219
- Missiaglia E, Jacobs B, D’Ario G, Narzo AFD, Soneson C, Budinska E, Popovici V, Vecchione L, Gerster S, Yan P, *et al* (2014) Distal and proximal colon cancers differ in terms of molecular, pathological, and clinical features. *Ann Oncol* 25: 1995–2001
- Mohammad KS, Javelaud D, Fournier PGJ, Niewolna M, McKenna CR, Peng XH, Duong V, Dunn LK, Mauviel A & Guise TA (2011) TGF- β -RI Kinase Inhibitor SD-

208 Reduces the Development and Progression of Melanoma Bone Metastases. *Cancer Res* 71: 175–184

Morin PJ, Sparks AB, Korinek V, Barker N, Clevers H, Vogelstein B & Kinzler KW (1997) Activation of β -Catenin-Tcf Signaling in Colon Cancer by Mutations in β -Catenin or APC. *Science* 275: 1787–1790

Munn DH & Bronte V (2016) Immune suppressive mechanisms in the tumor microenvironment. *Curr Opin Immunol* 39: 1–6

Musella M, Manic G, Maria RD, Vitale I & Sistigu A (2017) Type-I-interferons in infection and cancer: Unanticipated dynamics with therapeutic implications. *Oncoimmunology* 6: e1314424

Ogino S, Nosho K, Irahara N, Shima K, Baba Y, Kirkner GJ, Meyerhardt JA & Fuchs CS (2009) Prognostic Significance and Molecular Associations of 18q Loss of Heterozygosity: A Cohort Study of Microsatellite Stable Colorectal Cancers. *J Clin Oncol* 27: 4591–4598

Park CG, Hartl CA, Schmid D, Carmona EM, Kim H-J & Goldberg MS (2018) Extended release of perioperative immunotherapy prevents tumor recurrence and eliminates metastases. *Sci Transl Med* 10: eaar1916

Patnaik A, Haluska P, Tolcher AW, Erlichman C, Papadopoulos KP, Lensing JL, Beeram M, Molina JR, Rasco DW, Arcos RR, *et al* (2016) A First-in-Human Phase I Study of the Oral p38 MAPK Inhibitor, Ralimetinib (LY2228820 Dimesylate), in Patients with Advanced Cancer. *Clin Cancer Res* 22: 1095–1102

Peinado H, Zhang H, Matei IR, Costa-Silva B, Hoshino A, Rodrigues G, Psaila B, Kaplan RN, Bromberg JF, Kang Y, *et al* (2017) Pre-metastatic niches: organ-specific homes for metastases. *Nat Rev Cancer* 17: 302–317

Perica K, Varela JC, Oelke M & Schneck J (2015) Adoptive T Cell Immunotherapy For Cancer. *Rambam Maimonides Medical J* 6: e0004

Pesch V van, Lanaya H, Renauld J-C & Michiels T (2004) Characterization of the murine alpha interferon gene family. *J Virol* 78: 8219–8228

Piehler J, Thomas C, Garcia KC & Schreiber G (2012) Structural and dynamic determinants of type I interferon receptor assembly and their functional interpretation. *Immunol Rev* 250: 317–334

Ratti F, Catena M, Palo SD, Staudacher C & Aldrighetti L (2016) Impact of totally laparoscopic combined management of colorectal cancer with synchronous hepatic metastases on severity of complications: a propensity-score-based analysis. *Surg Endosc* 30: 4934–4945

- Rees PA & Lowy RJ (2018) Measuring type I interferon using reporter gene assays based on readily available cell lines. *J Immunol Methods* 461: 63–72
- Riihimäki M, Hemminki A, Sundquist J & Hemminki K (2016) Patterns of metastasis in colon and rectal cancer. *Sci Rep-uk* 6: 29765
- Rohaam MW, Wilgenhof S & Haanen JBAG (2019) Adoptive cellular therapies: the current landscape. *Virchows Arch* 474: 449–461
- Saidi H, Karuri D & Nyaim E (2008) Correlation of clinical data, anatomical site and disease stage in colorectal cancer. *E Afr Med J* 85: 259–262
- Sargent DJ, Marsoni S, Monges G, Thibodeau SN, Labianca R, Hamilton SR, French AJ, Kabat B, Foster NR, Torri V, *et al* (2010) Defective Mismatch Repair As a Predictive Marker for Lack of Efficacy of Fluorouracil-Based Adjuvant Therapy in Colon Cancer. *J Clin Oncol* 28: 3219–3226
- Sato T, Stange DE, Ferrante M, Vries RGJ, Es JH van, Brink S van den, Houdt WJ van, Pronk A, Gorp J van, Siersema PD, *et al* (2011) Long-term Expansion of Epithelial Organoids From Human Colon, Adenoma, Adenocarcinoma, and Barrett's Epithelium. *Gastroenterology* 141: 1762–1772
- Schindelin J, Arganda-Carreras I, Frise E, Kaynig V, Longair M, Pietzsch T, Preibisch S, Rueden C, Saalfeld S, Schmid B, *et al* (2012) Fiji: an open-source platform for biological-image analysis. *Nat Methods* 9: 676–682
- Schreckenbach T, Malkomes P, Bechstein WO, Woeste G, Schnitzbauer AA & Ulrich F (2015) The clinical relevance of the Fong and the Nordlinger scores in the era of effective neoadjuvant chemotherapy for colorectal liver metastasis. *Surg Today* 45: 1527–1534
- Schreiber G & Piehler J (2015) The molecular basis for functional plasticity in type I interferon signaling. *Trends Immunol* 36: 139–149
- Shakhar G & Ben-Eliyahu S (2003) Potential Prophylactic Measures Against Postoperative Immunosuppression: Could They Reduce Recurrence Rates in Oncological Patients? *Ann Surg Oncol* 10: 972–992
- Shih IM, Zhou W, Goodman SN, Lengauer C, Kinzler KW & Vogelstein B (2001) Evidence that genetic instability occurs at an early stage of colorectal tumorigenesis. *Cancer Res* 61: 818–22
- Shipkova M & Wieland E (2012) Surface markers of lymphocyte activation and markers of cell proliferation. *Clin Chim Acta* 413: 1338–1349
- Sieber OM, Heinimann K & Tomlinson IPM (2003) Genomic instability — the engine of tumorigenesis? *Nat Rev Cancer* 3: 701–708

- Siegel RL, Miller KD, Sauer AG, Fedewa SA, Butterly LF, Anderson JC, Cercek A, Smith RA & Jemal A (2020) Colorectal cancer statistics, 2020. *Ca Cancer J Clin* 70: 145–164
- Simone GD, Andreatta F, Bleriot C, Fumagalli V, Laura C, Garcia-Manteiga JM, Lucia PD, Gilotto S, Ficht X, Ponti FFD, *et al* (2021) Identification of a Kupffer cell subset capable of reverting the T cell dysfunction induced by hepatocellular priming. *Immunity*
- Sisirak V, Faget J, Gobert M, Goutagny N, Vey N, Treilleux I, Renaudineau S, Poyet G, Labidi-Galy SI, Goddard-Leon S, *et al* (2012) Impaired IFN- α Production by Plasmacytoid Dendritic Cells Favors Regulatory T-cell Expansion That May Contribute to Breast Cancer Progression. *Cancer Res* 72: 5188–5197
- Sitia G, Aiolfi R, Lucia PD, Mainetti M, Fiocchi A, Mingozi F, Esposito A, Ruggeri ZM, Chisari FV, Iannacone M, *et al* (2012) Antiplatelet therapy prevents hepatocellular carcinoma and improves survival in a mouse model of chronic hepatitis B. *Proc Natl Acad Sci USA* 109: E2165-72
- Snell LM, McGaha TL & Brooks DG (2017) Type I Interferon in Chronic Virus Infection and Cancer. *Trends Immunol* 38: 542–557
- Stark GR, Kerr IM, Williams BRG, Silverman RH & Schreiber RD (1998) HOW CELLS RESPOND TO INTERFERONS. *Annu Rev Biochem* 67: 227–264
- Steinert G, Schölch S, Koch M & Weitz J (2012) Biology and significance of circulating and disseminated tumour cells in colorectal cancer. *Langenbeck's Archives Surg* 397: 535–542
- Strilic B & Offermanns S (2017) Intravascular Survival and Extravasation of Tumor Cells. *Cancer Cell* 32: 282–293
- Subramaniam R, Mizoguchi A & Mizoguchi E (2016) Mechanistic roles of epithelial and immune cell signaling during the development of colitis-associated cancer. *Cancer Res Frontiers* 2: 1–21
- Sung H, Ferlay J, Siegel RL, Laversanne M, Soerjomataram I, Jemal A & Bray F (2021) Global Cancer Statistics 2020: GLOBOCAN Estimates of Incidence and Mortality Worldwide for 36 Cancers in 185 Countries. *Ca Cancer J Clin* 71: 209–249
- Świdarska M, Choromańska B, Dąbrowska E, Konarzewska-Duchnowska E, Choromańska K, Szczurko G, Myśliwiec P, Dadan J, Ładny JR & Zwierz K (2014) The diagnostics of colorectal cancer. *Contemp Oncol* 18: 1–6
- Tandon M, Salamoun JM, Carder EJ, Farber E, Xu S, Deng F, Tang H, Wipf P & Wang QJ (2015) SD-208, a Novel Protein Kinase D Inhibitor, Blocks Prostate Cancer Cell

Proliferation and Tumor Growth In Vivo by Inducing G2/M Cell Cycle Arrest. *Plos One* 10: e0119346

Tang Z, Kang B, Li C, Chen T & Zhang Z (2019) GEPIA2: an enhanced web server for large-scale expression profiling and interactive analysis. *Nucleic Acids Res* 47: W556–W560

Tauriello DVF, Palomo-Ponce S, Stork D, Berenguer-Llargo A, Badia-Ramentol J, Iglesias M, Sevillano M, Ibiza S, Cañellas A, Hernando-Momblona X, *et al* (2018) TGF β drives immune evasion in genetically reconstituted colon cancer metastasis. *Nature Publishing Group* 554: 538–543

Taylor DP, Burt RW, Williams MS, Haug PJ & Cannon–Albright LA (2010) Population-Based Family History–Specific Risks for Colorectal Cancer: A Constellation Approach. *Gastroenterology* 138: 877–885

Theodoratou E, Montazeri Z, Hawken S, Allum GC, Gong J, Tait V, Kirac I, Tazari M, Farrington SM, Demarsh A, *et al* (2012) Systematic Meta-Analyses and Field Synopsis of Genetic Association Studies in Colorectal Cancer. *Jnci J National Cancer Inst* 104: 1433–1457

Thiery JP & Sleeman JP (2006) Complex networks orchestrate epithelial–mesenchymal transitions. *Nat Rev Mol Cell Bio* 7: 131–142

Thommen DS & Schumacher TN (2018) T Cell Dysfunction in Cancer. *Cancer Cell* 33: 547–562

Tournigand C, André T, Achille E, Lledo G, Flesh M, Mery-Mignard D, Quinaux E, Couteau C, Buyse M, Ganem G, *et al* (2003) FOLFIRI Followed by FOLFOX6 or the Reverse Sequence in Advanced Colorectal Cancer: A Randomized GERCOR Study. *J Clin Oncol* 22: 229–237

Tran NL, Ferreira LM, Alvarez-Moya B, Buttiglione V, Ferrini B, Zordan P, Monestiroli A, Fagioli C, Bezzecchi E, Scotti GM, *et al* (2022) Continuous sensing of IFN α by hepatic endothelial cells shapes a vascular antimetastatic barrier. *Elife* 11

Trinchieri G (2010) Type I interferon: friend or foe? *J Exp Med* 207: 2053–2063

Trzpis M, McLaughlin PMJ, Leij LMFH de & Harmsen MC (2007) Epithelial Cell Adhesion Molecule More than a Carcinoma Marker and Adhesion Molecule. *Am J Pathology* 171: 386–395

Ueno H, Hashiguchi Y, Shimazaki H, Shinto E, Kajiwara Y, Nakanishi K, Kato K, Maekawa K, Miyai K, Nakamura T, *et al* (2013) Objective Criteria for Crohn-like Lymphoid Reaction in Colorectal Cancer. *Am J Clin Pathol* 139: 434–441

- Ueno H, Kajiwara Y, Shimazaki H, Shinto E, Hashiguchi Y, Nakanishi K, Maekawa K, Katsurada Y, Nakamura T, Mochizuki H, *et al* (2012) New Criteria for Histologic Grading of Colorectal Cancer. *Am J Surg Pathology* 36: 193–201
- Ueno H, Murphy J, Jass JR, Mochizuki H & Talbot IC (2002) Tumour ‘budding’ as an index to estimate the potential of aggressiveness in rectal cancer. *Histopathology* 40: 127–132
- Uhl M, Aulwurm S, Wischhusen J, Weiler M, Ma JY, Almirez R, Mangadu R, Liu Y-W, Platten M, Herrlinger U, *et al* (2004) SD-208, a Novel Transforming Growth Factor β Receptor I Kinase Inhibitor, Inhibits Growth and Invasiveness and Enhances Immunogenicity of Murine and Human Glioma Cells In vitro and In vivo. *Cancer Res* 64: 7954–7961
- Venkat SR, Mohan PP & Gandhi RT (2018) Colorectal Liver Metastasis: Overview of Treatment Paradigm Highlighting the Role of Ablation. *Am J Roentgenol* 210: 883–890
- Vidal-Vanaclocha F (2008) The Prometastatic Microenvironment of the Liver. *Cancer Microenviron* 1: 113–129
- Vilar E & Gruber SB (2010) Microsatellite instability in colorectal cancer—the stable evidence. *Nat Rev Clin Oncol* 7: 153–162
- Vousden DA, Cox E, Allemang-Grand R, Laliberté C, Qiu LR, Lindenmaier Z, Nieman BJ & Lerch JP (2018) Continuous manganese delivery via osmotic pumps for manganese-enhanced mouse MRI does not impair spatial learning but leads to skin ulceration. *Neuroimage* 173: 411–420
- Watanabe T, Wu T-T, Catalano PJ, Ueki T, Satriano R, Haller DG, Benson AB & Hamilton SR (2001) Molecular Predictors of Survival after Adjuvant Chemotherapy for Colon Cancer. *New Engl J Medicine* 344: 1196–1206
- Weber JS, Yang JC, Atkins MB & Disis ML (2015) Toxicities of Immunotherapy for the Practitioner. *J Clin Oncol* 33: 2092–2099
- Weitz J, Koch M, Debus J, Höhler T, Galle PR & Büchler MW (2005) Colorectal cancer. *Lancet* 365: 153–165
- Wu C (2018) Systemic Therapy for Colon Cancer. *Surg Oncol Clin N Am* 27: 235–242
- Xia A, Zhang Y, Xu J, Yin T & Lu X-J (2019) T Cell Dysfunction in Cancer Immunity and Immunotherapy. *Front Immunol* 10: 1719
- Zhang H, Yu P, Tomar VS, Chen X, Atherton MJ, Lu Z, Zhang H-G, Li S, Ortiz A, Gui J, *et al* (2022) Targeting PARP11 to avert immunosuppression and improve CAR T therapy in solid tumors. *Nat Cancer* 3: 808–820

- Zhang K-J, Yin X-F, Yang Y-Q, Li H-L, Xu Y-N, Chen L-Y, Liu X-J, Yuan S-J, Fang X-L, Xiao J, *et al* (2017) A Potent In Vivo Antitumor Efficacy of Novel Recombinant Type I Interferon. *Clin Cancer Res* 23: 2038–2049
- Zhang Z, Liu S, Zhang B, Qiao L, Zhang Y & Zhang Y (2020) T Cell Dysfunction and Exhaustion in Cancer. *Frontiers Cell Dev Biology* 8: 17
- Zhao M, Mishra L & Deng C-X (2018) The role of TGF- β /SMAD4 signaling in cancer. *Int J Biol Sci* 14: 111–123
- Zheng H, Qian J, Carbone CJ, Leu NA, Baker DP & Fuchs SY (2011) Vascular endothelial growth factor-induced elimination of the type 1 interferon receptor is required for efficient angiogenesis. *Blood* 118: 4003–4006
- Zijl F van, Krupitza G & Mikulits W (2011) Initial steps of metastasis: Cell invasion and endothelial transmigration. *Mutat Res Rev Mutat Res* 728: 23–34
- Zinser-Sierra JW, Rodríguez-Ramírez S, Villalobos-Valencia R & Ramírez-Márquez M (2011) Use of Bevacizumab in Metastatic Colorectal Cancer. *Drugs R D* 11: 101–111
- Zitvogel L, Galluzzi L, Kepp O, Smyth MJ & Kroemer G (2015) Type I interferons in anticancer immunity. *Nat Rev Immunol* 15: 405–414



7. Appendix

Table 7.1. Custom Taqman Array Cards genes list.

Gene Symbol	Probe ID	Gene Name
<i>Ifna1/Ifna6/Ifna5</i>	Mm03030145_gH	interferon alpha 1;interferon alpha 6;interferon alpha 5
<i>Ifna2</i>	Mm00833961_s1	interferon alpha 2
<i>Ifna4</i>	Mm00833969_s1	interferon alpha 4
<i>Ifna5</i>	Mm00833976_s1	interferon alpha 5
<i>Ifna6</i>	Mm01703458_s1	interferon alpha 6
<i>Ifna7</i>	Mm02525960_s1	interferon alpha 7
<i>Ifna9</i>	Mm00833983_s1	interferon alpha 9
<i>Ifna11/Ifna2</i>	Mm04207507_gH	interferon alpha 2,interferon alpha 11
<i>Ifna12</i>	Mm00616656_s1	interferon alpha 12
<i>Ifna13</i>	Mm01731013_s1	interferon alpha 13
<i>Ifna14</i>	Mm01703465_s1	interferon alpha 14
<i>Ifna15</i>	Mm01267666_sH	interferon alpha 15
<i>Ifna16</i>	Mm01703434_s1	interferon alpha 16
<i>Ifnab</i>	Mm00833443_s1	interferon alpha B
<i>Ifnb1</i>	Mm00439552_s1	interferon beta 1, fibroblast
<i>Ifne</i>	Mm00616542_s1	interferon epsilon
<i>Ifnk</i>	Mm02529417_s1	interferon kappa
<i>Ifnz</i>	Mm02525738_g1	interferon zeta
<i>Irgm1</i>	Mm00492596_m1	immunity-related GTPase family M member 1
<i>Stat1</i>	Mm01257286_m1	signal transducer and activator of transcription 1
<i>Stat2</i>	Mm00490880_m1	signal transducer and activator of transcription 2
<i>Stat3</i>	Mm01219775_m1	signal transducer and activator of transcription 3
<i>Irf7</i>	Mm00516793_g1	interferon regulatory factor 7
<i>Irf8</i>	Mm00492567_m1	interferon regulatory factor 8
<i>Oas1a</i>	Mm00836412_m1	2'-5' oligoadenylate synthetase 1A
<i>Oas1l</i>	Mm00455081_m1	2'-5' oligoadenylate synthetase-like 1
<i>Ifit1</i>	Mm00515153_m1	interferon-induced protein with tetratricopeptide repeats 1
<i>Ifit2</i>	Mm00492606_m1	interferon-induced protein with tetratricopeptide repeats 2
<i>Ifi202b</i>	Mm00839397_m1	interferon activated gene 202B
<i>Ifi205</i>	Mm01315309_m1	interferon activated gene 205
<i>Tmem173 (STING)</i>	Mm01158117_m1	transmembrane protein 173
<i>Aim 2</i>	Mm01295719_m1	absent in melanoma 2
<i>Ifi204</i>	Mm00492602_m1	interferon activated gene 204
<i>Ifitm2</i>	Mm00850080_g1	interferon induced transmembrane protein 2
<i>Ifitm3</i>	Mm00847057_s1	interferon induced transmembrane protein 3

<i>Cd86</i>	Mm00444540_m1	CD86 antigen
<i>Gbp2b</i>	Mm00657086_m1	guanylate binding protein 2b
<i>Cxcl10</i>	Mm00445235_m1	chemokine (C-X-C motif) ligand 10
<i>Usp18</i>	Mm01188805_m1	ubiquitin specific peptidase 18
<i>Socs3</i>	Mm00545913_s1	suppressor of cytokine signaling 3
<i>Dhx58</i>	Mm01302252_m1	DEXH (Asp-Glu-X-His) box polypeptide 58
<i>IFNAR1</i>	Mm00439544_m1	interferon (alpha and beta) receptor 1
<i>Tgfb1</i>	Mm01178820_m1	transforming growth factor, beta 1
<i>Axl</i>	Mm00437221_m1	AXL receptor tyrosine kinase
<i>Gas 6</i>	Mm00490378_m1	growth arrest specific 6
<i>CD274 (PDL1)</i>	Mm03048248_m1	CD274 antigen
<i>CTLA4</i>	Mm00486849_m1	cytotoxic T-lymphocyte-associated protein 4
<i>Pdcd1/PD1</i>	Mm01285676_m1	programmed cell death 1
<i>Tnfsf9</i>	Mm00437155_m1	tumor necrosis factor (ligand) superfamily, member 9
<i>Timd4</i>	Mm00724709_m1	T cell immunoglobulin and mucin domain containing 4
<i>IL1a</i>	Mm00439620_m1	interleukin 1 alpha
<i>IL1b</i>	Mm00434228_m1	interleukin 1 beta
<i>IL6</i>	Mm00446190_m1	interleukin 6
<i>TNFa</i>	Mm00443258_m1	tumor necrosis factor
<i>Tgfr2</i>	Mm03024091_m1	transforming growth factor, beta receptor II
<i>Lcn2</i>	Mm01324470_m1	lipocalin 2
<i>EIF2AK3 (PERK)</i>	Mm00438700_m1	eukaryotic translation initiation factor 2 alpha kinase 3
<i>CCR2</i>	Mm99999051_gH	chemokine (C-C motif) receptor 2
<i>Eif2ak2 (PKR)</i>	Mm01235643_m1	eukaryotic translation initiation factor 2-alpha kinase 2
<i>IDO2</i>	Mm00524210_m1	indoleamine 2,3-dioxygenase 2
<i>GAPDH</i>	Mm99999915_g1	glyceraldehyde-3-phosphate dehydrogenase
<i>TBP</i>	Mm01277042_m1	TATA box binding protein
<i>Psmc4</i>	Mm00457191_m1	proteasome (prosome, macropain) 26S subunit, ATPase, 4
18s	Hs99999901_s1	Eukaryotic 18S rRNA